Dynamics and Predictability of Large-Scale Atmospheric Waves

by

Girish Nigamanth Raghunathan

A Dissertation Presented in Partial Fulfillment
of the Requirements for the Degree
Doctor of Philosophy

Approved April 2021 by the
Graduate Supervisory Committee:

Huei-Ping Huang, Chair
Kangping Chen
Ronald Calhoun
Marcus Herrmann
Eric Kostelich

ARIZONA STATE UNIVERSITY

May 2021

ABSTRACT

Large amplitude westward propagating long waves in midlatitudes of Northern Hemisphere occasionally sustain coherent phase propagation over multiple weeks. Owing to the large amplitude and the life cycle of these waves previous studies have speculated their influence on extended-range weather forecasts but have not quantified them. The primary aim of this study is to establish an updated long-term catalog of Retrograde events which can then be used to investigate the statistics and structure of these waves. Guided by the newly created catalog the dynamics of these waves are further explored. A preliminary look into the dynamics of these waves reveal a sequence of poleward extrusion, westward migration and vortex shedding occurring frequently during certain strong Retrograde wave events. A strong connection between the westward moving low PV structures and the East Asian cold air outbreak is uncovered. Also, the initiation of the sequence of low PV extrusion and vortex shedding is found to be linked with the phase of propagating Wave-1 zonal component. Enhanced predictability of global midlatitude Geopotential Height at 500mb is noted during active period of strong Retrograde wave activity in comparison to inactive period. Skilled forecasts were produced almost (on an average) 12 days in advance during the active period of one of the winters (1995/96) as compared to 9 days during the inactive period of the season.

ACKNOWLEDGMENTS

I would like to express my utmost gratitude to Dr. Huei-Ping Huang for guiding through my PhD providing some valuable insights and direction throughout the process.

I also would like to thank Dr. Calhoun, Dr. Chen, Dr. Herrmann, and Dr. Kostelich for agreeing and being a valuable part of the Graduate committee.

This work was supported by National Science Foundation Grant AGS-1724555.

TABLE OF CONTENTS

Page

LIST OF TABLES vi

LIST OF FIGURES vii

CHAPTER

1 INTRODUCTION 1

Motivation for Study 1

Theoretical Background on Rossby Waves 4

Conservation of absolute vorticity 4

Rossby Wave dispersion relation 5

Geostrophic approximation and Rossby number 6

Potential Vorticity 8

Physical understanding of Potential Vorticity 9

Two Different Approaches in Studying Atmospheric Waves 11

Outline for Thesis 11

2 OBSERVATIONAL ANALYSIS OF RETROGRADE WAVES 13

Using Time Filtered Reanalysis to Identify Retrograde Wave Events 13

Event Selection Criteria and the Updated Catalog 14

Vertical Structure of Retrograde Waves 19

Statistics and Horizontal Structure of Retrograde Waves 21

Potential Vorticity Picture and Vortex Shedding 25

Summary and Future Work 31

CHAPTER Page

3 PREDICTABILITY ASSOCIATED WITH RETROGRADE WAVE DISTURBANCES 33

Introduction 33

Reforecast Dataset and Processing 34

Winters with Major Retrograde Wave Activity 36

Geographical Dependence of Increased Predictability 42

Vortex shedding event during February 1995 43

Blocking and Vortex shedding event during December 2010 47

Periods of increased predictability during December 1994 49

Further Discussion and Summary 55

4 TRANS-PACIFIC CONNECTION OF RETROGRADE DISTURBACNES TO EAST ASIAN COLD AIR OUTBREAK 57

Introduction 57

Vortex Shedding as an Effect of Westward Propagating Wave-1 Signal 58

January 1980 Retrograde Wave Event 58

January 1995 and December 2010 Retrograde Wave Events 63

Discussion on observed links 64

Possible Stratospheric Connection 66

Links to East Asian Cold Air Outbreaks 67

Using Reanalysis data to identify cold air outbreak events 69

Cold air outbreak events during winters of 1979/80 and 2010/11 71

Potential Vorticity during cold air outbreak 72

CHAPTER Page

Tracking of low PV centers....73

Summary and Further Discussion....76

5 CONCLUSION AND FUTURE DIRECTION....78

REFERENCES....81

APPENDIX

A BAND PASS FILTER....86

B SIGNIFICANCE OF INCREASED PREDICTABILITY....89

LIST OF TABLES

Table Page

1. The Retrograde-Wave Events, Organized by Year, as Identified by Criteria (1) and (2) in the Text. Each Event is Described by its Start Date (Month/day), Followed by Duration and Period in Days 16

2. Pressure Value Corresponding to Potential Temperature Levels - Based on Average of Monthly Mean Temperature over Pacific Region (Between 160^{o} E and 160^{o} W at 60^{o} N Latitude Circle) 27

LIST OF FIGURES

Figure Page

1. Zonal Mean Velocity During the January Of 1980 at 250mb Pressure Level 7

2. Geostrophic Flow in Atmosphere Source: Geophysical Flows by Omta.....8

3. . Conservation of Potential Vorticity with Changing Static Stability (Changing Distance between Isentropic *Surfaces)* Source: Dynamic Meteorology by Holton 10

4. . a) PV at 315K Isentropic Surface with Blue Contours Indicating PV Value Less than 1 PVU and Red Contours Indicating Values Greater than 1 PVU B) Geopotential Height Anomaly (Departure from Annual Mean) At 250mb Level with Red Contours Indicating Positive and Blue Contours Indicating Negative *Values*.....10

5. Hovmöller Diagrams of Wave-1 Component of Geopotential Height Anomaly along the Latitude Circle at 60oN, over the Period of December 1, 1979 - March 31, 1980. (a) 30 mb Level, (b) 250 mb Level, (c) 500 mb Level. Contour Intervals are 120 m for 30 mb, and 60 m for 250 and 500 mb. Red and Blue are Positive and Negative, and Zero Contours are in Black. (d) Similar to the Geopotential Height Anomalies but for the Wave-1 Component of the Anomaly of Surface Pressure. Contour Interval is 4 mb. 17

6. A Comparison of the Retrograde-Wave Events Documented in Table 1 of Madden and Speth (1989) and in our Table 1, for 1980-1987. Each Year is Represented by a Pair of Stripes, top from Madden and Speth and Bottom from this Work, that Indicate the Durations of the Events. The Date of the Year is Marked on the Abscissa. Blue Colored Segments Indicate a General Agreement between the Two Catalogs.....18

7. Variation of Zonal Wave-1 Geopotential Height Anomaly at 60oN Latitude with Pressure Level…….....20

Figure Page

8. A Composite of the Wave-1 Geopotential Height Anomalies as a Function of Latitude and Pressure, from the Days Listed in Table 1. It uses Band-Pass Filtered Daily Data at 14 Pressure Levels from 1000 to 30 mb. The Contours are the Amplitude with 25 m Contour Interval. The Relative Phase, Defined as the Phase Difference with Respect to the Reference Value at 60oN, 500 mb, is Shown as Phase Dials. It is Adjusted such that the Dial Points Upward at 60oN, 500 mb, and a Counterclockwise Rotation of the Dial Indicates a Westward Shift of the Ridge or Trough.……20

9. Figure 9. (a) Percentage of Days in a Month that are Identified as Part of a Retrograde-Wave Event in Table 1, Using the Data at 250 mb Level. (b) Similar to (a) But with the Screening of Retrograde-Wave Events Performed at 500 mb. 21

10. (a) Histogram of the Phase of Wave-1 Geopotential Height Anomalies from All Days Listed in Table 1, Using the 250 mb Data. The Phase is Defined as the Longitude where the Maximum (Ridge) of the Wave-1 Component is Located. (b) Similar to (a) But for the 500 mb Level. The Bin Width is 30°. The Abscissa is Essentially Longitude, and the Ordinate is Number of Days that are Sorted into Each Bin.....22

11. The First Two EOFs of the Geopotential Height Anomalies Truncated to Zonal Wavenumber 3, over the Global Domain, using All Days Listed in Table 1. The Calculations are Performed Separately at 30 mb, 250 mb, and 500 mb as Labeled. The Percentage of Variance Explained by the EOF (for the Respective Pressure Level) is also Indicated in Each Panel. Red and Blue Indicate Opposite Signs, and Contour Intervals are Arbitrary. The Abscissa and the Ordinate are Longitude and Latitude as Labeled. 23

Figure Page

12. Similar to Fig. 11, But with the Calculations Performed Using Geopotential Height Anomalies that Contain All Zonal Wavenumbers (Including Zonal Mean) over 20°N-90N° Domain. 24

13. The Projection Coefficients of Daily 250 mb Geopotential Height Anomalies onto the First Two EOFs at that Level as Given in the Middle Row of Fig. 8. Blue and Red are the Coefficients for EOF 1 and EOF2, Respectively. Units are Arbitrary. The Four Panels are for the Winter-Spring Season (November 1-April 30) of 1979-80, 1983-84, 1994-95 and 2010-11 as Labeled. The Dates are Indicated on the Abscissa. 25

14. Maps of Total Potential Vorticity on 315°K Isentropic Surface (Left Column) vs. Band-Pass Filtered 250 mb Geopotential Height Anomaly (right column) for the Sequence of December 23, 24, 26, 27, and 31 of 2010. The Domain Covers 80°E-60°W and 30°N-80°N as Labeled. The Contour Interval for Potential Vorticity is 1 PVU (= 10-6 m2s-1kg-1K), with the Darkest Blue Color Corresponding to the Areas below 1 PVU. The Contour Interval for Geopotential Height Anomalies is 60 m. Red and Blue are Positive and Negative, and Zero Contours are in Black. 28

15. a) Geopotential Height Anomaly Field over Northern Hemisphere (20oN – 90oN) on 7th January 1980 with the Black Semicircle Indicating 60oN Latitude, b) Same as a) on 13th January 1980, c) Solid Black and Red Lines Indicating Line Plots of Non-Fourier Transformed 60oN Geopotential Height Anomaly over the Entire Latitude on 7th and 13th January 1980 Respectively, Dashed Black and Red Lines Indicate Zonal Wavenumber-1 of the 60oN Geopotential Height Anomaly on 7th and 13th January 1980 Respectively. 29

Figure Page

16. Like Figure 14 but for the Sequence of January 3, 6, 7, 8, and 10 of 1980.....30

17. Like Figure 14 but for the Sequence of February 11, 12, 13, 14, and 15 of 1995.....31

18. Number of Days within November 1st to April 30th of Corresponding Seasons Considered to be Within Active Period (satisfying the criteria) with Changing Forecast Lead Time. 37

19. a) Anomaly Correlation, for Each Lead Times, Averaged over All Days (Solid Blue Lines), Active Period (Dashed Red Lines) and Inactive Period (Dot Dashed Yellow Line) between November 1st 1986 and April 30th 1987 Calculating using Geopotential Height Anomaly Field as it is, b) Same as a) but with Geopotential Height Anomaly Field Restricted to Zonal Wavenumber 1&2 c) Same as a) but with Geopotential Height Anomaly Field Restricted to Zonal Wavenumbers 5 to 9. 38

20. Same as Figure 19 but for Period between November 1st, 1994 and April 30th, 1995....39

21. Same as Figure 19 but for Period between November 1st, 1995 and April 30th, 1996....40

22. Same as Figure 19 but for Period between November 1st, 2010 and April 30th, 2011....40

23. 0-16-Day Anomaly Correlations, with 0-Day being the Starting Point Each Day between Nov 1st to April 30th for Years a) 1995-96, b) 2010-11, and c) 2000/01. Red Curves Indicate 0-16-Day Forecasts with 10-Day Anomaly Correlation Value Exceeding 0.6 and the Red Bars on Top are Days of Retrograde Wave Activity Chosen from Table1.....42

24. Distribution of Average Anomaly Correlation between 40^{o}-70^{o} N Along each 10^{o} Longitude Band between 0 -359^{o} E of Greenwich Meridian During the Four Winters Examined. Solid Lines (Red 8-Day and Blue 12-Day Forecast Average) Being Average over Inactive between 1st November and 30th April of Corresponding Winters and Dashed Lines being Average over Active Period of Retrograde Wave Events. 44

25. Anomaly Correlation between Observed and Forecast Geopotential Height Anomaly Field (Considering All Wavenumbers between 40o-70oN) with Forecasts Initialized on Respective Days as Mentioned in the Legend. 45

26. Time Evolution of a) Error Growth (Measured as the Difference in Geopotential Height Anomaly Values between Observation and Forecast) along 60oN Latitude b) Observed Geopotential Height Anomaly along 60o N Latitude Circle and c) Forecast Geopotential Height Anomaly Values along the 60o N Latitude Circle. a) b) and c) are Plotted for Cases where the Forecasts were Initialized Starting 1st, 4th, and 7th February 1995 from Top to Bottom Respectively. Positive Anomalies are Indicated by Red Contours, Negative Anomalies by Blue and Black Lines Denoting the Zero-Contour Level. 45

27. Geopotential Height Anomaly (Within 30^{o}-80^{o}N and 50^{o}-270^{o}E) with Contour Level of 80m Observed on a) 4th February 1995, b) 8th February 1995, and c) 11th February 1995. The Corresponding Forecast Geopotential Height Anomaly for Forecast Initialized on 4th February 1995 Showing d) 0-Day Forecast for 4th February 1995, e) 4-Day Forecast for 8th February 1995, and f) 7-Day Forecast for 11th February 1995. In Each of These

Figure Page

Contour Plots Red Lines Indicate Positive Geopotential Height Anomaly Contours, Blue Lines Indicate Negative Geopotential Height Anomaly Contours and the Black Lines Indicate the Zero-Contour Level. 47

28. Same as Figure 27 but Observed Geopotential Height Anomaly on a) 14th February 1995, b) 17th February 1995 and c) 20th February 1995 Along with Corresponding Forecasts d) 10-Day Forecast for 14th February 1995, e) 13-Day Forecast for 17th February 1995 and f) 16-Day Forecast for 20th February 1995. 47

29. Same as Figure 27 but Observed Geopotential Height Anomaly on a) 23rd December 2010, b) 26th December 2010 and c) 29th December 2010 Along with Corresponding Forecasts d) 10-Day Forecast for 23rd December 2010, e) 13-Day Forecast for 26th December 2010 and f) 16-Day Forecast for 29th December 2010. 48

30. Same as Figure 23 but for Year 1994/95. 49

31. Same as Figure 27 but Observed Geopotential Height Anomaly on a) 12th December 1994, b) 16th December 1994 and c) 19th December 1994 Along with Corresponding Forecasts d) 0-Day Forecast for 12th December 1994, e) 4-Day Forecast for 16th December 1994 and f) 7-Day Forecast for 19th December 1994. 50

32. Same as Figure 27 but Observed Geopotential Height Anomaly on a) 12th December 1994, b) 16th December 1994 and c) 19th December 1994 Along with Corresponding Forecasts d) 0-Day Forecast for 12th December 1994, e) 4-Day Forecast for 16th December 1994 and f) 7-Day Forecast for 19th December 1994. 51

Figure Page

33. Like Figure 26 but for Single 16-Day Forecast Starting 12th December 1994.....52

34. Anomaly Correlation (40o-70oN) Calculated from Seasonal Forecasts with Black Line for a Forecast Starting 1st September 2010 and Red Line for a Forecast Starting 1st October 2010 Calculated at 500hpa Level from Geopotential Height Anomalies at that Level....……54

35. Hovmoller Diagram of Wave-1 Geopotential Height Anomaly at 500hpa level a) for the Forecast Starting 1st September 2010 b) Observation Starting 1st September 2010 with a Contour Interval of 30m Red Lines Indicating Positive Anomaly and Blue Lines Indicating Negative Anomaly. Black Lines Represent the 0-Contour Level. 55

36. Sequence of Potential Vorticity Maps at 315K level on Dates 2nd, 4th, 6th, 8th, 10th, 12th, 14th, 16th, and 18th January 1980. The Domain is between 50oE-270oE and 20oN-80oN. Blue Contours Indicating Contour Levels between 0 and 1 with an Increment of 0.25 and Red Contours Indicating Contour Levels between 1 and 7 with an Increment of 2..... 60

37. Like Figure 36 but on Dates 20th, 22nd, 24th, 26th, 28th, 30th January 1st, 3rd, and 5th February 1980. 61

38. Like Figure 36 but for Sequence of Potential Vorticity Maps at 315K Level on Dates 7th, 9th, 11th,13th,15th,17th, 19th, 21st, and 23rd February 1980. 61

39. Hovmöller Diagrams of Wave-1 Component of Geopotential Height Anomaly Along the Latitude Circle at 60^{o}N (0^{o} - 360^{o}), over the Period of November 1, 1979 – April 30, 1980. The Contour Interval is a) 100m for 30mb, b) 60m for 250mb, c) 40m for 500mb and d) 40m for 1000mb Levels with Red and Blue Being Positive and Negative

Anomalies and Black Indicating the 0-Contour Level. Three Green Lines on January 6, January 28 and February 13, 1980 Indicate Days of Vortex Shedding Occurrence.....62

40. Sequence of Geopotential Height Anomaly Field at 250mb Level During the Days 2nd, 4th, 6th, 8th, 10th, 12th, 14th, 16th, and 18th January 1980. The Red and Blue Contours Denote Positive and Negative Geopotential Height Anomalies with a Contour Level of 100m between Them. The Green Circle Indicates the 60oN Latitude Circle.....63

41. Like Figure 39 but for Duration between a) November 1, 1994 – April 30, 1994 and b) November 1, 2010 – April 30, 2011. The Green Lines are for Days a) December 10, 2010, December 26, 2010 and January 15, 2011, b) January 22, 1995, February 12, 1995, and February 28, 1995 at 500mb *Level.*.....64

42. Like Figure 36 with PV Maps on a) 10th December 2010 b) 26th December 2010, c) 15th January 2011, d) 22nd January 1995, e) 15th February 1995 and f) 28th February 1995.....65

43. Similar to Figure 40 but at 30mb Level Instead 67

44. a) The Change in Averaged 2-m Temperature (Four-Times Daily Averaged for Each Day and Over the Region 115o-120oE and 25o-30oN) Over the Period between January 1st to March 25th 1980 b)Change in the Maximum Value of Four-Times Daily Averaged 1000 Hpa Geopotential Height with the Region 20o-70oN and 50o-150oE during the Same Period..... 69

45. Like Figure 44 but for Period between 1st December 2010 and 23rd Feb 2011.....69

Figure Page

46. Geopotential Height at 1000hpa Pressure Level during Periods Identified to have Cold Air Outbreak on a) 26th January 1980, b) 30th January 1980, c) 14th December 2010, and d) 16th December 2010. Blue Contours Indicating Total Geopotential Height Value Less Than 200m and Red Contours Indicating Values Greater than 200m with Contour Interval of 60m between Each Contour Lines over the Domain between 0o-80oN and 50o-150oE. 70

47. Like Figure 46 but for Days a) 22nd December 2010, b) 25th December 2010, c) 12th January 2011, and d) 15th January 2011. 71

48. 1.1 PVU (10-6 m2s-1K kg-1) Potential Vorticity Contour Line over the Domain 50o-270oE and 20o-80oN) during a) Black Contour – 26th January 1980 and Red Contour - 29th January 1980, b) Black Contour – 12th December 2010 and Red Contour – 15th December 2010, c) Black Contour – 22nd December 2010 and Red Contour – 25th December 2010, and d) Black Contour – 12th January 2011 and Red Contour – 15th January 2011. 73

49. Like Figure 48 but During a) Black Contour – 10th March 1993 and Red Contour - 13th March 1993, b) Black Contour – 14th March 1996 and Red Contour – 17th March 1996, c) Black Contour – 28th March 1996 and Red Contour – 31st March 1996, and d) Black Contour – 9th March 2006 and Red Contour – 12th March 2006. 74

50. Position of low-PV Anomaly Center from the PV Tracking Algorithm during Each Day between 20th January 1980 and 30th January 1980 Along Corresponding Latitude and Longitude. 75

Figure Page

51. Like Figure 50 but for Each Day between 19th December 2010 and 29th December 2010..... 75

52. Like Figure 36 but for Days 23rd, 24th, 25th, 26th, 27th and 28th December 2010 (from Top Left to Bottom Right) with '*' Indicating Tracked Low-PV Centers. 76

53. The Response Functions of the High-Pass (Blue) and Low-Pass (Red) Filters. The Two Dashed Vertical Lines Mark τ = 8 Days and 30 Days. 88

54. Percentage Confidence on the Hypothesis that Datasets Containing Event Day Anomaly Correlations has a Larger Cumulative Distribution Function Compared to the Non-Event Day Anomaly Correlations for Each of the Forecast Lead Times Based on KS and T Statistics with Purple, Red, Yellow and Blue Lines Indicating Periods November 1st to April 30th of 1986-87, 1994-95, 1995-96 and 2010-11 Respectively. 91

CHAPTER 1

INTRODUCTION

Motivation for Study

The idea of predicting a future state of the atmosphere based on current state has its roots traced back to early 20th century when Vilhelm Bjernkes in a paper published in 1904 asserted that if it was true that a subsequent state of the atmosphere developing from a previous state is governed by certain laws of physics then knowing accurately the current state of the atmosphere and the laws that govern this transition to the next state, it is possible for us to predict this subsequent atmospheric state. Using this idea as a basis Richardson made the first ever attempt at weather forecasting while using weather conditions over northern Europe at 4 A.M on 20th May 1910 as initial condition. He computed a six-hour forecast for which he took over two years and the forecast too was found to be inaccurate primarily because the proposed equations were too accurate (Vulpiani, 2014). Uncertainties in forecasts increases over time primarily because of the inability to resolve weather features occurring within the smallest grid size chosen. Even with the improvement in high-speed computing, it still is impossible to resolve such processes due to the lack of observational readings at such small length scales. Thus, most weather models today resort to the use of parametrization to capture the effects of processes like radiation, convection, and cloud microphysics. In light of these ever-present inaccuracies in the initial condition and the non-periodic nature of the atmospheric states, finding accurate solutions for a long-range forecast would be impossible and there exist a limit to the predictability of these atmospheric states proportional to the scale of phenomenon to be predicted (Lorenz, 1963 & 1969). In a

1982 study examining numerical forecast models from the European Centre for Medium Range Weather Forecasts (ECMWF), Lorenz found that skillful forecast over the midlatitudes to be between 7 to 10 days during the northern hemisphere winter. He also theorized that incorporating previously unknown features into the forecast model can help increase lead time for a skillful forecast to about 2 weeks.

In this context, there have been several observational studies that have investigated long lived atmospheric fluctuation patterns in an attempt to understand previously unknown weather features. These long-lived circulations were of specific interest as their propagation were undeterred by instabilities due to small amplitude perturbations which cause upscale error cascading. For example, Madden and Julian (1971) observed a 40-50-day oscillation in the zonal wind component at 850mb and 150mb levels around the tropical region. These oscillations (later called as Madden-Julian Oscillations) are a part of eastward moving large-scale circulation cells (Madden and Julian, 1972) which during a strong event consist of regions of enhanced convective phase aiding rainfall over the region and suppressed convective phase inhibiting rainfall (Rui and Wang, 1990). Due to the nature of the phenomena, it is linked to anomalous rainfall over regions like West Africa (Lavender and Mathews 2009), western North America (Lorenz and Hartman, 2006) and Asia (Lawrence and Webster, 2002). Given the impact it has on a wide range of weather systems they play a major role in medium and extended range weather forecasts. Despite having a great impact on week 3 and week 4 forecasts (Lin et al., 2008) their impact on medium range weather prediction (week 1 to 2) is comparatively less primarily due to its slow propagating nature (Hamill and Khiladis, 2014).

Following the observation of the Madden-Julian Oscillation and armed with increasingly available satellite observation data, several studies attempted to uncover previously unknown long-lived patterns in the atmosphere in other regions as well. A time and spatial spectral analysis done on the 500mb Geopotential Height dataset found that fluctuations of more than 10 days in the northern hemisphere midlatitude winter times were dominated by low frequency westward moving patterns (Blackmon, 1976). A Complex Empirical Orthogonal Function (CEOF) analysis of the 500mb Geopotential Height data performed over the region revealed a global westward travelling feature during the 1979/80 Winter season persisting about 4 months with a period of 23 days (Branstator, 1987). This westward travelling structure was dominated by Zonal Wavenumbers 1 & 2 Fourier components. When Isolating this travelling pattern to the pacific sector of the northern hemisphere, a cycle of increasing and decreasing 500mb geopotential height amplitude lasting 3-4 weeks was observed (Kushnir, 1987). Madden and Speth (1989) based on observation data between 1979-87 tabulated the occurrences of all such major westward propagating event during the period using Zonal Wave-1 component of the 250mb Geopotential Height. However, despite its potential importance in influencing medium range weather prediction over Northern Hemisphere midlatitudes, there has been very little progress with respect to the long-term observational analysis and dynamics of these oscillations beyond these classical observational studies. Still, there have been several follow up studies linking this westward propagating signal to alternating wet and dry periods over California (Mo 1999), onset of Euro-Atlantic blocking (Michelangeli 1997) and East Asian cold air outbreak (Takaya and Nakamura 2005).

With majority of these observational studies speculating their period to be around 3 weeks and with studies linking their presence to some short-term weather events, these westward propagating waves are predicted to heavily influence week-2 weather forecasts (Branstator 1987). They are also among the only known features in the midlatitudes with a period between 7-30 days with the another being atmospheric blocking. With the availability of latest reanalysis data set for over a 40-year period starting 1979 (satellite era beginning) over a much finer grid, it is now possible to perform a long-term observational analysis of this relatively understudied phenomena and use an update list of strong westward propagating (Retrograde Wave) events to study its dynamics and influence on midlatitude predictability.

Given this background, the objective of this study is to try understanding Retrograde Waves and answer some of the key questions in the process like 1) When and where do they occur? 2) Under what conditions does the initiation happen? (Chapter 2) 3) Do they play a role in enhanced week 2 (8-14-day) weather prediction? (Chapter 3) 4) What role do they play in the initiation of some of the extreme weather events in the midlatitudes like East Asian cold air outbreak and blocking? (Chapter 4)

Theoretical Background on Rossby Waves

Conservation of absolute vorticity. To explain the observed variations in pressure over the upper troposphere over midlatitudes, Rossby studied the changes in vorticity purely due to the displacement of an air column across latitudes leading to the theorized existence of large-scale wave patterns.

The starting point for this analysis is the assumption of a homogenous, incompressible atmosphere with purely horizontal motion. Thus, in 2D local coordinates x and y momentum equations are as follows.

$$\frac{\partial u}{\partial t} + u\frac{\partial u}{\partial x} + v\frac{\partial u}{\partial y} = -\frac{1}{\rho}\frac{\partial p}{\partial x} + fv \qquad \textbf{(1)}$$

$$\frac{\partial v}{\partial t} + u\frac{\partial v}{\partial x} + v\frac{\partial v}{\partial y} = -\frac{1}{\rho}\frac{\partial p}{\partial y} - fu \qquad \textbf{(2)}$$

Where $f = 2\Omega \sin\varphi$ comes from the Coriolis force term $2\Omega \times U$. Differentiating equation 1 with respecting to y and equation 2 with respect to x, subtracting 1 from 2 and using the relation of vorticity $\zeta = \frac{\partial v}{\partial x} - \frac{\partial u}{\partial y}$ along the vertical direction we get the following equation after simplification

$$\frac{D}{Dt}(\zeta + f) = -(\zeta + f)\left(\frac{\partial u}{\partial x} + \frac{\partial v}{\partial y}\right) + \frac{1}{\rho^2}\left(\frac{\partial \rho}{\partial x}\frac{\partial p}{\partial y} - \frac{\partial \rho}{\partial y}\frac{\partial p}{\partial x}\right) \qquad \textbf{(3)}$$

The second term of the right-hand side which is the solenoidal term arising from $\nabla p \times \nabla \rho$ becomes 0 under the assumption of barotropic flow. In the first term, which is the divergence term, $\frac{\partial u}{\partial x} + \frac{\partial v}{\partial y} = -\frac{\partial w}{\partial z}$ due to incompressibility. Since a purely horizontal motion is assumed, this term then will be 0. Thus, we would get

$$\frac{D\zeta_a}{Dt} = 0 \qquad \textbf{(4)}$$

Which is the conservation of absolute vorticity following the air parcel where $\zeta_a = \zeta + f$

Rossby Wave dispersion relation. Based on the conservation of absolute vorticity it can be inferred that any air column moving towards higher latitudes will experience a reduction in its vorticity translating to a less cyclonic motion and in contrary air column

towards lower latitudes would mean increased cyclonic motion. Expanding equation 4 we obtain

$$\frac{D\zeta}{Dt} = -v\frac{\partial f}{\partial y} = -\beta v \qquad \textbf{(5)}$$

Where $\beta = \frac{\partial f}{\partial y} = \frac{2\Omega \cos\varphi}{R}$ is the gradient of Coriolis parameter with R being mean radius of the earth.

Assuming a tiny perturbation over the constant zonal mean flow of velocity U with horizontal and vertical velocities u' and v' equation 5 will become

$$\frac{\partial \zeta}{\partial t} + U\frac{\partial \zeta}{\partial x} = -\beta v' \qquad \textbf{(6)}$$

Comparing this to a 1D wave equation with an eastward phase speed of c, propagation speed is derived from equation 6 as

$$c = U - \frac{\beta}{K^2} \qquad \textbf{(7)}$$

With $K = \sqrt{{k_x}^2 + {k_y}^2}$ being horizontal zonal wavenumber, k_x along x direction and k_y along y direction. The phase speed is seen to depend inversely to the square of zonal wavenumber and westward propagation occurs when the term $\frac{\beta}{K^2} > U$.

Geostrophic approximation and Rossby number. When the pressure gradient force in equations 1 and 2 is balanced only by the Coriolis parameter, the x and y component momentum equations are simplified to

$$-\frac{1}{\rho}\frac{\partial p}{\partial x} \approx -fv\,; \qquad -\frac{1}{\rho}\frac{\partial p}{\partial y} \approx fu \tag{8}$$

This is called as geostrophic approximation and a measure of when such an approximation is valid is given by Rossby number which is the ratio of the acceleration term as compared to the Coriolis force term.

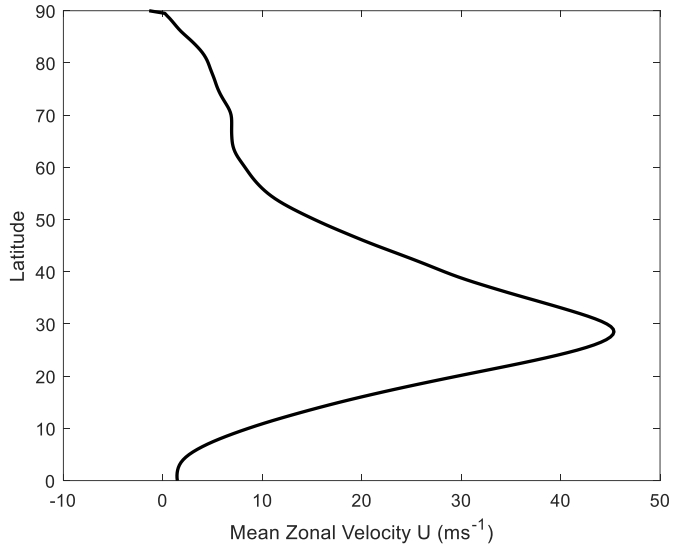

Figure 1. Zonal Mean Velocity During the January Of 1980 at 250mb Pressure Level

$$Ro = \frac{\frac{U^2}{L}}{fU} = \frac{U}{fL} \tag{9}$$

The smaller the value of Rossby number, greater the validity of geostrophic approximation. For example, for a synoptic scale flow within midlatitudes with $L \approx 1000\ km, u \cong v \cong 10\ ms^{-1}\ and\ f \cong\ 10^{-4}$ the value of Rossby number $Ro = 0.1$. However even for large scale flows when moving closer to the equator the value of $f \sim 0$ and thus the value of Ro is much higher.

The extratropic regions around the upper troposphere are characterized by the presence of a strong jet stream due to the north-south temperature gradient especially in

the winter as shown in Figure 1. Any perturbation, especially in the y-direction (as discussed in the previous section) would cause large meandering of these jets since the restoring force in the form of gradient in planetary vorticity grows weaker towards the poles. From Figure 1 we can see that the zonal mean velocity decreases drastically above these jet streams and has an increasing presence of wavelike pattern in the region above (Figure 2). From the relation for phase speed (equation 7) it can be interpreted that under such circumstances, a dominant wave pattern of zonal wavenumber 1-3 would have a greater propensity to travel westward.

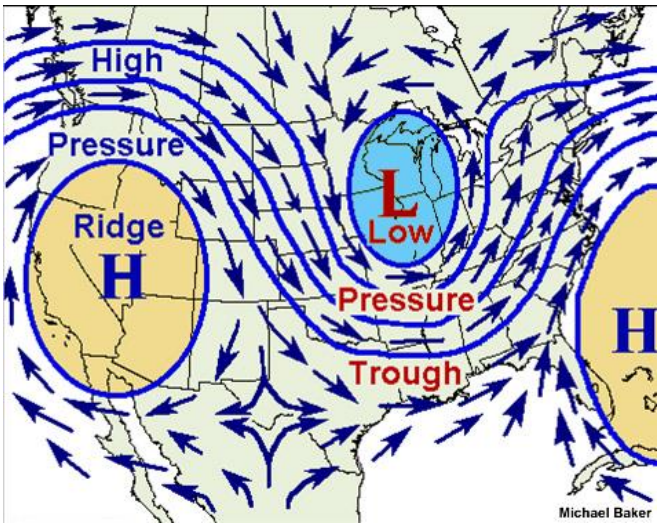

Figure 2. Geostrophic Flow in Atmosphere, Source: Omta, 2020.

Potential Vorticity. Rossby realized that for a barotropic air parcel of depth h, it is possible to derive from equation 3 that

$$\frac{D}{Dt}\left(\frac{\zeta + f}{h}\right) = 0 \qquad \textbf{(10)}$$

Where $\frac{\zeta+f}{h}$ is the barotropic potential vorticity the conservation of which describes creation of vorticity due to the vertical stretching of the vortex tube. Assuming an adiabatic process, this change in depth of the fluid column can be given by hydrostatic approximation $h = -\frac{\delta p}{\rho g}$.

This conserved quantity of barotropic potential vorticity was still an effect of several approximations. Ertel (1942) to include the full three-dimensional frictionless vorticity equation, identified that a similar conserved quantity can be obtained if we use isentropic surfaces as vertical coordinates. The quantity Potential Temperature (θ) which is a constant over isentropic surfaces physically denotes the temperature of the air parcel if it were to be brought to a standard pressure level adiabatically from current pressure level. Thus, taking a scalar product of $\nabla\theta$ with full 3-D vorticity equation to convert it to isentropic coordinate system yields

$$\frac{DP}{Dt} = 0; \quad where\ P = (\zeta_\theta + f)\left(-g\frac{\partial\theta}{\partial p}\right) \tag{11}$$

With P being the isentropic potential vorticity and $\zeta_\theta$being vorticity over an isentropic surface.

Physical understanding of Potential Vorticity. The conservation of potential vorticity can be understood by considering horizontal moving air column bound between two isentropic surfaces (adiabatic motion). Thus, with the change in static stability and increase or decrease of distance between isentropic surfaces, the vorticity either increases (cyclonic) or decreases (anti-cyclonic). This can be seen from Figure 3 which follows the frictionless, adiabatic motion of air parcel along isentropic surface. An example of this in real atmosphere is shown in Figure 4. In the PV map, a positive PV anomaly compared to

the zonal PV value would mean vorticity greater than the planetary vorticity (cyclonic circulation) and while a negative PV anomaly would mean vorticity lesser than planetary vorticity (anti-cyclonic circulation). This is evident upon comparison with the Geopotential height anomaly where-in a positive anomaly would mean a high-pressure and negative anomaly would mean a low-pressure circulation.

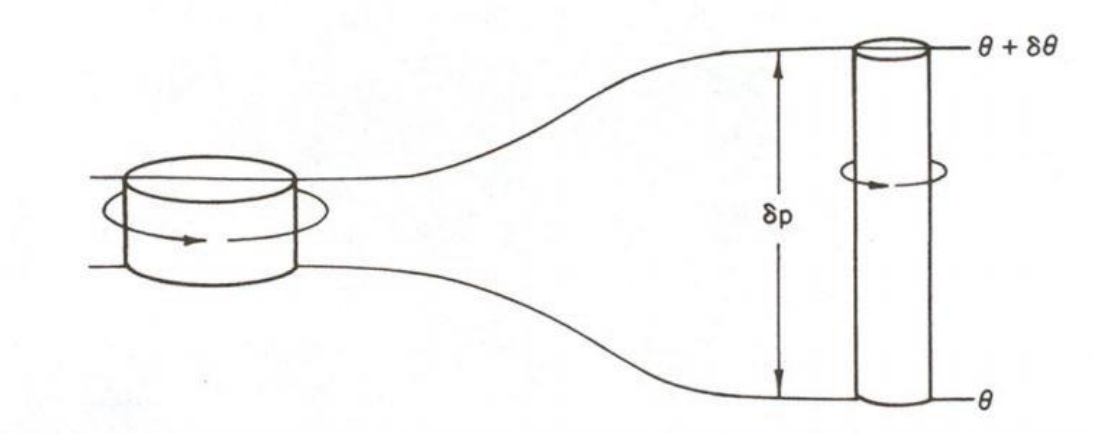

Figure 3. Conservation of Potential Vorticity with Changing Static Stability (Changing Distance between Isentropic Surfaces) Source: Holton, 2013.

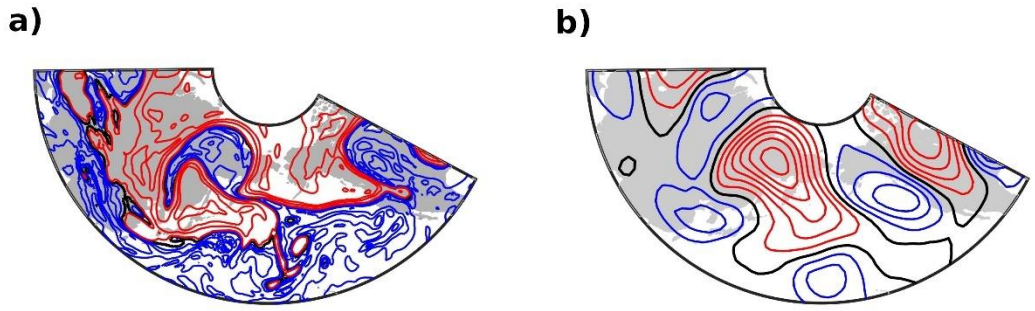

Figure 4. a) PV at 315K Isentropic Surface with Blue Contours Indicating PV Value Less than 1 PVU and Red Contours Indicating Values Greater than 1 PVU B) Geopotential Height Anomaly (Departure from Annual Mean) At 250mb Level with Red Contours Indicating Positive and Blue Contours Indicating Negative Values.

Two Different Approaches in Studying Atmospheric Waves

Studies have traditionally approached the propagation of atmospheric waves from the perspective of linear wave dispersion. For instance, studies by Branstator and Held (1995) and Huang and Robinson (1995) identified westward propagating disturbances to be similar to the leading unstable mode in solving non-linear barotropic vorticity linearized with the assumption of a zonally asymmetric basic state. However, with the increasing availability of daily isentropic PV maps, it is possible to get the full non-linear picture of these waves by analyzing the PV maps instead. For instance, Hoskins (1997) identified that it is possible associate Blocking with poleward moving low PV air which remain stationary as an anti-cyclone, cyclone pair when looking into isentropic PV maps.

Outline for Thesis

The primary goal of this study is to explore the dynamics and predictability associated with westward propagating waves. The first step in this process, presented in Chapter 2, is to identify and update the catalog of major Retrograde wave events between 1979 and 2017 using reanalysis dataset for Geopotential Height. This comprehensive catalog is then used as a basis for recovering the statistics and structure of these waves. A brief look into the dynamics of these waves is also presented based on PV maps during periods of Retrograde Wave activity as identified using the updated catalog. Majority of this work presented in the chapter has already been published in Raghunathan and Huang (2019) including the description of the band-pass filter presented in Appendix A.

Following this in Chapter 3, predictability associated with these waves studied using the periods of Retrograde Wave activity from the updated catalog are presented.

Using global Reforecast dataset for Geopotential Height at 500mb level, predictability is presented in terms of anomaly correlation for four major winters during active and inactive period of Retrograde Wave activity. Following this, individual structures of enhanced predictability during such events are also identified.

Chapter 4 investigates the mechanism for initiation of these Vortex shedding type of structures identified during periods of Retrograde Wave activity in Chapter 2 along with the influence of such evolved structures in triggering a cold air outbreak event over East Asia. The spatial and temporal connection between evolved low PV structures and initiation of cold air outbreak are shown.

Finally, Chapter 5 summarizes the results from the three different studies presented in Chapters 2, 3 and 4 along with possible future directions of research based on results from those studies.

CHAPTER 2

OBSERVATIONAL ANALYSIS OF RETROGRADE WAVES

In this chapter the results from an updated observational analysis of the Northern Hemisphere retrograde disturbances by making use of the available long-term repository of reanalysis data set of over 39-year period. The new catalog of Retrograde Wave events over the course of this 39-year period is established based on a set of criteria delimiting the days that can be considered as event days. This elaborate catalog is then used to extract some basic statistics and spatial and temporal structures of these retrograde disturbances. The catalog is also used to perform some preliminary analysis into the mechanism of retrograde waves by analyzing the isentropic potential vorticity maps over the pacific sector during periods of Retrograde wave activity. A brief discussion is presented on the frequent occurrence of poleward extruding low-PV air mass, westward shift, and vortex-shedding during periods of Retrograde Wave activity.

Using Time Filtered Reanalysis to Identify Retrograde Wave Events

The first step is to identify Retrograde disturbances which manifest as westward propagation in midlatitude Northern Hemispheric geopotential height particularly in low frequencies (Branstator 1987). Madden and Speth (1989) in his analysis used the zonal wavenumber 1 component in Geopotential height anomalies to identify these disturbances. We use a similar framework for our analysis using the ERA-Interim reanalysis dataset (Dee et al 2011) between January 1979 and December 2017 provided

by ECMWF. In particular the four-times daily Geopotential height dataset over a global domain with $2.5^o \times 2.5^o$ resolution at multiple pressure levels is used.

The daily average of this is then found to eliminate diurnal variations. To focus on the submonthly timescale (8-30-day period) which also happens to be the timescale of Retrograde disturbances (Madden and Speth 1989) appropriate time filtering of this reanalysis data is done. As a first step, the annual cycle defined by the annual mean and the first two harmonics (Hsu and Wallace 1976) is identified from the multiyear average of daily geopotential height at each grid point. Mean and the first two wavenumbers from Fourier analysis of the multiyear average, which is the annual cycle, is then subtracted from the daily geopotential height at each grid point to get the daily geopotential height anomaly. Subsequently the data at each grid point is then filtered further using an 8-day low pass filter and a 30-day high pass filter to eliminate variations less than 8 days and more than 30 days. The 8-day low pass filter uses a 30 day running average and the 25-day high pass filter uses a 121 day running average and thus a total of 72 days at the beginning (From January 1st 1979) and end (before December 31st 2017) of the 39-year data is unavailable for analysis.

Event Selection Criteria and the Updated Catalog

The retrograde disturbances noted in the classical observational studies have all been identified to in the midlatitudes of Northern Hemisphere. Madden and Speth (1989) in his analysis to identify these disturbances focused on the 60^o N latitude Zonal Wavenumber 1 component of geopotential height anomaly at the 250mb pressure level. We use this study as a basis for our analysis, defining a unique set of criteria based on the amplitude

and phase of this Zonal Wavenumber 1 component of band pass filtered geopotential height quantity (hereafter referred to as Geopotential Height anomaly). Thus, after computing the Fourier Wavenumber 1 of Geopotential height anomaly at 250mb pressure level around 60^{o} N latitude, the day is chosen as Retrograde Wave event if following conditions are satisfied.

(1) If the 5-day running average of the amplitude of the wave-1 component exceeds the threshold of 60m and the phase of the wave-1 component exhibits westward propagation during the whole 5-day window for averaging, the given day at the center of the 5-day window is said to satisfy the "retrograde-wave condition".

(2) A retrograde-wave event is established if the "retrograde-wave condition" given in (1) is satisfied for at least 8 consecutive days and, further, the crest of the wave-1 Fourier component travels westward by at least half of the latitude circle over the span of the entire event (which could be longer than 8 days).

In contrast to the study by Madden and Speth (1989) which uses a similar condition to identify retrograde waves, this study includes a threshold for amplitude in order to exclude events particularly in boreal summers which may have smaller amplitude considering that these events are less likely to have an impact on predictability or in improving our understanding of retrograde waves. Also, an additional 5-day averaging of amplitude is used to avoid any discontinuity in identifying long episodes due to impact of shorter scale weather events. The summary of all such events between 1979 and 2017 is presented in *Table 1* containing events listed with start date, duration of the event and the average period of wave-1 component during the event.

Table 1

The Retrograde-Wave Events, Organized by Year, as Identified by Criteria (1) and (2) in the Text. Each Event is Described by its Start Date (Month/day), Followed by Duration and Period in Days.

Year	Starting Date (Duration, Period)					
1979	3/15 (15,16)	8/17 (17,19)	11/1 (10,19)	11/14 (16,21)		
1980	1/5 (76,20)	7/25 (29,19)	10/5 (12,17)	10/27 (27,20)	12/3 (11,14)	12/29 (21,14)
1981	1/27 (16,21)	3/11 (31,16)	4/13 (13,15)	5/20 (11,18)	11/23 (26,18)	
1982	1/5 (20,20)	1/30 (36,19)	11/30 (14,17)	12/24 (15,20)		
1983	2/28 (10,13)	5/24 (8,15)				
1984	1/5 (42,21)	2/25 (10,20)	10/13 (12,19)			
1985	1/13 (18,17)	4/11 (21,18)	5/21 (18,17)			
1986	2/22 (20,15)	4/6 (20,22)				
1987	1/20 (16,15)	2/16 (63,19)	9/25 (14,16)	11/4 (10,17)	11/28 (9,17)	12/13 (23,22)
1988	2/10 (14,17)	3/3 (21,16)	4/3 (12,21)	4/27 (13,20)	6/6 (14,22)	10/1 (31,16)
1989	2/21 (30,16)	4/6 (16,20)	6/19 (10,15)	11/20 (16,17)	12/12 (23,20)	
1990	2/11 (19,15)	3/21 (52,18)	11/6 (8,16)			
1991	1/21 (22,19)	4/4 (24,20)	5/26 (8,15)	10/17 (22,19)	11/15 (9,16)	12/15 (13,16)
1992	3/9 (14,16)	5/2 (16,16)	12/6 (20,19)			
1993	1/13 (14,16)	2/16 (39,19)	4/3 (19,16)	5/9 (12,17)	10/7 (11,15)	
1994	2/17 (11,19)	4/3 (19,22)	10/3 (17,18)			
1995	1/18 (59,17)	3/25 (9,13)	4/20 (18,13)	11/8 (9,17)	11/25 (11,18)	12/12 (25,18)
1996	1/26 (28,15)	2/27 (23,22)	3/28 (11,16)	11/15 (17,26)	12/3 (15,19)	12/21 (13,26)
1997	3/4 (15,15)	4/11 (13,12)	10/17 (21,15)	12/12 (8,15)		
1998	2/21 (21,15)	9/18 (13,14)	10/21 (15,18)	12/1 (46,17)		
1999	1/17 (17,18)	3/14 (21,16)	9/17 (14,18)			
2000	3/29 (20,14)					
2001	3/10 (21,19)	4/14 (12,23)	9/18 (15,20)	12/24 (24,22)		
2002	3/24 (20,22)	4/29 (11,18)	7/23 (10,18)	12/12 (16,15)		
2003	1/8 (22,21)	2/26 (23,21)	4/15 (17,17)	10/26 (46,21)		
2004	2/18 (22,17)	11/16	12/28 (18,18)			
2005	2/27 (10,15)	3/19 (17,18)	4/16 (20,17)	10/9 (19,21)	11/14 (20,14)	12/7 (17,15)
2006	1/16 (8,16)	2/19 (13,17)	3/5 (27,17)	5/1 (14,17)	11/27 (11,16)	
2007	1/21 (9,15)	2/6 (28,20)	3/18 (11,16)	4/8 (21,15)	5/17 (9,15)	6/9 (12,14)
2008	1/29 (15,15)	3/17 (18,24)	12/2 (19,15)			
2009	1/14 (13,15)	1/30 (10,18)	3/19 (20,15)	5/18 (18,15)	8/28 (22,17)	9/20 (27,18)
2010	1/17 (23,18)	2/11 (16,23)	3/6 (15,25)	5/26 (10,19)	12/5 (52,18)	
2011	2/3 (29,17)	3/19 (22,17)	11/10 (14,19)	11/30 (9,15)		
2012	1/8 (12,18)	5/3 (9,13)	10/3 (30,18)	12/13 (19,25)		
2013	1/3 (14,20)	3/9 (8,15)	5/13 (8,14)	9/15 (13,15)	10/3 (16,20)	11/14 (11,19)
2014	2/6 (17,22)	3/4 (29,16)	4/27 (12,17)			
2015	1/13 (9,15)	3/11 (19,19)	6/8 (14,17)	9/24 (25,16)		

2016	2/5 (17,23)	3/3 (24,17)	5/6 (17,18)	12/28 (12,15)
2017	1/13 (11,18)	2/4 (26,21)	3/9 (14,21)	4/30 (21,18)

One of the striking episodes of strong retrograde wave activity recovered in *Table 1* is the 76-day event starting 5th January 1980 which has been presented extensively in studies by Branstator (1987) and Madden and Speth (1989). Recent study by Watt-Meyer and Kusner (2015) on decomposition of standing and travelling wave patterns also illustrated a similar picture. The plot of Zonal Wavenumber 1 Geopotential height anomaly at 60° N and at different pressure levels starting from Surface pressure level (1000 mb) to lower stratospheric level (30mb) depicts clearly this retrograde wave propagation (Figure 5) and is also consistent with the one depicted in Madden and Speth (1989).

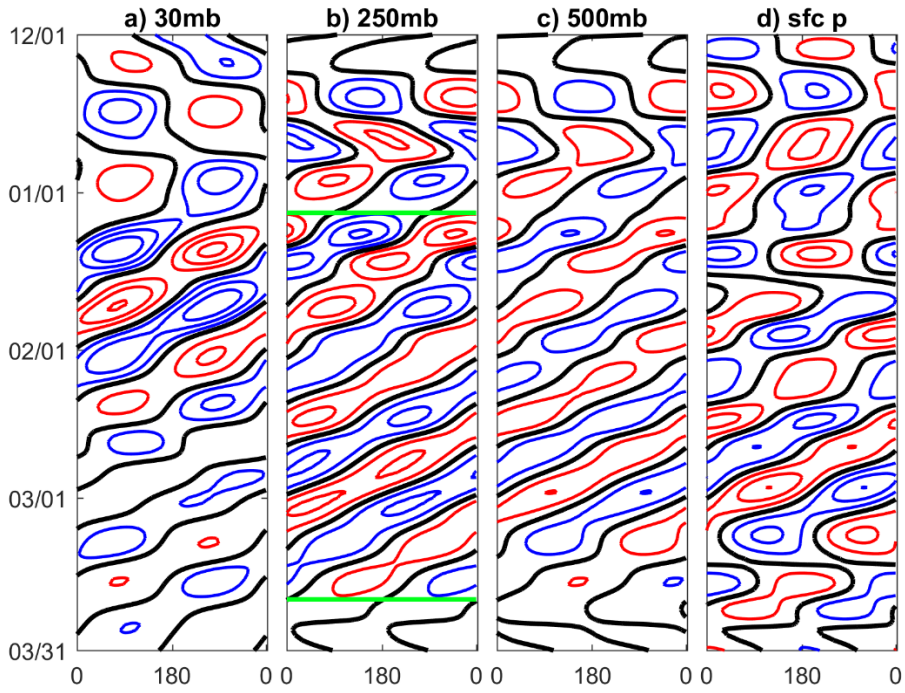

Figure 5. Hovmöller Diagrams of Wave-1 Component of Geopotential Height Anomaly along the Latitude Circle at 60°N, over the Period of December 1, 1979 - March 31, 1980.

(a) 30 mb Level, (b) 250 mb Level, (c) 500 mb Level. Contour Intervals are 120 m for 30 mb, and 60 m for 250 and 500 mb. Red and Blue are Positive and Negative, and Zero Contours are in Black. (d) Similar to the Geopotential Height Anomalies but for the Wave-1 Component of the Anomaly of Surface Pressure. Contour Interval is 4 mb.

A clear barotropic structure of Zonal Wavenumber-1 with amplitude increasing proportionally with increase in pressure levels, as it was proposed by previous studies, can be noted from these plots in Figure 5. The green bars in the plot for 250mb pressure level indicates the time period identified in *Table 1* considered to have Retrograde wave propagation with presence of clear westward phase propagation seen within the green bars.

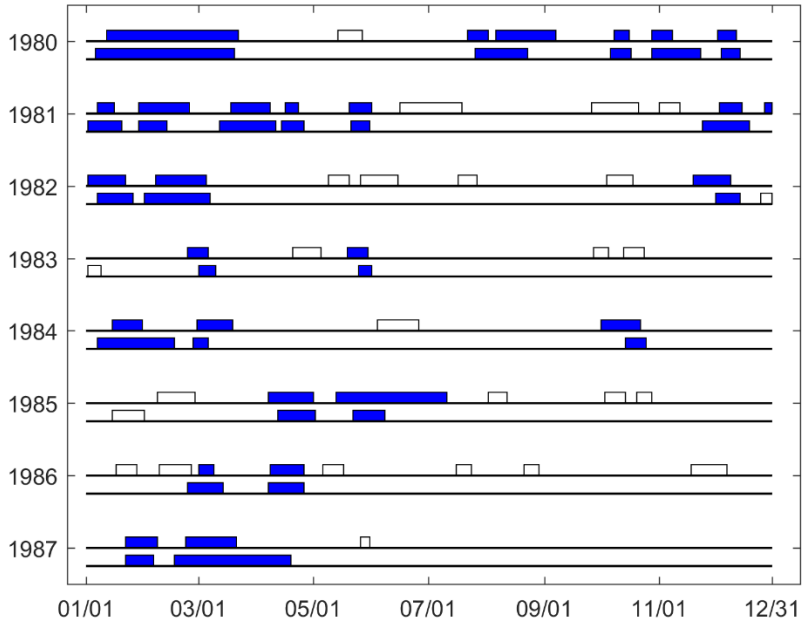

Figure 6. A Comparison of the Retrograde-Wave Events Documented in Table 1 of Madden and Speth (1989) and in our Table 1, for 1980-1987. Each Year is Represented by a Pair of Stripes, top from Madden and Speth and Bottom from this Work, that Indicate the Durations of the Events. The Date of the Year is Marked on the Abscissa. Blue Colored Segments Indicate a General Agreement between the Two Catalogs.

For the most part the events presented in *Table 1* broadly matches with those in a shorter table of events by Madden and Speth (1989). The comparison between the two table is shown in Figure 6 with solid blue color indicting presence of selected events in both the catalog. The mismatch in event between the two catalogs appear in the form of missing events during boreal summer in the new updated catalog presented in this study due to the additional condition on amplitude threshold in order to select an event as discussed in the previous section.

Vertical Structure of Retrograde Waves

Given the equivalent barotropic nature of these events, if we were to pick the events for Table 1 based on a different pressure level, the threshold amplitude chosen would change appropriately depending on the pressure level. Figure 7 shows the average Zonal Wave-1 amplitude of geopotential height anomaly at 60^{o}N for different levels considering all days between 1979 and 2017 which shows how amplitude increases with increase in pressure level all the way to lower stratosphere level of 30mb.

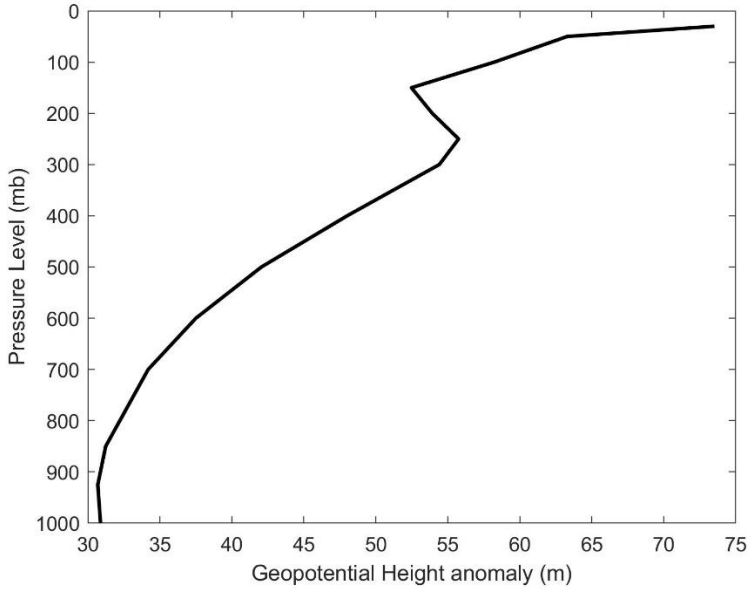

Figure 7. Variation of Zonal Wave-1 Geopotential Height Anomaly at 60°N Latitude with Pressure Level

The equivalent barotropic nature of these waves can be further visualized from Figure 8 showing the vertical structure of these waves using composite of the amplitude and phase relative to that at 60°N, 500mb Zonal Wave-1 geopotential height anomaly at different latitudes and different pressure level. The compositing is done for days picked from Table 1. The figure shows relatively small phase tilt across the pressure levels as it has been noted in the previous studies (Madden and Speth 1989, Branstator 1987).

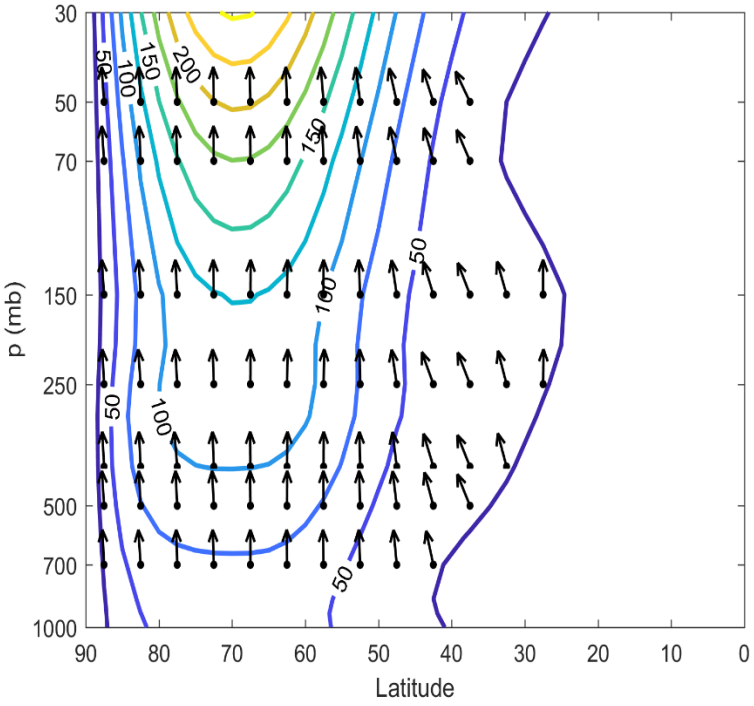

Figure 8. A Composite of the Wave-1 Geopotential Height Anomalies as a Function of Latitude and Pressure, from the Days Listed in Table 1. It uses Band-Pass Filtered Daily Data at 14 Pressure Levels from 1000 to 30 mb. The Contours are the Amplitude with 25 m Contour Interval. The Relative Phase, Defined as the Phase Difference with Respect to the Reference Value at 60°N, 500 mb, is Shown as Phase Dials. It is Adjusted such that the Dial Points Upward at 60°N, 500 mb, and a Counterclockwise Rotation of the Dial Indicates a Westward Shift of the Ridge or Trough.

Statistics and Horizontal Structure of Retrograde Waves

The catalog of event days in Table 1 is used to extract some key statistics on Retrograde Waves. For example, Figure 9 shows the average percentage of days containing Retrograde Wave event in those months at 250mb level (Figure 9a) and from a separate analysis at 500mb level (Figure 9b) with amplitude threshold condition of 50m. It can be seen from these plots that the percentage of events during boreal summer is much smaller compared to the winter months in the northern hemisphere evidently due to small Wave-1 amplitude during the summer months (as noticed by Blackmon 1976). Another statistic that is shown in Figure 10 is the distribution of Phase during periods of Retrograde Wave activity to determine if there is a preferred phase. Like Figure 9, Figure 10 also is plotted at 250mb (Figure 10a) and 500mb (Figure 10b) levels.

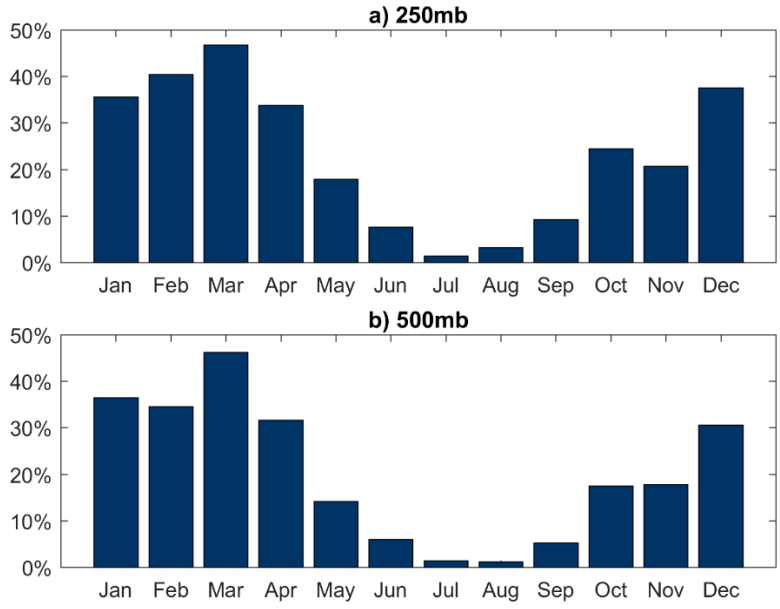

Figure 9. (a) Percentage of Days in a Month that are Identified as Part of a Retrograde-Wave Event in Table 1, Using the Data at 250 mb Level. (b) Similar to (a) But with the Screening of Retrograde-Wave Events Performed at 500 mb.

The distribution of phase is relatively constant since the Wave-1 component propagates westward around the latitude during the periods of Retrograde Wave activity. However, there is still a peak found in the histogram around the pacific sector the reason to which will be discussed in subsequent sections.

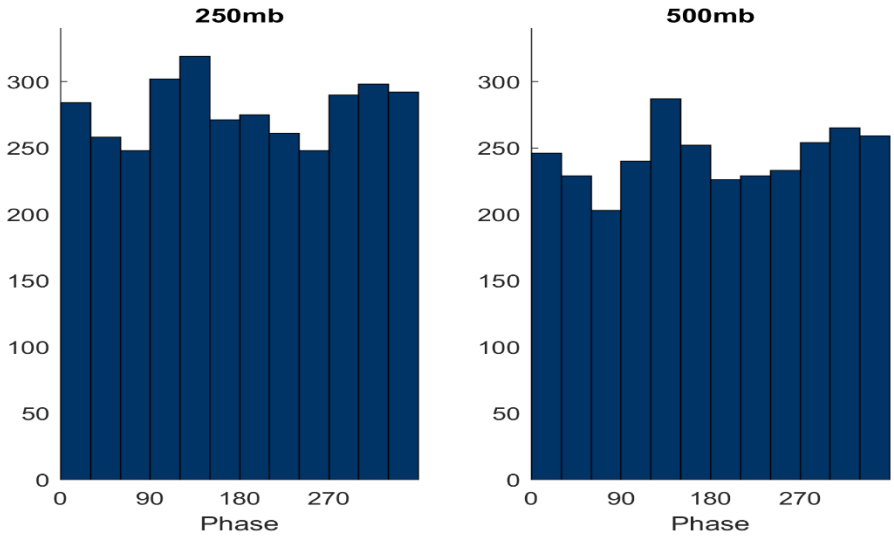

Figure 10. (a) Histogram of the Phase of Wave-1 Geopotential Height Anomalies from All Days Listed in Table 1, Using the 250 mb Data. The Phase is Defined as the Longitude where the Maximum (Ridge) of the Wave-1 Component is Located. (b) Similar to (a) But for the 500 mb Level. The Bin Width is 30°. The Abscissa is Essentially Longitude, and the Ordinate is Number of Days that are Sorted into Each Bin.

An Empirical Orthogonal Function (EOF) analysis, which is done to extract dominant spatial features during periods selected, is performed on days of Retrograde Wave activity listed in Table 1. For this analysis we use two different datasets, one containing global domain of Geopotential Height anomaly with Zonal Fourier components restricted to Wavenumber 1, 2 and 3 the results of which is shown in Figure 11. The other retaining all the Zonal Fourier components including the Zonal mean value but on the Northern Hemisphere domain between 20^{o}N and 90^{o}N is shown in Figure 12. Each of these

analyses is done at 3 different levels (30mb, 250mb and 500mb) and the grid points are area weighted with the square root of cosine of the latitude multiplied to the grid points in those corresponding latitudes. Each figure contains the percentage of variance explained by those corresponding EOFs at the top the individual plots. A common phase quadrature between EOF 1 and EOF 2 is seen across Figure 11 and Figure 12. Since the EOFs are orthogonal to each other, any phase quadrature between them is indicative of a propagating feature. Also as evidenced from the vertical structure, the equivalent barotropic behavior is evident in these EOFs as well with dominant structure restricted to Zonal Wavenumber-1 feature in the stratosphere (30mb) level as compared to a possible Zonal Wavenumber-2 features existing in the middle-upper troposphere level (500mb and 250mb). This result is consistent with the one obtained by Branstator (1987) in their analysis.

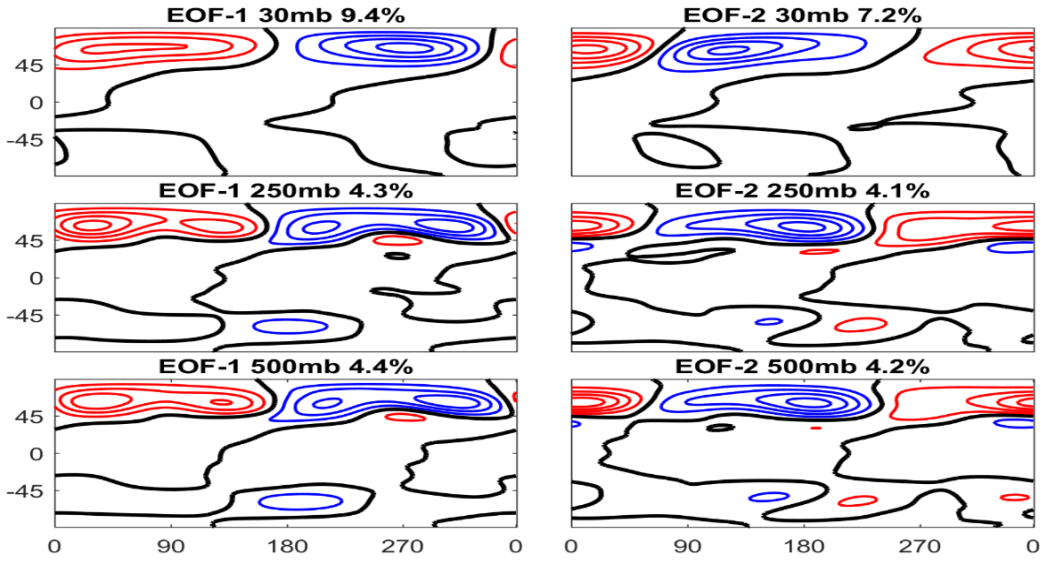

Figure 11. The First Two EOFs of the Geopotential Height Anomalies Truncated to Zonal Wavenumber 3, over the Global Domain, using All Days Listed in Table 1. The Calculations are Performed Separately at 30 mb, 250 mb, and 500 mb as Labeled. The Percentage of Variance Explained by the EOF (for the Respective Pressure Level) is also

Indicated in Each Panel. Red and Blue Indicate Opposite Signs, and Contour Intervals are Arbitrary. The Abscissa and the Ordinate are Longitude and Latitude as Labeled.

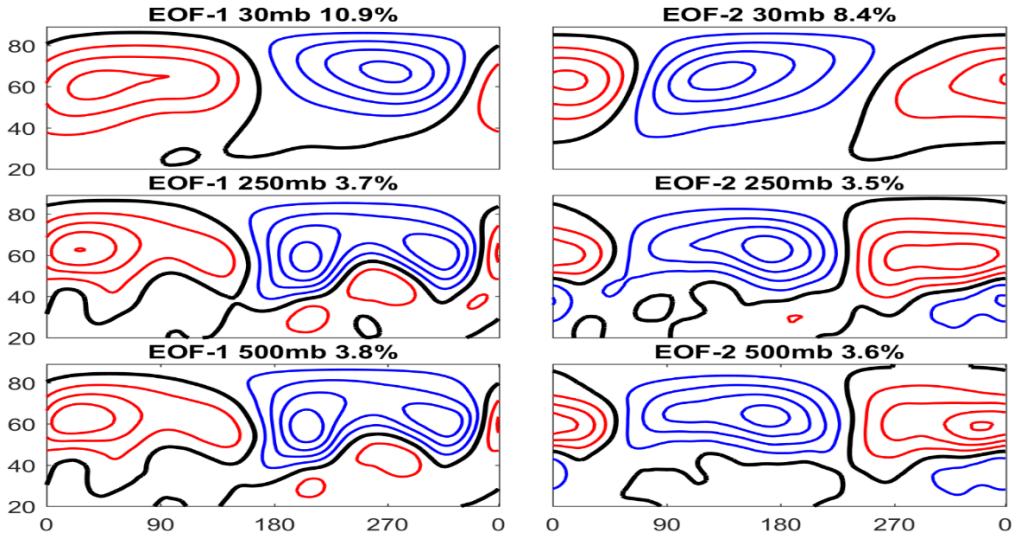

Figure 12. Similar to Fig. 11, But with the Calculations Performed Using Geopotential Height Anomalies that Contain All Zonal Wavenumbers (Including Zonal Mean) over 20°N-90N° Domain.

The study by Speth et al. (1992) on Retrograde waves in southern hemisphere noted the non-existence of any correspondence between Retrograde waves in the northern and the southern hemisphere. This seems to be the case from the global domain EOF analysis in Figure 11 showing how northern hemispheric feature is mostly dominant.

The phase quadrature seen in the composites can be more clearly spotted in Figure 13 that shows the time evolution of projection coefficients upon projecting the geopotential height anomalies onto the EOFs 1 and 2 shown by blue and red lines respectively in the figure. The time evolution plot is made for four different winters (1979/80, 1983/84, 1994/95 and 2010/11) with each panel showing projection coefficient for one winter between Nov 1st and April 30th and the periods of retrograde wave activity marked by a red bar over these plots. The EOFs 1 and 2 chosen for this analysis is obtained from

analysis over 20°N-90°N domain with Zonal Fourier components restricted to Wavenumber 1,2 and 3.

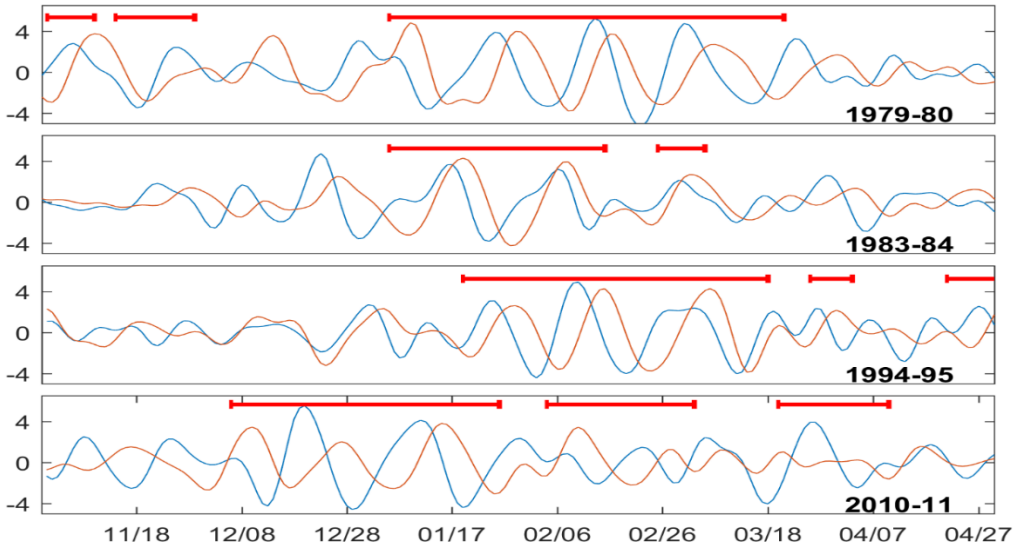

Figure 13. The Projection Coefficients of Daily 250 mb Geopotential Height Anomalies onto the First Two EOFs at that Level as Given in the Middle Row of Fig. 8. Blue and Red are the Coefficients for EOF 1 and EOF2, Respectively. Units are Arbitrary. The Four Panels are for the Winter-Spring Season (November 1-April 30) of 1979-80, 1983-84, 1994-95 and 2010-11 as Labeled. The Dates are Indicated on the Abscissa.

Potential Vorticity Picture and Vortex Shedding

Despite the lack of comprehensive studies into dynamics of submonthly Retrograde waves, there have been few previous studies that have attempted to explain its mechanism. For instance, the studies by Branstator and Held (1995) and Huang and Robinson (1995) revealed that Retrograde waves result from the leading unstable mode upon imposing a zonally asymmetric basic state on to the barotropic vorticity equation. Huang and Robinson (1995) went further to indicate the possible point of origin to be around the jet exit region which would serve as an energy source for generating these waves. Lau and Nath (1999) speculated that the dynamics of these waves were governed

by the Rossby wave dynamics with a dominating β effect in the midlatitudes and consequent weak mean flow leading to a westward propagation. Mo (1999) related the 22-day mode westward propagating mode found in his analysis to tropical connection. Polvani et al. (1999) in examining westerly flow response to shallow water simulation with a localized mountain, presented the resulting stream function and potential vorticity fields from their simulation. One of their results revealed a pattern of poleward extruding low-PV air which undergoes westward shift and vortex shedding upon entering the higher latitudes. This result, even though is based only on numerical simulation, motivates us into looking at the Retrograde waves from a Potential Vorticity standpoint as it could help change the perspective of this phenomenon as relating to wave breaking and vortex shedding rather than viewing it from a traditional Rossby wave point of view. It is also noted that great improvements in our understanding of large-scale dynamics is possible with the usage of isentropic potential vorticity to study these waves (McIntyre and Palmer 1983).

For this part of the study Isentropic potential vorticity data obtained from ERA-Interim archive is used. From a brief calculation of Potential Temperature over 60^{o} N during winter period using values of average temperature during the period and at 250 mb pressure level is done using the following relation

$$\theta = T\left(\frac{P_0}{P}\right)^k \qquad \textbf{(12)}$$

With T being Temperature at current pressure level, P_0 the standard pressure level (1000 mb), P the current pressure level and $k = \frac{R}{c_p}$ for dry air.

The Potential Temperature value at 250 mb pressure level was found to be around 315K during winter period and approximately 330 K during the summer months of Northern Hemisphere at around 60^{o}N. Table 2 contains pressure levels corresponding to the potential temperature values during the corresponding months. The unfiltered Potential Vorticity data at 315K is mainly used.

Table 2

Pressure Value Corresponding to Potential Temperature Levels - Based on Average of Monthly Mean Temperature over Pacific Region (Between 160^{o} E and 160^{o} W at 60^{o} N Latitude Circle)

Month	Potential Temperature (in K)	Pressure (in mb)
Jan-80	315	260
Feb-80	315	261
Mar-80	315	277
Apr-80	330	240
May-80	330	251
Jun-80	330	258
Jul-80	330	259
Aug-80	330	252
Sep-80	330	244
Oct-80	330	242
Nov-80	315	277
Dec-80	315	266

A comparison of Daily total PV with the bandpass filtered daily Geopotential Height anomaly presented as a sequence during 23rd, 24th, 26th, 27th, 31st December 2011 which was the part of a major retrograde wave event from Table 1 starting December 5th, 2011 for a period of 52 days is shown in Figure 14. The pattern of slow westward propagation of positive geopotential height anomaly that can be noted in these plots is seen to be translated to a extruding low-PV air to higher latitudes, followed by a

westward shift and eventual shedding of the westward shifting vortex. It is also to be noted that the point of origin of this low-PV extrusion as seen from the PV map is around the international date line where a slight peak in the phase distribution was noted in Figure 10.

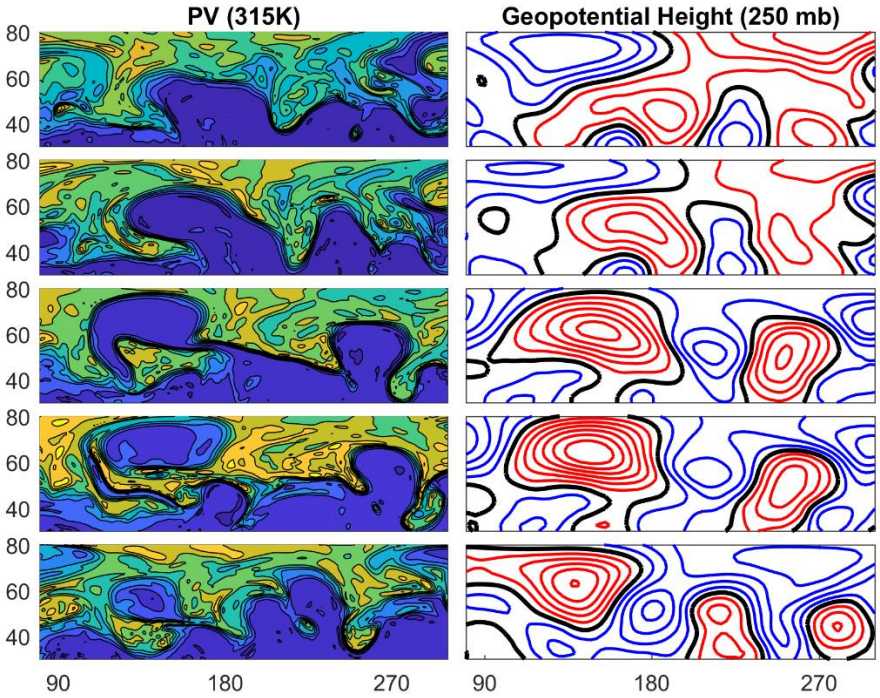

Figure 14. Maps of Total Potential Vorticity on 315°K Isentropic Surface (Left Column) vs. Band-Pass Filtered 250 mb Geopotential Height Anomaly (right column) for the Sequence of December 23, 24, 26, 27, and 31 of 2010. The Domain Covers 80°E-60°W and 30°N-80°N as Labeled. The Contour Interval for Potential Vorticity is 1 PVU (= 10^{-6} $m^2s^{-1}kg^{-1}K$), with the Darkest Blue Color Corresponding to the Areas below 1 PVU. The Contour Interval for Geopotential Height Anomalies is 60 m. Red and Blue are Positive and Negative, and Zero Contours are in Black.

As per our discussion into the physical understanding of Potential Vorticity in section 1.2.5, we know that a negative PV anomaly as compared to the zonal PV would indicate an anti-cyclonic circulation as is the case with a positive Geopotential height anomaly. This way we can understand how a small westward shifting low PV signal could translate into global Zonal Wave-1 westward propagation which is also explained

in Figure 15 where it can be noted that a westward shift in the peak of non-Fourier transformed Geopotential height anomaly of around 50^{o} in longitude translates to a westward movement in phase of Wave-1 Geopotential Height anomaly of about 130^{o} over a period of 6-days.

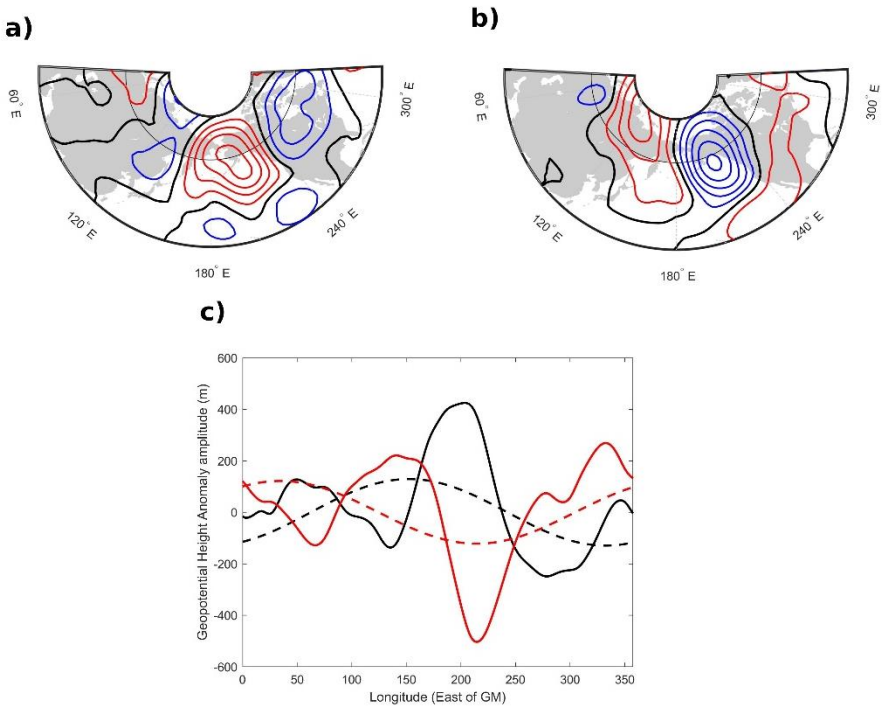

Figure 15. a) Geopotential Height Anomaly Field over Northern Hemisphere (20^{o}N – 90^{o}N) on 7th January 1980 with the Black Semicircle Indicating 60^{o}N Latitude, b) Same as a) on 13th January 1980, c) Solid Black and Red Lines Indicating Line Plots of Non-Fourier Transformed 60^{o}N Geopotential Height Anomaly over the Entire Latitude on 7th and 13th January 1980 Respectively, Dashed Black and Red Lines Indicate Zonal Wavenumber-1 of the 60^{o}N Geopotential Height Anomaly on 7th and 13th January 1980 Respectively.

A comparison like the one done in Figure 14, a different sequence of PV and Geopotential Height anomaly field are shown in Figure 16 for the days between 3rd and 10th January 1980 belonging to the strong Retrograde Wave activity during the winter of 1979/80. The sequence displays a similarity with the one seen in Figure 14 with a hint of separating vortex over the higher latitude seen around the 10th January 1980. Figure 17

shows the sequence for another event in February 1995 during a similarly strong Retrograde wave activity. Thus, the commonality across these different sequences is the (1) Poleward extrusion of low PV air into higher latitudes followed by (2) a slight westward shift and vortex shedding of this low PV air.

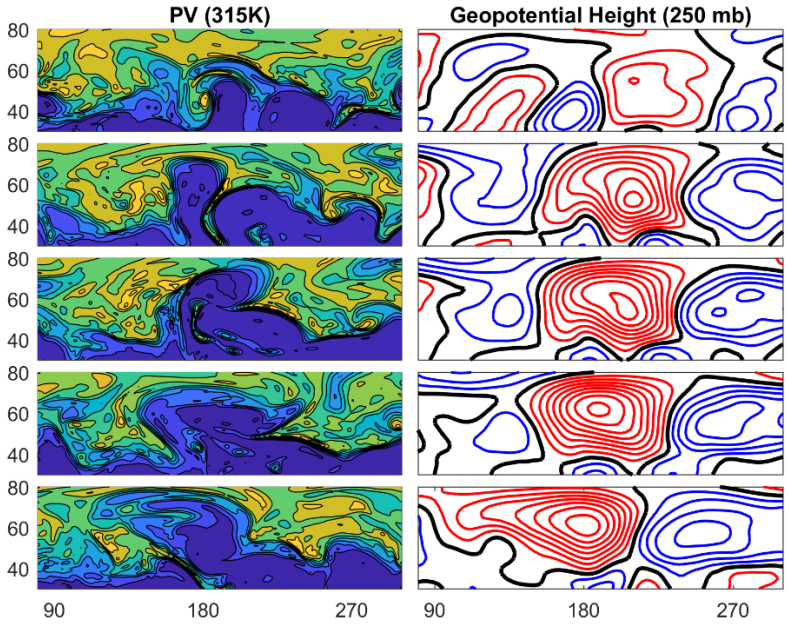

Figure 16. Like Figure 14 but for the Sequence of January 3, 6, 7, 8, and 10 of 1980.

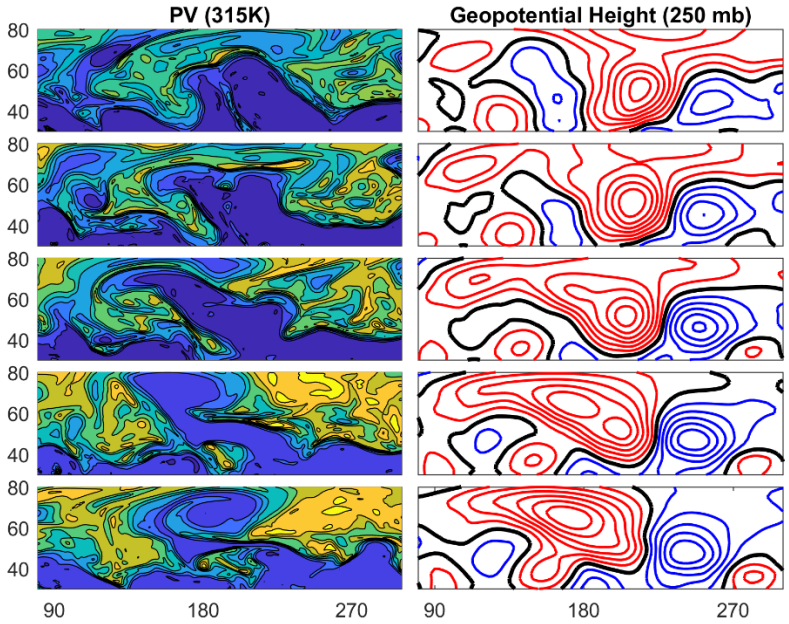

Figure 17. Like Figure 14 but for the Sequence of February 11, 12, 13, 14, and 15 of 1995.

Summary and Future Work

The primary aim of producing a new updated catalog of Retrograde Wave events and using this extended catalog of events spanning 39 years to reexamine the statistics, horizontal and vertical structure of these waves is accomplished. Through this analysis it was established that the statistics and structure of Retrograde waves for the most parts matches were consistent with those presented in classical studies. As an example of usefulness of this new updated catalog in examining the wave dynamics, a brief analysis based on the evolution Potential Vorticity structures during specific periods of Retrograde propagation is presented linking them to wave breaking and vortex shedding.

These prospective links warrant a deeper study into these Potential Vorticity structures in understanding their role in influencing some commonly observed weather events in the midlatitudes like blocking, East Asian cold air outbreak etc. For instance, Hoskins (1997) in examining the evolution of PV during episodes of blocking identified similar poleward extruding low PV structures which however remained stationary over the Euro-Atlantic region. Similarly, in a study on persistent anomalies over Northern Hemisphere. Miller et al. (2019) identified hint of northward shift in positive anomalies over the pacific sector. There have also been studies linking Westward travelling upper-tropospheric anti-cyclonic disturbances to East Asian cold air outbreak (Takaya and Nakamura 2005) which will be looking into in more detail in Chapter 4.

Another paradigm where the new catalog can be put to use is in investigating the influence of Retrograde waves on extended-range weather prediction. Chapter 3

discusses in detail the extent to which this influence is present while examining predictability using the 33 years reforecast during overlapping periods of Retrograde wave activity.

CHAPTER 3

PREDICTABILITY ASSOCIATED WITH RETROGRADE WAVE DISTURBANCES

Guided by the newly created catalog of Retrograde Wave events introduced in the previous chapter, the aim of the work presented in this chapter is to explore the presence of increased predictability during active period of retrograde wave propagation. Using reforecast dataset and quantifying predictability based on correlation between Observation and n-day forecast comparison is done between periods of active and inactive retrograde wave activity during some of the winter with strong retrograde wave events. Individual forecasts with increased predictability are presented highlighting structures that are preserved in these forecasts during active period.

Introduction

The potential influence of large-amplitude retrograde waves on extended-range weather prediction despite having been proposed by the classical studies (Branstator 1987) have not been explored further. With the proposed theoretical predictability limit for midlatitude being around two weeks during Northern hemisphere winters (Lorenz 1969) and the potential for improvement in this predictability limit with incorporation of previously unknown features in atmosphere (Lorenz 1982), the need to study its influence becomes exacerbated. Evidences from past studies on increasing this predictability limit have pointed towards such low frequency temporal variations having a period of predictability proportional to their time scale (Vandendool and Saha 1989). With retrograde wave events having a period of around three weeks which extends well into

Week-2 region past the two-week predictability limit mark, their influence becomes worthy of being explored into.

Though not aplenty, there has been some evidence from previous studies suggesting the influence of Retrograde Waves in increasing predictability. For instance, Zang et al. (2017) in exploring predictability of midlatitude weather identified a slow error westward travelling error growth as compared to rapidly developing error signals related to eastward propagating baroclinic wave packets. Stan and Krishnamurthi (2019) identified submonthly oscillations with a 28-day period resembling Retrograde Waves which upon being used in a statistical model to predict 2-m temperature increased the predictability to up to 20 days. Given the worthiness of exploring the problem as suggested by literature and guided by the availability of a long-term catalog of Retrograde Waves event from Chapter 2, it will be useful to investigate the skill of forecast during active period of Retrograde wavs event as compared to inactive period.

Reforecast Dataset and Processing

Evaluation of predictability during active periods can be done by analyzing past forecasts available as Reforecast datasets. In specific, we use the NOAA GEFS Reforecast II dataset containing the 11-members ensemble mean values of global Geopotential Height data at 500 mb level over a grid of $1^o \times 1^o$. Each of these daily datasets between 1st December 1984 and 31st December 2017 containing 0-16day forecasts (0hr, 24hr, 48hr… etc.) with the 0-day forecast (0hr) considered to be observation for that day were used for this analysis. The first 8 days forecasts (0hrs – 192hrs forecast) the models were run at a T254L42 resolution which corresponds to approximately 40 km at 40^oN and from day 7.5 the models are run at T190L42 resolution

which corresponds to approximately 54 km at 40^{o}N which is then stored from day 8 to day 16 (186hrs – 384hrs). In our case we used the High-resolution dataset from 0 to 8-day forecasts (0-192hrs) and Low-resolution dataset from 9-day to 16-day forecasts (216hrs – 384hrs) (Hamill et al 2013).

As a further step in processing this dataset, the mean climatological cycle, in this case considered to be the mean and first three wavenumbers from the Fourier analysis of multiyear average, is subtracted from each grid point Geopotential Height data to obtain the Geopotential Height anomaly field. This step is performed individually to each of the forecasts (0-16-day forecasts) separately calculating mean climatology for each of those forecasts separately. For example, in order to obtain 3-day forecast climatology at a certain grid point, first 3-day forecast for each day between January 1st 1985 till December 31st 2017 is isolated (72hr forecast on December 29th 1984 would be the 3-day forecast for January 1st 1980). A multiyear average to obtain annual cycle and Fourier mean and Wavenumbers 1-3 of this annual mean is subtracted from these accumulated 3-day forecasts to obtain 3-day forecast Geopotential Height anomaly field. This way any model biases in these forecasts are eliminated.

The skill of these forecasts can be evaluated by calculating the Anomaly Correlation (AC) which is a scalar quantity indicative of the similarity between Observed Geopotential Height anomaly field and the corresponding forecast. It can be found using the following relation.

$$AC = \frac{\sum O'F'}{\sqrt{\sum O'^2 \sum F'^2}} \quad \textbf{(13)}$$

Where O' is the Observation anomaly which in this case is the 0hrs forecast for the particular and F' is the Forecast anomaly for the day. Summation is done over every grid point which in this study is chosen to be all the longitude grid points within 40°N – 70°N. A forecast is considered skillful if this value of Anomaly Correlation is greater than 0.6 (Hollingsworth et al. 1980).

Winters with Major Retrograde Wave Activity

Four winters with each containing dominant retrograde activity are chosen and the Anomaly Correlation is calculated between observation and each n-day forecast (0-16day) geopotential height anomaly of all the days from November 1st to April 30th. The Anomaly Correlations are then averaged over these periods separately for each of these n-day forecasts resulting in a relation between the averaged Anomaly Correlation and the forecast lead time.

This procedure is performed separately picking only those days chosen to be within active period which is based on Table 1. A given day is chosen to have active retrograde wave activity if all the days between the day the forecast was made and the day the forecast is for (which is the current day) are within the catalog events in Table 1. For example, if say January 20th is to be chosen as an active period while calculating averaged Anomaly Correlations for 9-day forecasts, then there must be a Retrograde Wave event encompassing all the days between January 11th (day the 9-day forecast was made) and January 20th (day the 9-day forecast is for). Any day that does not satisfy this criterion is considered inactive period of Retrograde Wave activity. As it can be noted,

number of days chosen within active period would then vary with forecast lead time and Figure 18 gives the number of days chosen to as active period as a function of forecast lead time for the four major winter months analyzed (1986/87, 1994/95, 1995/96, 2010/11).

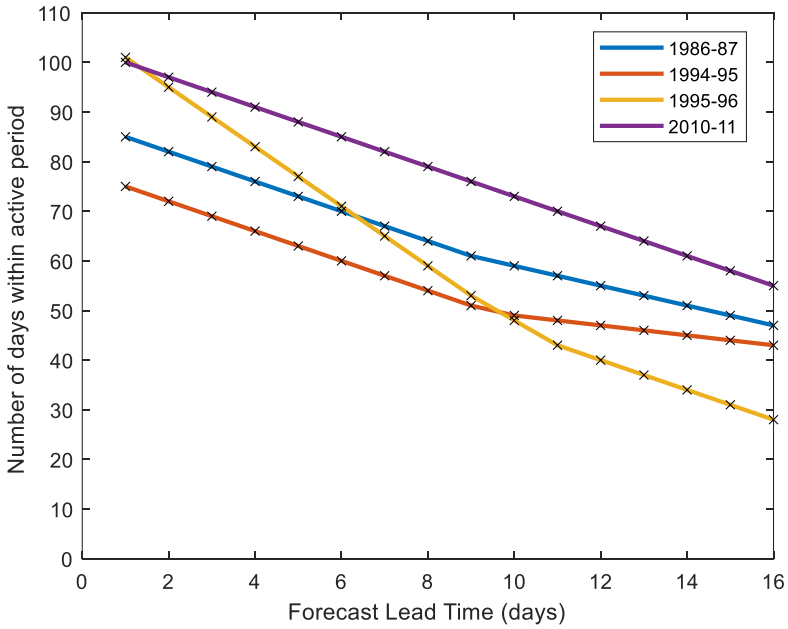

Figure 18. Number of Days within November 1st to April 30th of Corresponding Seasons Considered to be Within Active Period (satisfying the criteria) with Changing Forecast Lead Time.

Each of the three panels in Figure 19 through Figure 22 show the averaged Anomaly Correlation during all days (solid blue line), Active period (dashed red lines) and inactive period (dot dashed yellow lines). Calculations performed on the Geopotential Height anomaly field (observation and forecast) as it is shown in the first panel, calculations performed on Geopotential Height anomaly field truncated to Zonal Wavenumbers 1 & 2 shown in the second panel and those performed on Geopotential Height anomaly field truncated to Zonal Wavenumbers 5 to 9 in the third panel. The idea is to examine predictability of long waves (Zonal Wavenumber 1&2) and short waves

(Zonal Wavenumber 5 to 9) separately to see if there is any correspondence between the two.

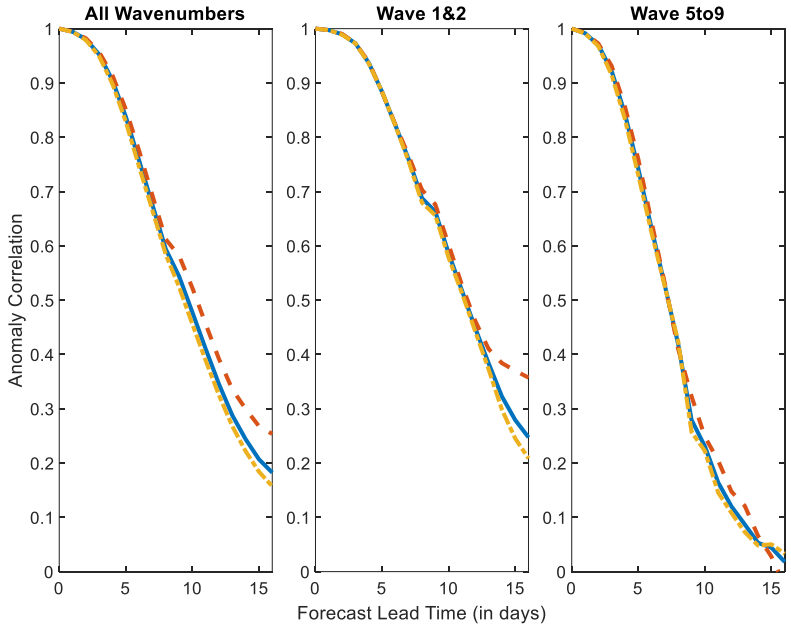

Figure 19. a) Anomaly Correlation, for Each Lead Times, Averaged over All Days (Solid Blue Lines), Active Period (Dashed Red Lines) and Inactive Period (Dot Dashed Yellow Line) between November 1st 1986 and April 30th 1987 Calculating using Geopotential Height Anomaly Field as it is, b) Same as a) but with Geopotential Height Anomaly Field Restricted to Zonal Wavenumber 1&2 c) Same as a) but with Geopotential Height Anomaly Field Restricted to Zonal Wavenumbers 5 to 9.

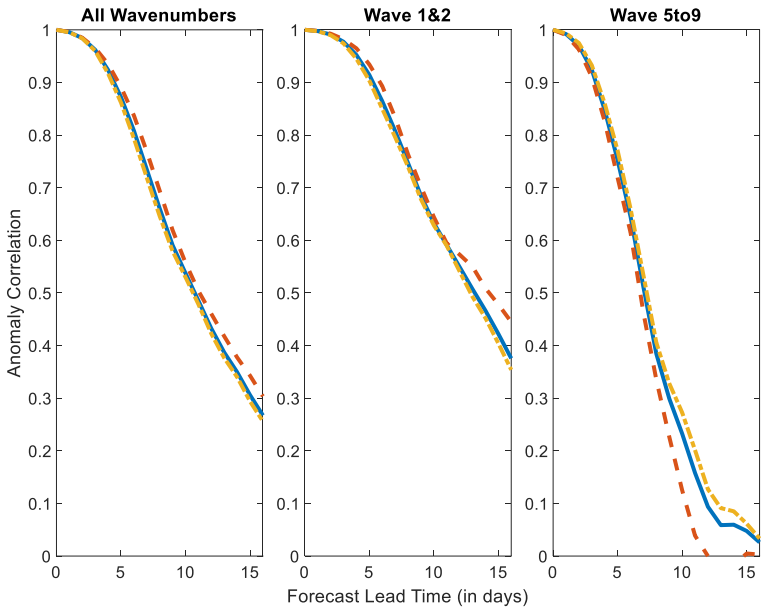

Figure 20. Same as Figure 19 but for Period between November 1st, 1994 and April 30th, 1995.

The results indicate increased averaged Anomaly Correlation value during active period as compared to the inactive period during all the four winter when considering the all wavenumbers case (unrestricted Geopotential Height anomaly field) and the Zonal Wavenumbers 1& 2 case. However, no such pattern can be discerned for the case with restriction of Zonal Wavenumbers 5 to 9. Despite the noticeable trend of increased Anomaly Correlation during active period as compared to inactive period, the net increase in the value is not uniform across the episodes. A possible explanation is the presence of other phenomena occurring outside the active period not picked up in Table 1 which may contribute to increase predictability. For example, Bian He (2018) in studying persistent maxima reported an increase in predictability by about 1 day during these events. A more detailed argument with a case study is presented in the upcoming section.

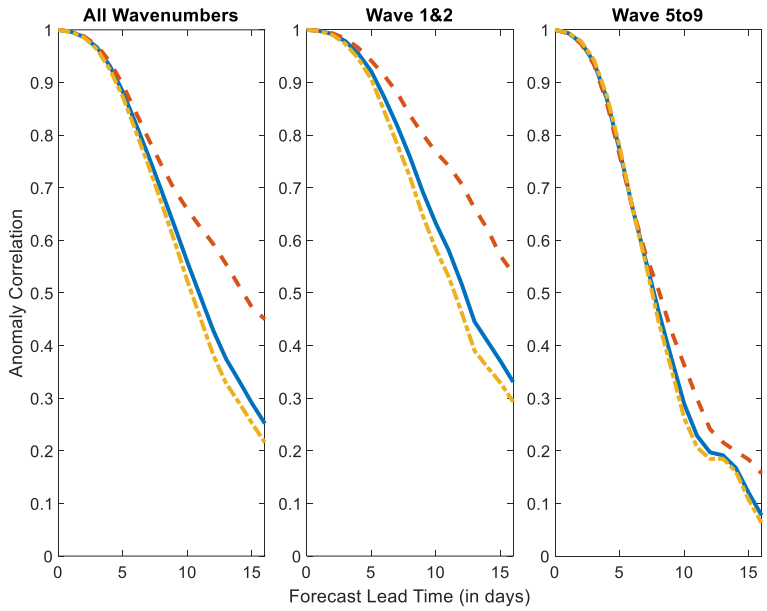

Figure 21. Same as Figure 19 but for Period between November 1st, 1995 and April 30th, 1996.

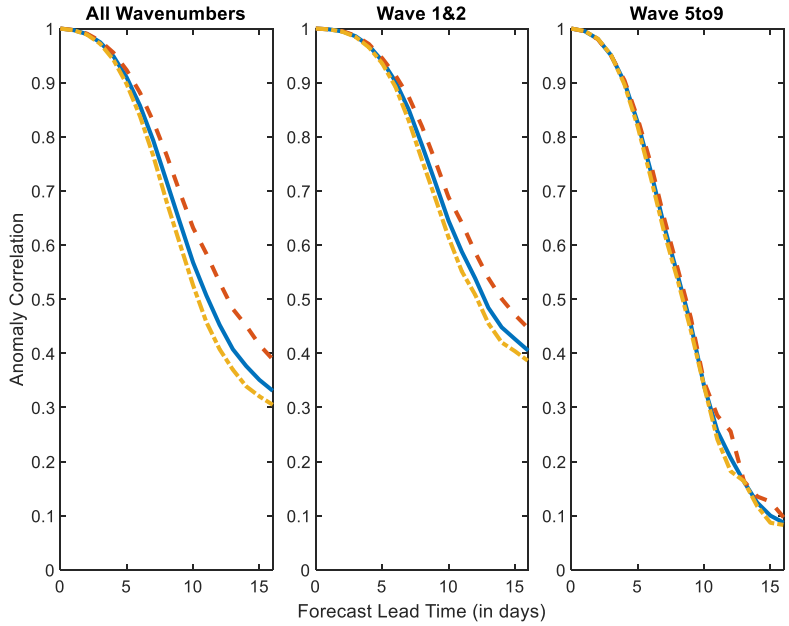

Figure 22. Same as Figure 19 but for Period between November 1st, 2010 and April 30th, 2011.

The 1995/96 winter along with 2010/11 winter stand out with significant increase in averaged anomaly correlation noted during active period as compared to inactive period. The increased predictability during active period of 1995/96 winter seems to be spread across both long waves (Zonal Wavenumbers 1&2) and short waves (Zonal Wavenumbers 5 to 9). For this case over the midlatitudes, the average lead time for a skillful forecast during Active period is around 12 days in contrast to a 9-day lead time for skillful forecast during inactive period. A similar increased lead time for skillful forecast is noted during active period of 2010/11 winter as well. Two sample statistical test between active period and inactive period Anomaly Correlation values prove with more 95% significance that the two sample belong to different distributions. Result are shown in detail in the Appendix.

The daily 0-16-day forecast Anomaly Correlation during for forecasts made each day between November 1st and April 30th for different winters is shown in Figure 23 with curves highlighted in red indicating that the 10-day forecast Anomaly Correlation value is greater than 0.6 (high skilled 10-day forecast) and red lines on the top denoting periods from Table 1. Most of these curves with high skilled 10-day forecast fall within periods of Retrograde Wave event days for the 1995/96 and 2010/11 cases which would explain the sharp increase in average Anomaly Correlation during active period noted in Figure 21 and Figure 22. In contrast the 2000/01 winter case which has reduced Retrograde wave activity is also marked by reduced number of high skilled 10-day forecast.

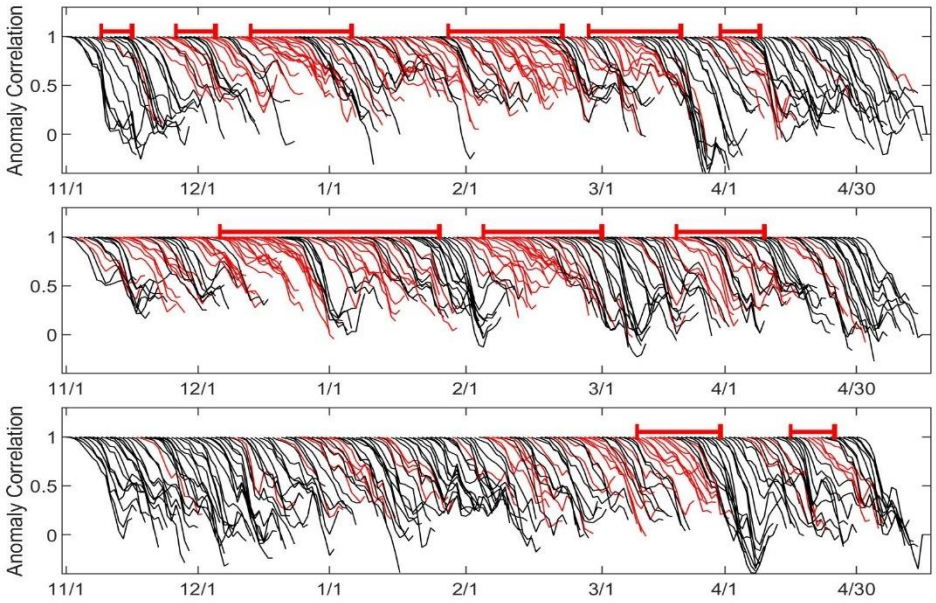

Figure 23. 0-16-Day Anomaly Correlations, with 0-Day being the Starting Point Each Day between Nov 1st to April 30th for Years a) 1995-96, b) 2010-11, and c) 2000/01. Red Curves Indicate 0-16-Day Forecasts with 10-Day Anomaly Correlation Value Exceeding 0.6 and the Red Bars on Top are Days of Retrograde Wave Activity Chosen from Table1.

Geographical Dependence of Increased Predictability

The calculation of Anomaly Correlation in the previous sections were done by averaging it over entire band of grid points between 40°N and 70°N. However, we have seen in the previous chapter on how Retrograde Wave event are dominated by low PV extrusion and westward movement over pacific sector. This being the case, it becomes useful for us to see if these individual structures of westward moving anti-cyclonic circulations are predicted well by the forecasts and if they in-turn are responsible for the increase predictability we noted during the four winter seasons analyzed in the previous section.

As a first step, we look at Anomaly Correlation values averaged over 40^{o}-70^{o}N band over the four winters but over each 10^{o} longitude band between 0-359^{o}E of Greenwich Meridian presented in Figure 24. A considerably high anomaly correlation in noted over 100-200^{o} E during active period as compared to inactive period in almost all these plots (for both 8-day and 12-day forecasts) with a few exceptions (for example 12-day correlation during 1994/95). The westward moving anti-cyclonic circulation, though it has its point of origin over east pacific region (160-200^{o}E), remains within the 40-70^{o}N band as it travels westward to over East Asia, which could possibly explain the noted increased predictability over the entire sector. We get a clearer picture into this when looking at individual forecasts with increased predictability later in this section.

Vortex shedding event during February 1995. The first case considered is the vortex shedding event in February 1995 which can be seen in Figure 17. Studies on predictability associated with other travelling and stationary wave features like Madden Julian Oscillations (Kim et al. 2014) and blocking (Tibaldi 1990) respectively have shown that the forecasts predicted them better when initialized with the presence of a strong event of the respective phenomenon than when the event occurs few days into the forecast.

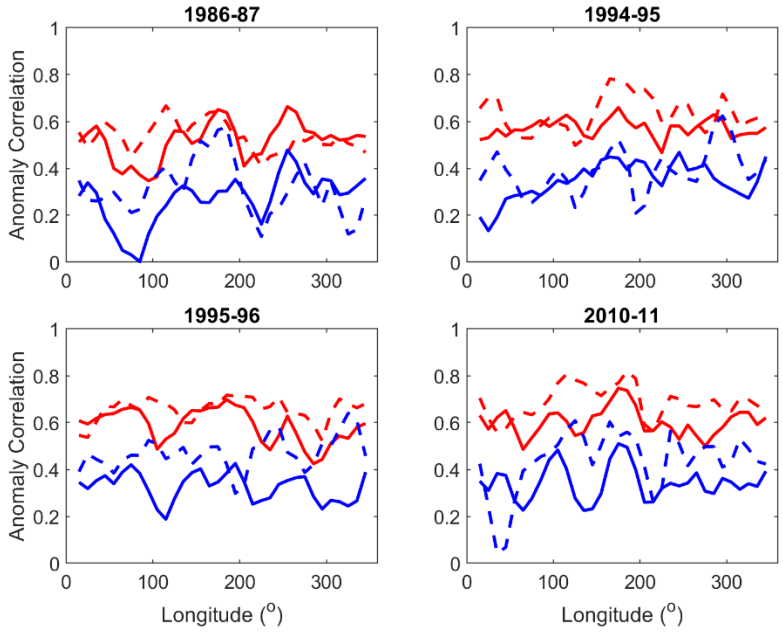

Figure 24. Distribution of Average Anomaly Correlation between 40°-70° N Along each 10° Longitude Band between 0 -359° E of Greenwich Meridian During the Four Winters Examined. Solid Lines (Red 8-Day and Blue 12-Day Forecast Average) Being Average over Inactive between 1st November and 30th April of Corresponding Winters and Dashed Lines being Average over Active Period of Retrograde Wave Events.

A similar result is obtained for Retrograde Wave events as well when comparing Figure 25 and Figure 26, with Figure 25 containing four different 0-16-day Anomaly Correlation curves initialized starting 1st, 4th, 7th, and 10th February 1995 and Figure 26 containing the Error growth, Forecast and Observed geopotential height values along 60°N. A clear westward propagation is noted along starting around 7th February 1995 as seen from the observed geopotential height anomaly in Figure 26 and with forecasts starting on both 4th and 7th February predict this westward propagation well it can be noted that these forecasts are initialized following the emergence of positive geopotential height anomaly along the 60°N latitude. A reflection of this predictability is noted in the Anomaly Correlation curves in Figure 25 wherein the values for forecasts initialized on

4th Feb 1995 remain at around 0.7 even for the 16-day forecasts, a value far higher than average during the entire winter from Figure 20.

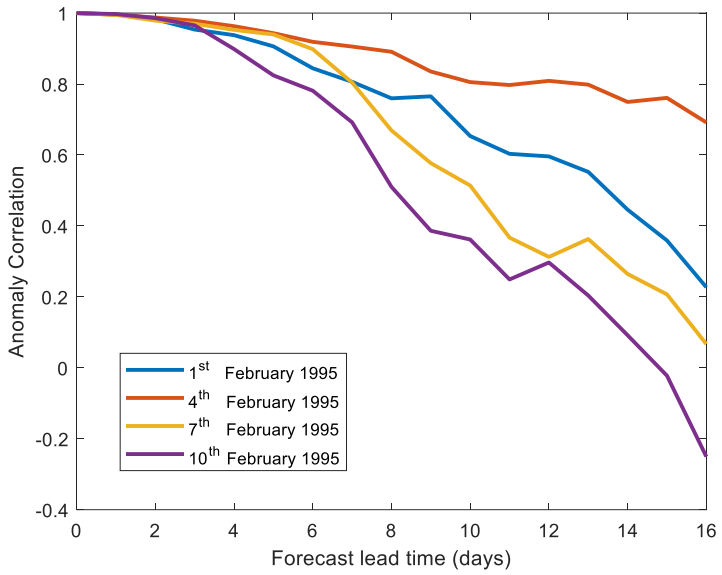

Figure 25. Anomaly Correlation between Observed and Forecast Geopotential Height Anomaly Field (Considering All Wavenumbers between 40°-70°N) with Forecasts Initialized on Respective Days as Mentioned in the Legend.

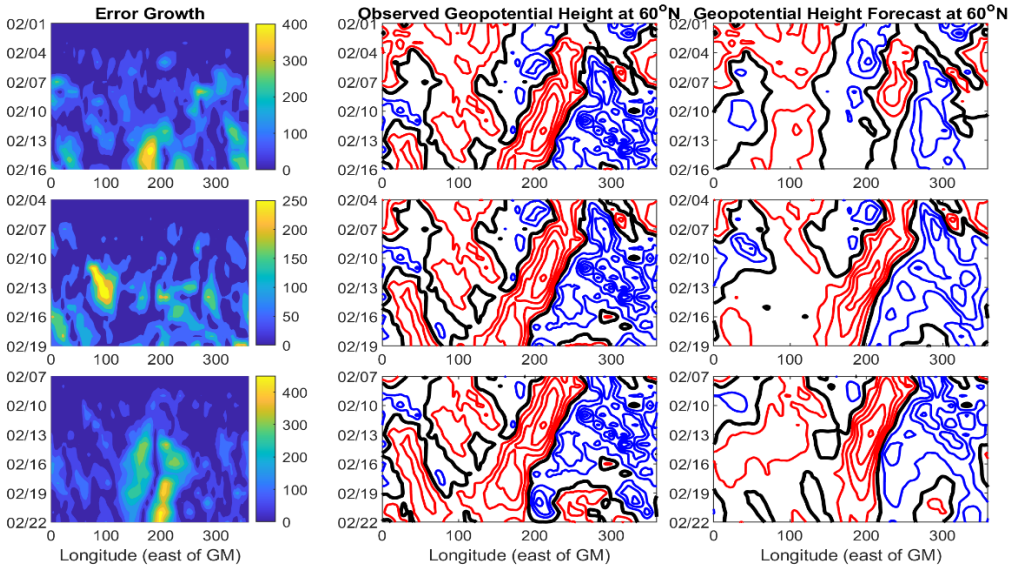

Figure 26. Time Evolution of a) Error Growth (Measured as the Difference in Geopotential Height Anomaly Values between Observation and Forecast) along 60°N Latitude b) Observed Geopotential Height Anomaly along 60° N Latitude Circle and c)

Forecast Geopotential Height Anomaly Values along the 60^{o} N Latitude Circle. a) b) and c) are Plotted for Cases where the Forecasts were Initialized Starting 1st, 4th, and 7th February 1995 from Top to Bottom Respectively. Positive Anomalies are Indicated by Red Contours, Negative Anomalies by Blue and Black Lines Denoting the Zero-Contour Level.

A parallel look at the Error growth during these forecasts reveal the source of error to be poor prediction of the eastward moving positive and negative anomaly and the emergence of a negative anomaly. These aspects can be explored better examining the full Geopotential Height anomaly Observation and Forecast field in Figure 27 and Figure 28 where it can be seen that the patterns of westward shifting positive geopotential height anomalies (anti-cyclonic circulations) emerging over North America spotted in the Observations are captured well in the forecasts explaining abnormally high Anomaly Correlation values during this period.

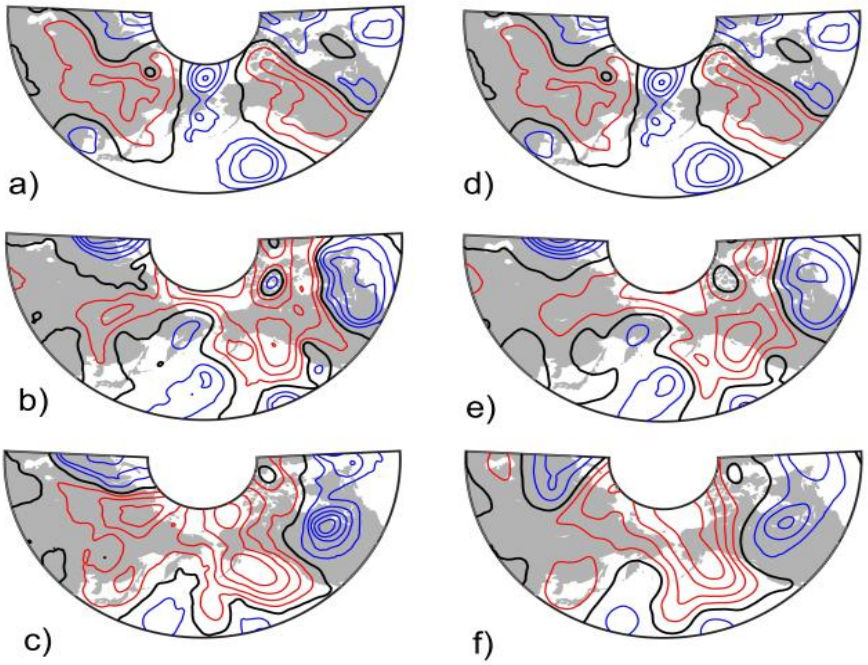

Figure 27. Geopotential Height Anomaly (Within 30°-80°N and 50°-270°E) with Contour Level of 80m Observed on a) 4th February 1995, b) 8th February 1995, and c) 11th February 1995. The Corresponding Forecast Geopotential Height Anomaly for Forecast Initialized on 4th February 1995 Showing d) 0-Day Forecast for 4th February 1995, e) 4-Day Forecast for 8th February 1995, and f) 7-Day Forecast for 11th February 1995. In Each of These Contour Plots Red Lines Indicate Positive Geopotential Height Anomaly Contours, Blue Lines Indicate Negative Geopotential Height Anomaly Contours and the Black Lines Indicate the Zero-Contour Level.

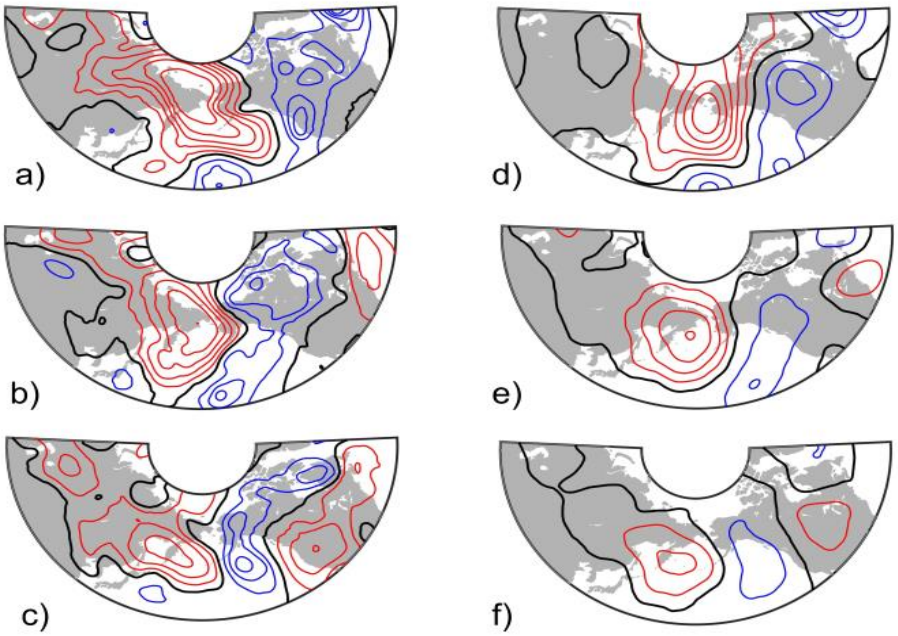

Figure 28. Same as Figure 27 but Observed Geopotential Height Anomaly on a) 14th February 1995, b) 17th February 1995 and c) 20th February 1995 Along with Corresponding Forecasts d) 10-Day Forecast for 14th February 1995, e) 13-Day Forecast for 17th February 1995 and f) 16-Day Forecast for 20th February 1995.

Blocking and Vortex shedding event during December 2010. Similar analysis of other Retrograde Wave events with periods of increased predictability revealed similar results with up to 16-day forecasts retaining these westward travelling anti-cyclonic structures (another such case presented in Appendix). One another interesting case presented in this section is during a prominent vortex shedding event in December 2010

which was seen in Figure 14. The enhanced predictability of this evolving low PV structure, its westward shift which resulted in a block over the region of japan causing the occurrence of an extended cold spell in the region was discussed in the study by Hoskins (2013). When talking about improvements in predictive capabilities of current forecast models beyond Week-1, he cited this example and how Japanese meteorological models had predicted accurately this cold spell two weeks in advance. From a similar analysis of comparing observations and forecasts starting 13th December 2010 (during one of the long Retrograde wave events from Table 1) shown in Figure 29 encompassing the start of this cold spell shows the retention of westward travelling vortex shedding structure even in the 16-day forecast.

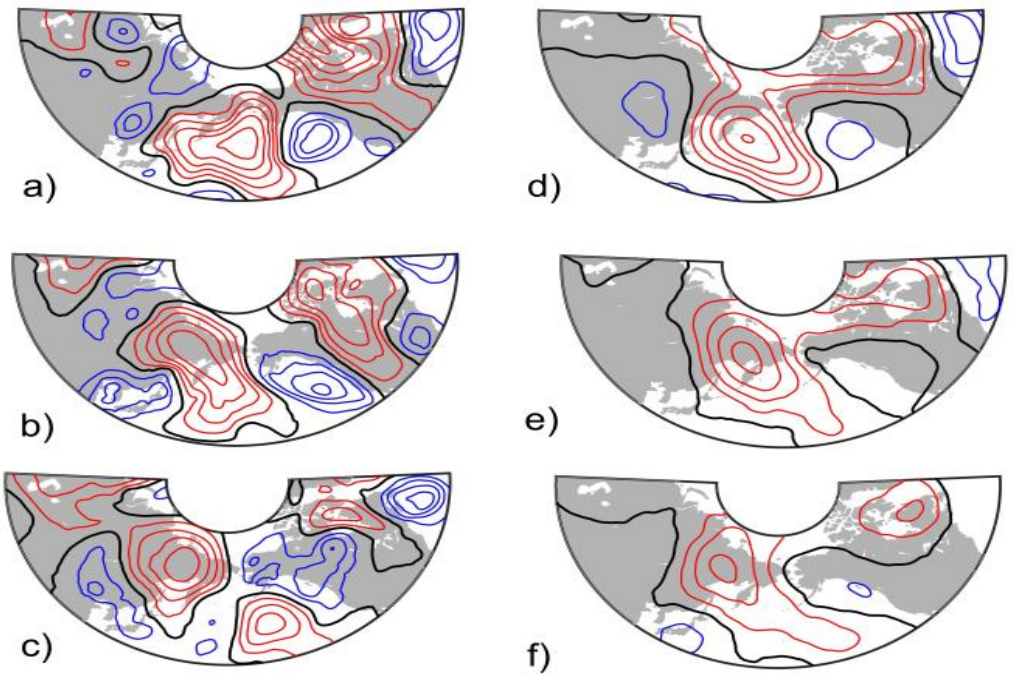

Figure 29. Same as Figure 27 but Observed Geopotential Height Anomaly on a) 23rd December 2010, b) 26th December 2010 and c) 29th December 2010 Along with

Corresponding Forecasts d) 10-Day Forecast for 23rd December 2010, e) 13-Day Forecast for 26th December 2010 and f) 16-Day Forecast for 29th December 2010.

Periods of increased predictability during December 1994. In the previous section we had briefly discussed the probability of other atmospheric features like blocking that may occur during the periods chosen to find average Anomaly correlation which may influence the midlatitude predictability. Here we look at one such example of a band of high anomaly correlation days found during December 1994 outside the days present in Table 1 in Figure 30.

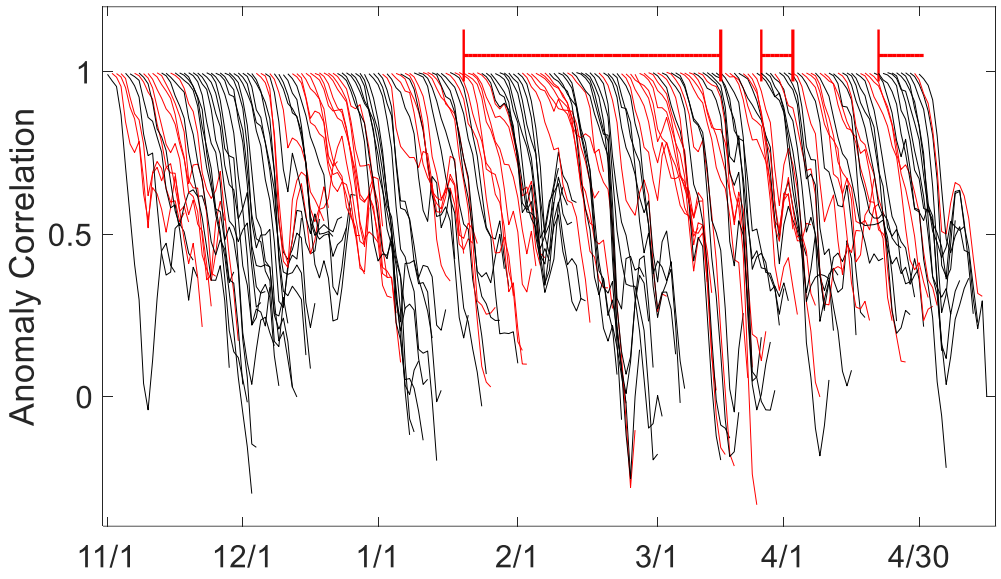

Figure 30. Same as Figure 23 but for Year 1994/95.

Examining the individual forecast in Figure 31 and Figure 32 reveals the presence of positive Geopotential Height anomaly over North America remaining stationary over the region which is also captured well in the forecasts explaining the noted high value of Anomaly Correlation during that period. This stationary feature resembles the heavily

studied Persistent Anomalies with proven links to higher predictability. The Hovmoller diagram of Geopotential Height anomaly evolution in Observation and Forecast in Figure 33 depicts clearly the relatively stationary positive anomaly picked up clearly in the 0-16 day Forecast starting 12th December 1994.

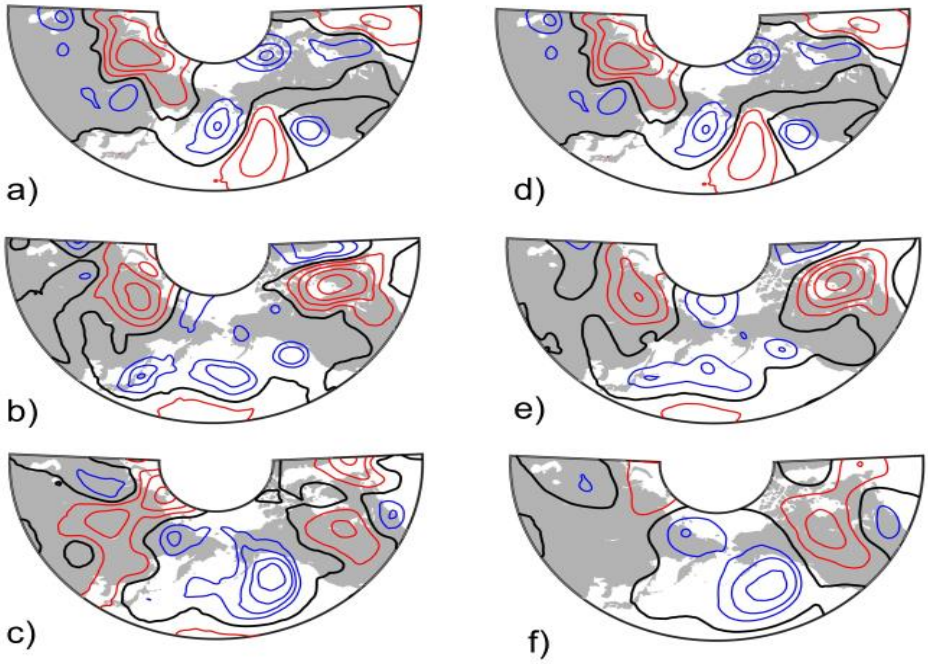

Figure 31. Same as Figure 27 but Observed Geopotential Height Anomaly on a) 12th December 1994, b) 16th December 1994 and c) 19th December 1994 Along with Corresponding Forecasts d) 0-Day Forecast for 12th December 1994, e) 4-Day Forecast for 16th December 1994 and f) 7-Day Forecast for 19th December 1994.

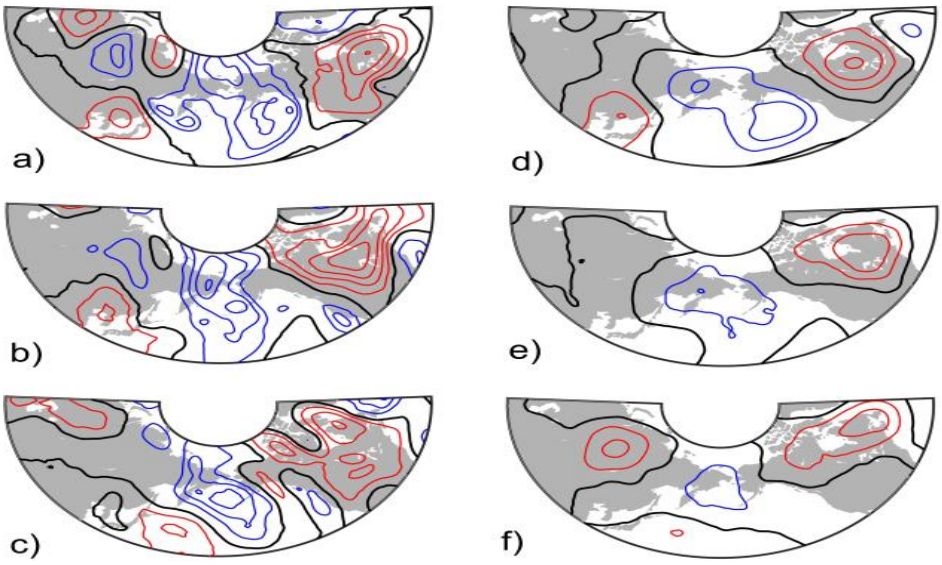

Figure 32. Same as Figure 27 but Observed Geopotential Height Anomaly on a) 12th December 1994, b) 16th December 1994 and c) 19th December 1994 Along with Corresponding Forecasts d) 0-Day Forecast for 12th December 1994, e) 4-Day Forecast for 16th December 1994 and f) 7-Day Forecast for 19th December 1994.

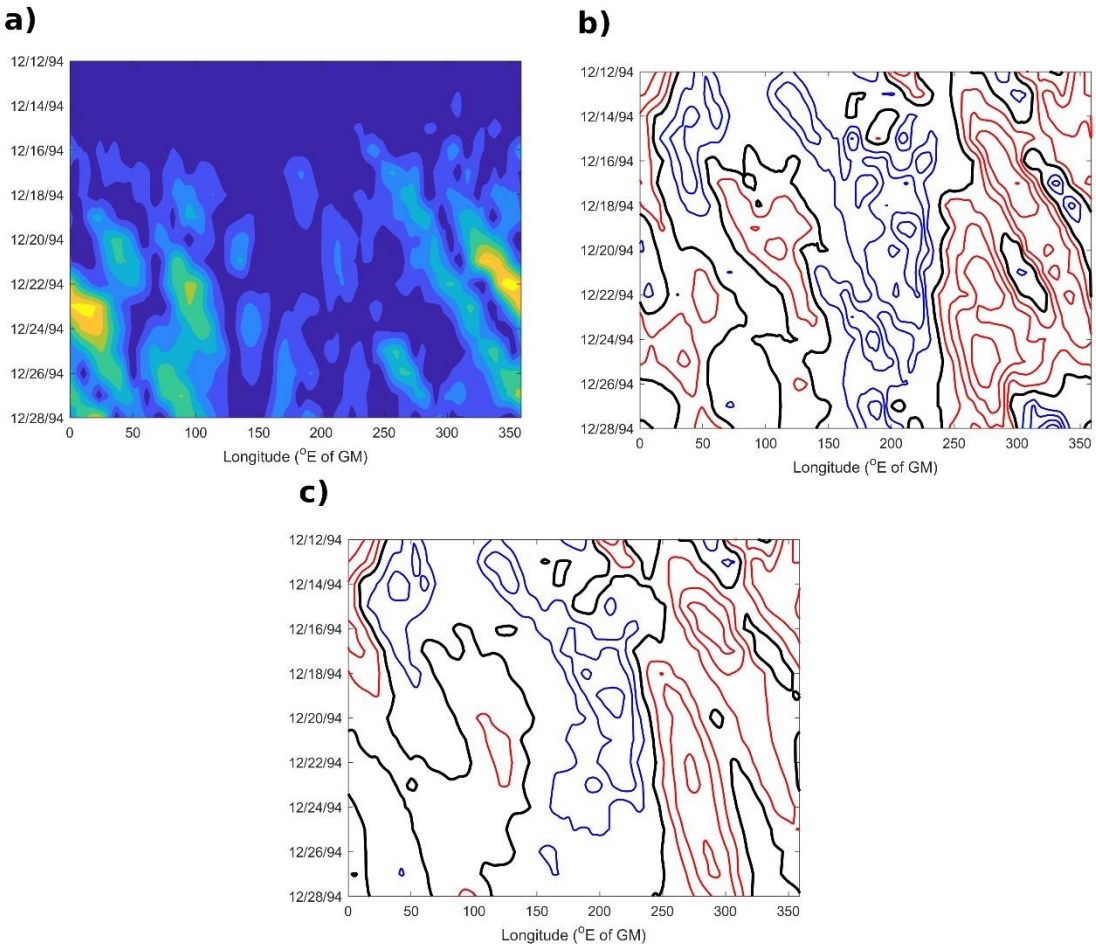

Figure 33. Like Figure 26 but for Single 16-Day Forecast Starting 12th December 1994.

Analysis of Extended-Range Forecasts

Anderson and Van Den Dool (1994) while looking into the skill associated with extended-range forecasts determined that forecasts produced after 12-days are indistinguishable from a random no-skill forecast and that any possible return of skill can occur by change. However, since Retrograde Waves (like the one in January 1980) are known to sustain over a large period of time, its possible influence in these extended range forecasts is worth looking into.

Seasonal Forecast from ECMWF. For this analysis we use the daily Seasonal Forecast dataset SEAS5 from ECMWF containing twice daily Geopotential Height

forecasts at 500hpa level extending up to 215 days. The dataset from system 4 with Hindcast starting September 1st and October 1st of 2010 containing 15-member ensemble was used. The starting point for these forecasts were the reanalysis ERA-Interim dataset on those respective days, thus we use the available ERA-Interim Geopotential Height dataset at 500hpa level as observations for corresponding forecasts. The forecast anomalies are found subtracting the climatology found using ERA-Interim dataset as described in Chapter 2 from individual daily averaged 15-member ensemble mean forecasts and are compared with observed anomalies to determine the Anomaly Correlation values (between 40^{o}-70^{o}N) as described in previous sections.

Seasonal Forecast for 2010/11 Winter. First, we look at the Anomaly Correlation plot starting September 1st, 2010 and October 1st, 2010 (Figure 34). The two forecast anomaly correlations are made into the same plot to make sure a local increase in value is not purely by chance. For instance, we note a period of increased Anomaly Correlation during February 2011 (February 16th – March 3rd, 2011) which also falls within active Retrograde Wave period from Table 1. A similar brief period of high correlation is noted between January 5th and 8th, 2011. However, examining the capability of the seasonal forecast model to capture the westward propagating Wave-1 anomaly reveal a poor performance by the model in doing so as it can be witnessed from Figure 35. This result was expected as Retrograde Waves have a relatively shorter time scale (period of 21 days) compared to some of the features that are captured well in Seasonal Forecasts like El-Nino Southern Oscillations. For instance, Doi et al., (2013) attributed the prediction of extreme warm ocean surface event over the west cost of Australia in February-March 2011 9 months in advance to high predictability associated with La Nina

in the pacific. Thus, it might be possible that the increased Anomaly correlation over the midlatitudes noted might be a result of interaction of this global propagating Wave-1 anomaly with a well predicted stationary phenomena like La-Nina. However, no direct correlation can be established between Retrograde Waves and periods of increased Anomaly Correlation in seasonal forecasts.

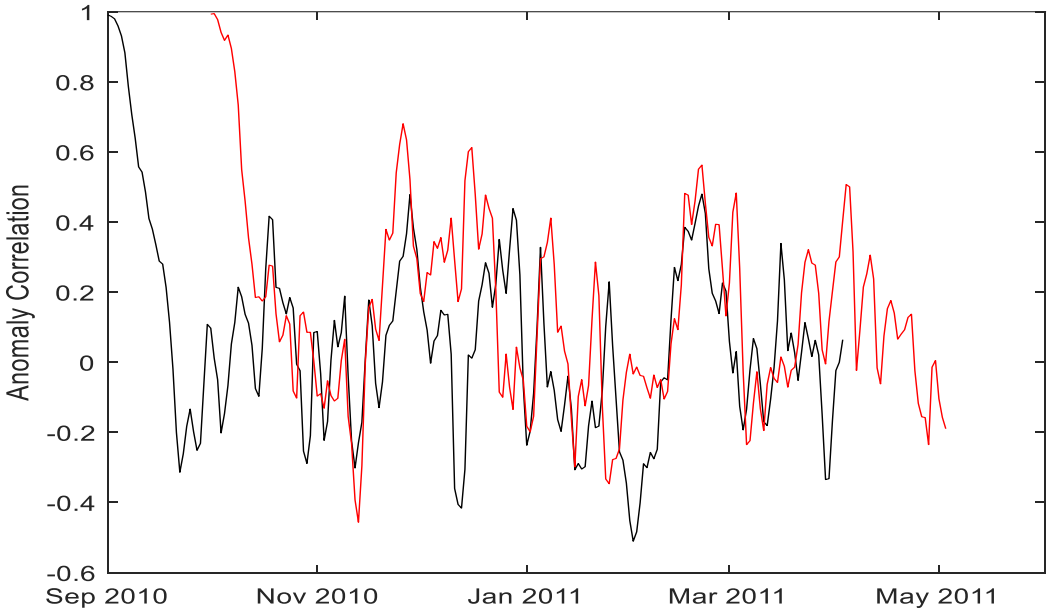

Figure 34. Anomaly Correlation (40°-70°N) Calculated from Seasonal Forecasts with Black Line for a Forecast Starting 1st September 2010 and Red Line for a Forecast Starting 1st October 2010 Calculated at 500hpa Level from Geopotential Height Anomalies at that Level.

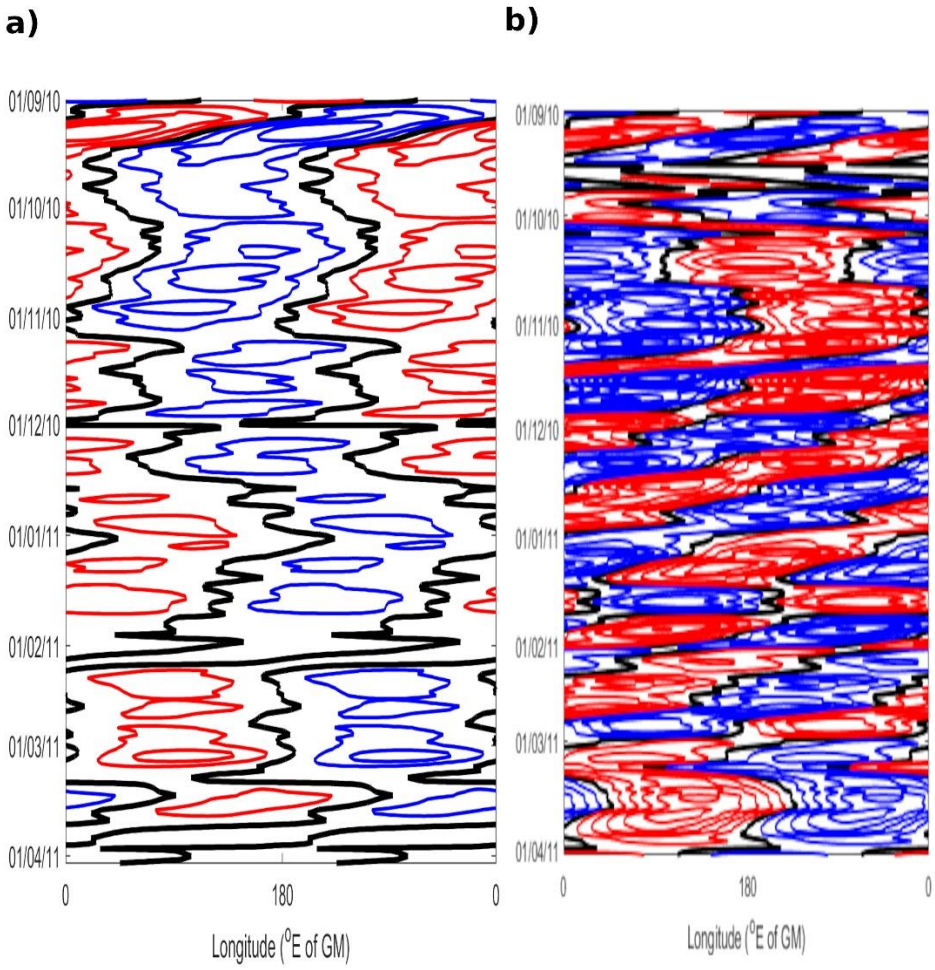

Figure 35. Hovmoller Diagram of Wave-1 Geopotential Height Anomaly at 500hpa level a) for the Forecast Starting 1st September 2010 b) Observation Starting 1st September 2010 with a Contour Interval of 30m Red Lines Indicating Positive Anomaly and Blue Lines Indicating Negative Anomaly. Black Lines Represent the 0-Contour Level.

Further Discussion and Summary

The predictability associated with Retrograde waves assessed using Reforecast data revealed a generally higher forecast skill active period as compared to inactive period of Retrograde disturbances. The winter of 1995/96 in was specific revealed to be an extra-ordinary case with an average lead time for producing skilled forecast to be around 12 days during active period compared to inactive period average of around 9 days.

The individual Geopotential Height anomaly forecast were seen to display good skill in retaining westward propagating structures especially when poleward extrusion and westward shift in low PV structure was observed. This skill apart from increasing the overall predictability in midlatitude weather during winters, could also prove useful in predicting some of the extreme weather events as evidenced from the work by Hoskins (2013) discussed in the four of this chapter. These westward shifting upper-tropospheric positive Geopotential Height anomalies picked out and predicted clearly by forecasts are also speculated play a role in the amplification of Siberian high resulting in an outbreak of cold weather over East Asia (Takaya and Nakamura 2005). A more detailed discussion into these links is presented in Chapter 4.

CHAPTER 4

TRANS-PACIFIC CONNECTION OF RETRGORADE DISTURBANCES TO EAST ASIAN COLD AIR OUTBREAK

Following a brief discussion on enhanced predictability of evolving low PV structures during certain Retrograde Wave episodes, the aim of this chapter is to dive deeper into the genesis of such shedding low PV vortices, how they might influence certain prominent weather features along pacific ocean and even far west toward the East Asian continent. We, in specific, will look at its connection in the amplification of Siberian High and the result cold air outbreak over East Asia.

Introduction

The large-amplitude Retrograde Wave events in the midlatitudes are accompanied by poleward extruding low PV structures that shift westward. We have seen cases of this westward shifting low PV structures as far as East Asia. The winter climate over the East Asian continent is regulated by a surface level high pressure system (called Siberian High) which upon a further increase in pressure dissipates and moves toward the south east along with a sharp drop in surface temperature over the region. (Compo, 1999). Zhang et al. (1997) identified that on an average 13 such cold air outbreak occurs over a year with 2 strong cold air outbreak events based on data between 1979-95. Attempts have been made to ascertain its causes with one possible explanation involving the interaction between Upper level PV anomalies and surface high (Mechanism if Intraseasonal Amplification of Cold Siberian High, Takaya, and Nakamura, 2005). In looking at the geographical dependence of these upper level PV anomalies, their analysis revealed a ‘pacific origin’ with a westward moving anti-cyclonic anomaly originating

over the north pacific, resembling the westward moving low PV structures identified during Retrograde disturbances, along with an 'Atlantic origin'.

The aim of the study presented in this chapter is to first ascertain the frequency and mechanism of these evolving low PV structures during Retrograde disturbances and to later examine their role in the East Asian cold air outbreak based on definitions of cold air outbreak by Takaya and Nakamura (2005) and tracking these low PV structures over the periods of cold air outbreak events.

Vortex Shedding as an Effect of Westward Propagating Wave-1 Signal

From a simple calculation using the Equation 7 for Rossby wave dispersion we can ascertain that around 60^{o} N the Wave-1 zonal component (k=1) will almost always propagate westwards. However due to the changes midlatitude geopotential height on a day to day basis due to evolution of local weather phenomena, the westward propagation is usually incoherent. It is using this background that Madden and Speth (1989) identified Retrograde disturbances as a coherent westward propagating wave-1 signal during the period of occurrence for their catalog. The identification of coherent westward propagation in our study is substituted using the condition for a threshold amplitude.

We had a brief discussion in chapter 2 as to how signals of poleward shift low PV air, followed by a westward shift and vortex shedding were spotted in the PV maps during few of the days of Retrograde disturbances. Following that study, in this chapter we decided to look at long term PV maps to identify the frequency of occurrence of clear vortex shedding signals through different events (some of the major Retrograde events). However, a maximum of two or three such events with clear vortex shedding was spotted among events that are more than 50 days long. But there were several instances of

poleward movement in PV spread out across the event days which would mean a poleward movement of positive Geopotential Height anomaly. Thus, it is possible that the probable cause of westward moving Wave-1 signal in the midlatitudes is this poleward moving positive Geopotential Height anomaly over north pacific which in absence of other positive Geopotential Height anomaly during the period along the latitude resulting in a large amplitude Wave-1 signal with the tendency to move westward. This type of a discussion was previously noted by Lau and Nath (1999) in trying to explain the origin of these Retrograde disturbances. Thus if we stick to a more traditional discussion into westward propagation viewing them as dispersion of strong westward propagating Wave-1 signal, it is possible that the vortex shedding identified during some of these days from Table-1 could be an effect of the propagating wave-1 signal with some kind of non-linear interaction between them.

January 1980 Retrograde Wave Event. To test this hypothesis, we first look at one of the strong Retrograde Wave events starting 5th January 1980. Looking through various PV maps at 315K level during this period, we see poleward extrusions in low PV air around 4th January, right before the start of the long event (Figure 36). We eventually spot the shedding of vortex around 10th January. Following this there a signal of Vortex shedding between January 26th and 29th 1980 (Figure 37) and another one between 12th and 15th (Figure 38). In Comparing the vortex shedding events occurring at frequent intervals with the Zonal Wave-1 Hovmoller diagram of the bandpass filtered Geopotential Height data (at 60^{o}N and 250mb, 500mb pressure levels) we can see a strong correspondence between the timing of Vortex shedding and the phase of this travelling Wave-1 component (Figure 39). A similar vortex shedding event (a much

smaller event however) was also spotted between February 29th and March 3rd (not shown). With the start of a large amplitude Wave-1 propagation at the end of December, we can see that the poleward extrusion reinforces a strong Wave-1 amplitude which continues to propagate westward following the vortex shedding event around 10th January 1980.

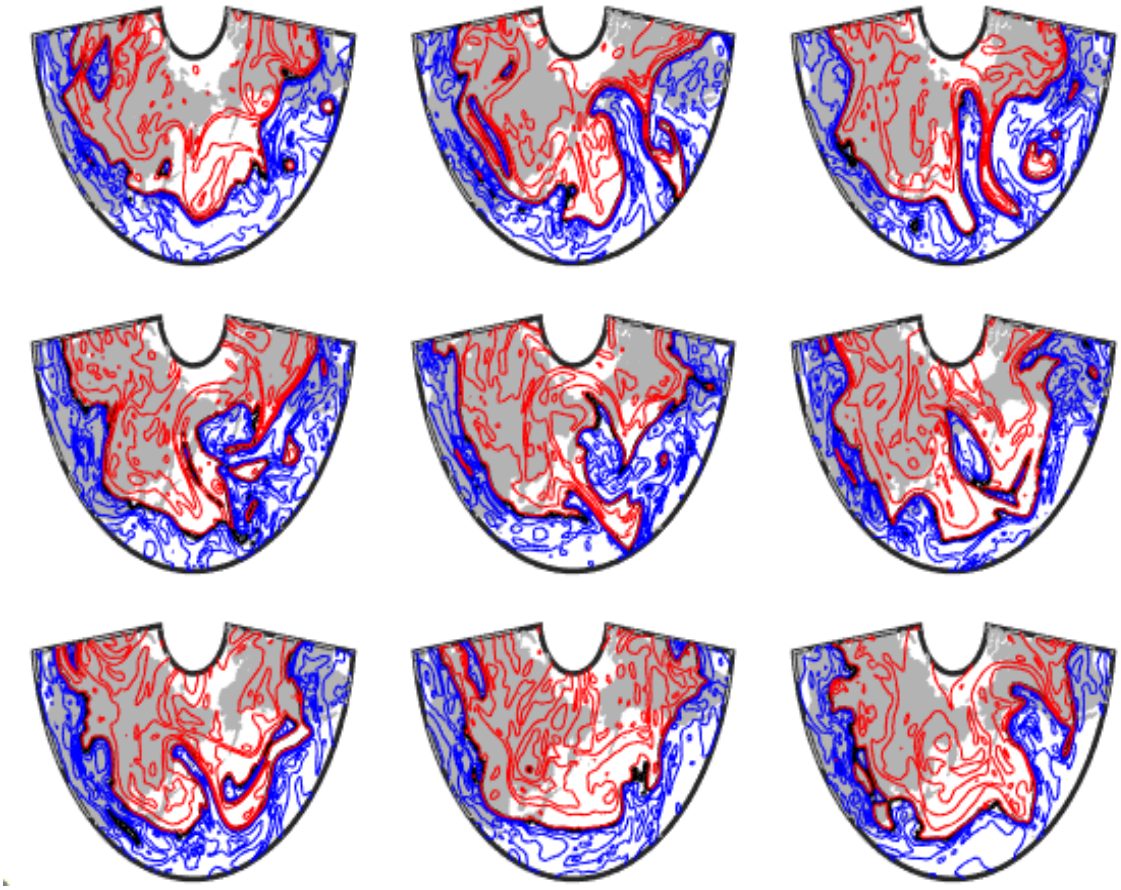

Figure 36. Sequence of Potential Vorticity Maps at 315K level on Dates 2nd, 4th, 6th, 8th, 10th, 12th, 14th, 16th, and 18th January 1980. The Domain is between 50°E-270°E and 20°N-80°N. Blue Contours Indicating Contour Levels between 0 and 1 with an Increment of 0.25 and Red Contours Indicating Contour Levels between 1 and 7 with an Increment of 2.

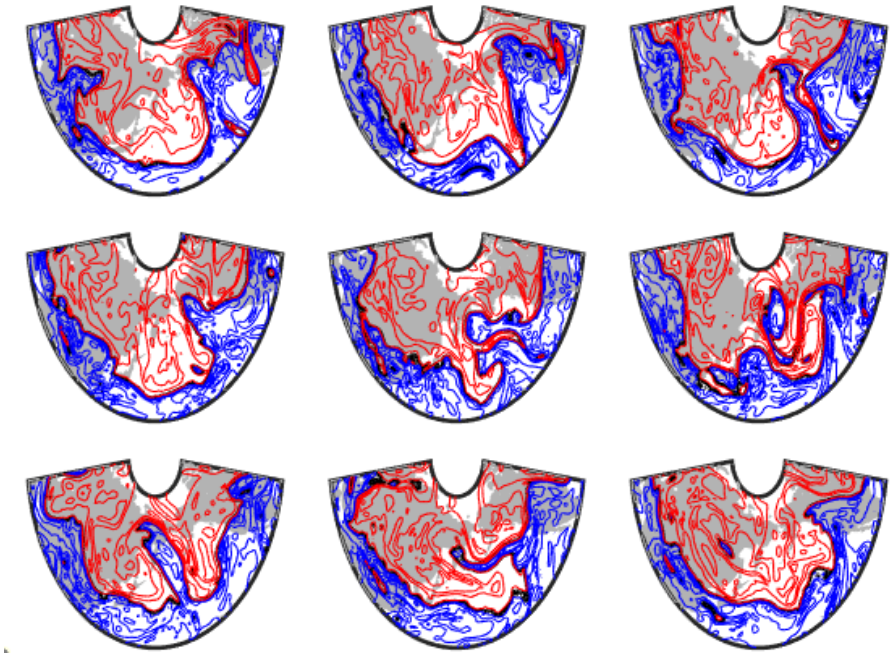

Figure 37. Like Figure 36 but on Dates 20th, 22nd, 24th, 26th, 28th, 30th January 1st, 3rd, and 5th February 1980.

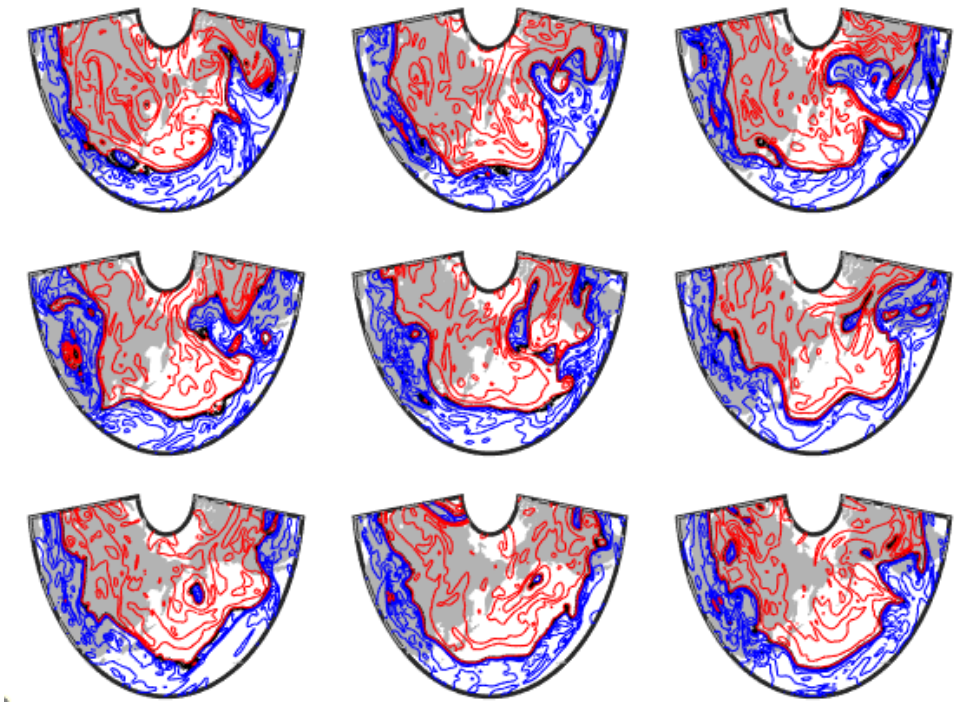

Figure 38. Like Figure 36 but for Sequence of Potential Vorticity Maps at 315K Level on Dates 7th, 9th, 11th,13th,15th,17th, 19th, 21st, and 23rd February 1980.

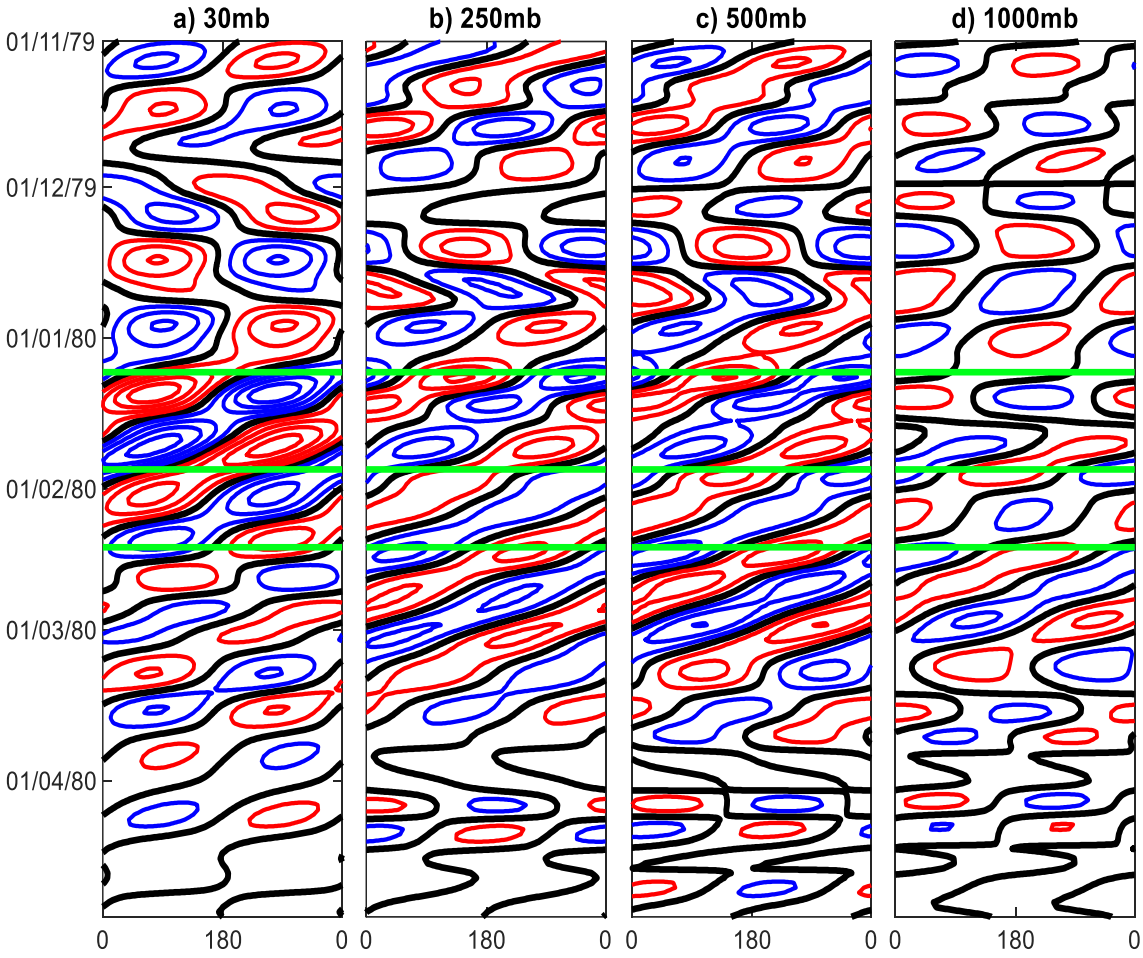

Figure 39. Hovmöller Diagrams of Wave-1 Component of Geopotential Height Anomaly Along the Latitude Circle at 60°N (0° - 360°), over the Period of November 1, 1979 – April 30, 1980. The Contour Interval is a) 100m for 30mb, b) 60m for 250mb, c) 40m for 500mb and d) 40m for 1000mb Levels with Red and Blue Being Positive and Negative Anomalies and Black Indicating the 0-Contour Level. Three Green Lines on January 6, January 28 and February 13, 1980 Indicate Days of Vortex Shedding Occurrence.

From Figure 40 showing the evolution of 250mb Geopotential Height anomaly (not bandpass filtered) field during this period starting 2nd January shows how this poleward motion of positive Geopotential Height anomaly linked to the low PV air (between 6th and 10th January) induces a net large amplitude Wave-1 motion as it can be witnessed from the sequence following this poleward movement.

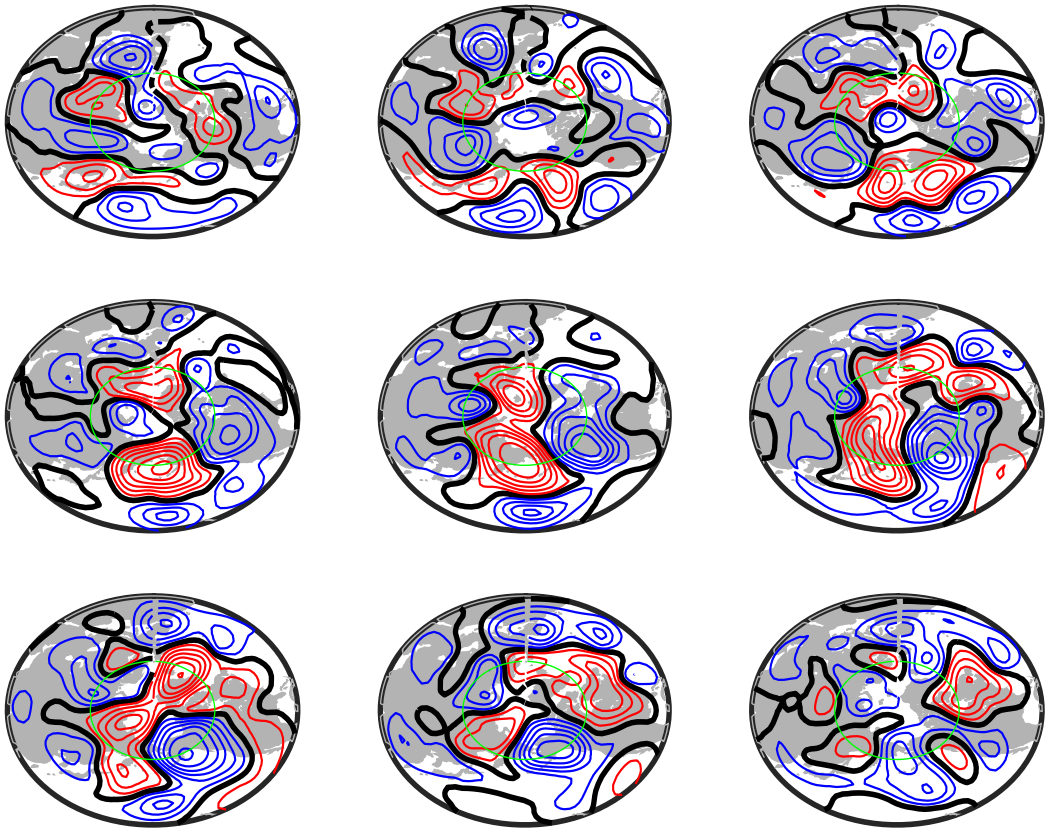

Figure 40. Sequence of Geopotential Height Anomaly Field at 250mb Level During the Days 2nd, 4th, 6th, 8th, 10th, 12th, 14th, 16th, and 18th January 1980. The Red and Blue Contours Denote Positive and Negative Geopotential Height Anomalies with a Contour Level of 100m between Them. The Green Circle Indicates the 60°N Latitude Circle.

January 1995 and December 2010 Retrograde Wave Events. The evolution of PV and the corresponding comparison with retrograding Wave-1 anomaly reveal a similar pattern. Similar pattern in observed when comparing the Hovmoller diagram during the Retrograde Wave events in January 1980 and January 1995. During days prior to the vortex shedding marked by green lines in Figure 41a and Figure 41b, the high amplitude westward propagating wave-1 structure reaches over the north Pacific Ocean. The corresponding PV maps during days of vortex shedding during these two events is shown in Figure 42.

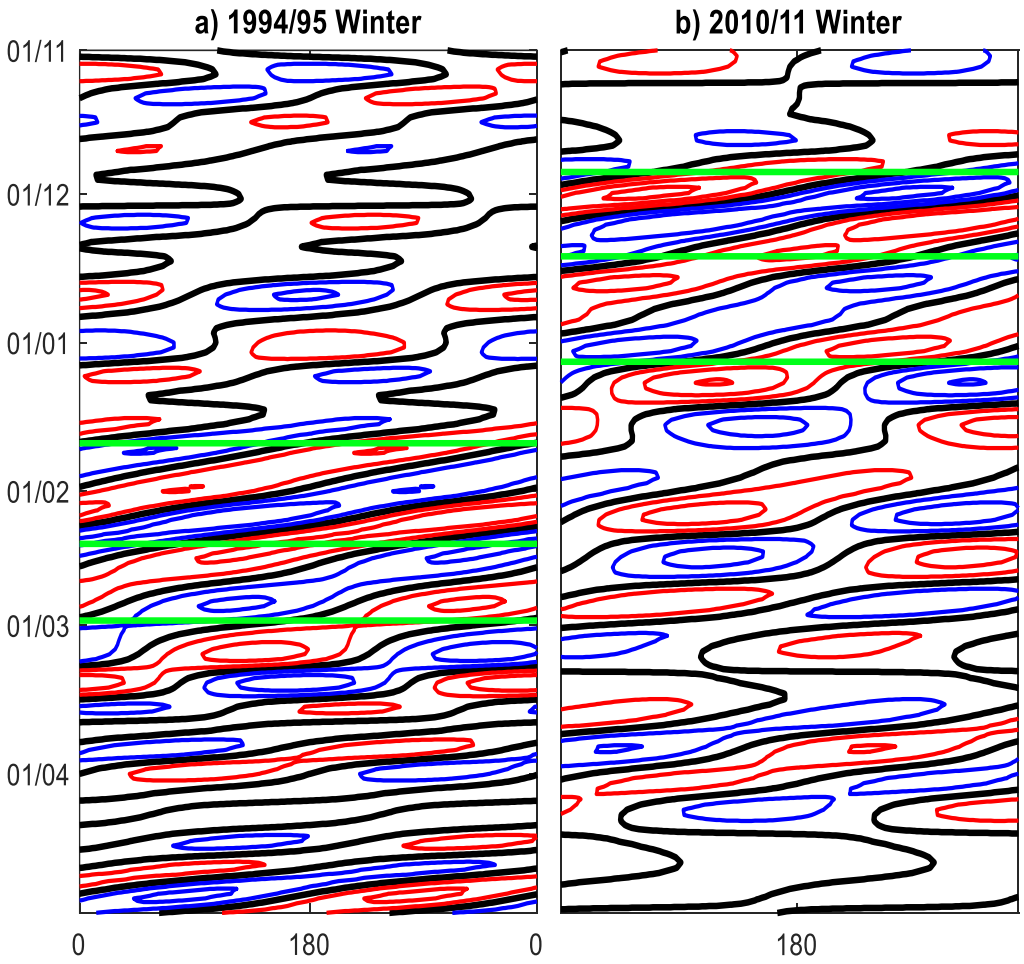

Figure 41. Like Figure 39 but for Duration between a) November 1, 1994 – April 30, 1994 and b) November 1, 2010 – April 30, 2011. The Green Lines are for Days a) December 10, 2010, December 26, 2010 and January 15, 2011, b) January 22, 1995, February 12, 1995, and February 28, 1995 at 500mb Level.

Discussion on the observed links. The observed vortex shedding over the North Pacific Ocean is more or less periodic within these major Retrograde Wave events indicative of its links to the travelling Zonal Wave-1 pattern. Another common observation between difference instances of Vortex Shedding is the pre-existence of a fairly large amplitude Wave-1 component. For instance, during the start of Vortex shedding event on 6th January 1980 (which is also the start of Retrograde Wave event as

per Table-1) there is already a presence of a large amplitude wave. However, this is absent at the beginning of Retrograde Wave event in December 2010.

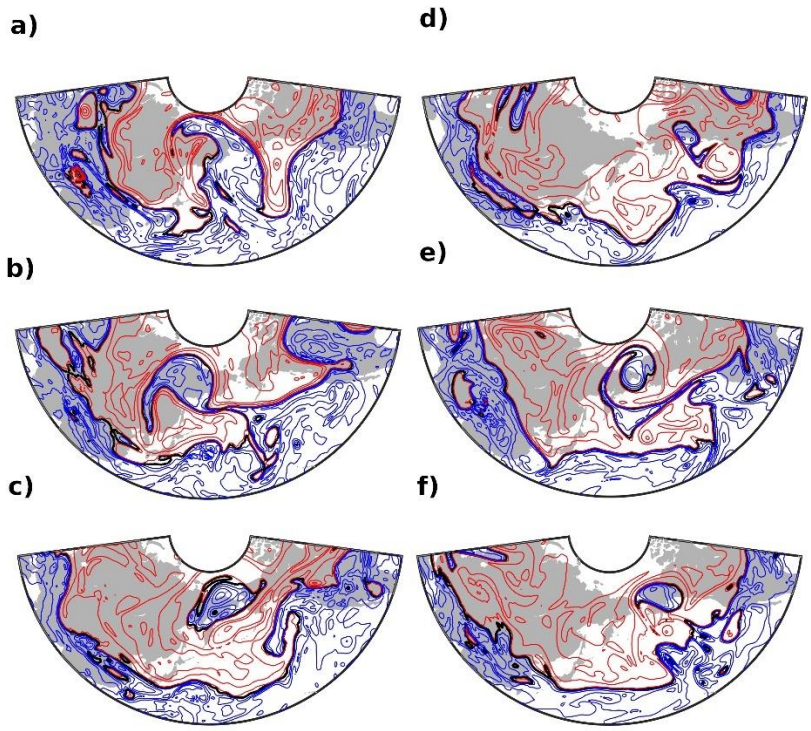

Figure 42. Like Figure 36 with PV Maps on a) 10th December 2010 b) 26th December 2010, c) 15th January 2011, d) 22nd January 1995, e) 15th February 1995 and f) 28th February 1995.

Thus, based on these observations it is possible that there might be a certain minimum amplitude of background Wave-1 flow which would then trigger the start of the observed Vortex Shedding event. One way to understand this link is from a Rossby Wave breaking perspective. For instance, the study by Hsu and Plumb (2000) on numerical simulations of a shallow water model with a strong imposed asymmetric mean wind over a forced anticyclonic circulation produced similar periodically shed eddies out of the anti-cyclonic circulation. It was also argued that the tendency of the circulation to become unstable and shed vortex depends on maintenance of a strong asymmetry. The using of an imposed

zonally asymmetric basic state as we can recall is similar to the arguments made by Branstator and Held (1995) and Huang and Robinson (1995) related to the thus produced leading unstable modes as a probable cause of the observed low frequency westward propagating pattern. It is interesting to note that from the examples we have seen in this section it is possible that the observed vortex shedding events would also more or less be periodic if the position of the pacific jet exit region were to remain constant through the strong Retrograde event given that the period of westward Wave-1 oscillation remains more or less a constant.

Possible Stratospheric Connection

Given the barotropic nature of Retrograde Waves, the pattern westward propagating large-amplitude Wave-1 signal is also witnessed in the lower stratosphere especially following the specific Vortex Shedding events discussed in the previous section (Figure 39). Studies have indicated the influence of planetary scale Rossby waves in upper troposphere disrupting the circulation pattern in the stratosphere as result of an upward transfer of angular momentum during such propagations (Baldwin and Dunkerton, 2001). An examination of Geopotential Height anomaly at 30mb level (Figure 43) revealed the emergence of a large anti-cyclonic anomaly and a split in polar vortex which appears similar to what is defined as a split-type SSW event in Butler et al. (2015). However, this was not among the strong SSW events cataloged in the supplemental material of the same study, but there was one SSW event occurring during the January 1980 Retrograde event on February 29th which was a result of a standing positive geopotential height anomaly over the arctic over several previous days (not shown). However this kind of upward propagation during vortex shedding event is also

witnessed following the other two vortex shedding events in Winter of 1979/80 as it can be witnessed as large amplitude Wave-1 signals following the three events in Figure 39.

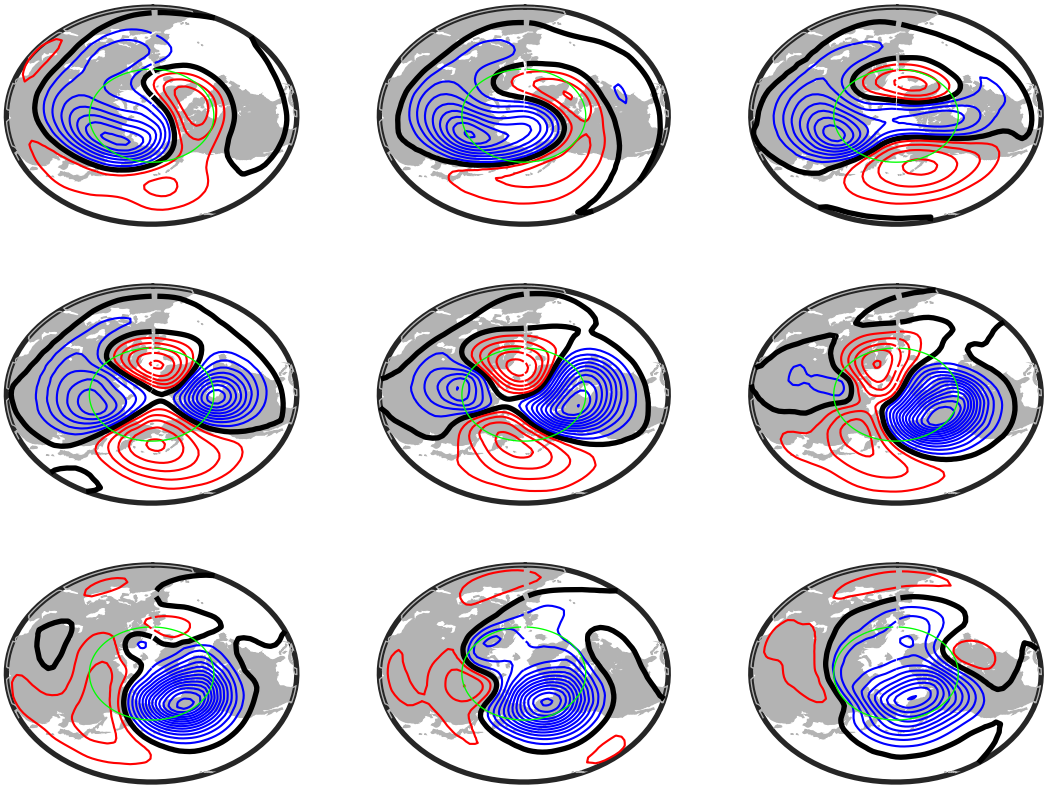

Figure 43. Similar to Figure 40 but at 30mb Level Instead

Links to East Asian Cold Air Outbreaks

Several studies looking into East Asian cold air outbreaks have had different definitions of them to identify individual strong events. For instance, Takaya and Nakamura (2005) used a low pass filtered 1000 hpa geopotential height anomaly and calculated the maximum value of it within a 1000km radius making a composite of 20 such strong events with largest maximum values around a target grid point. A similar composite at 250hpa level during those days revealed the presence of a quasi-stationary anticyclonic upper level circulation over an intensifying surface level high pressure. In

our study we use the condition by Zang et al. (1997) which uses the absolute value of sea level pressure and defines a cold air outbreak when this Sea Level Pressure exceeds 1035hpa and the temperature decrease over the region in East Asia (115^{o} – 120^{o}E and 25^{o}-30^{o}N specified as region 3 in their study) exceeds 6^{o}C during the 48hr period following the intensification of Siberian High. We use a similar definition in our study looking at major cold air outbreak event during two winters with strong Retrograde Wave activity (one starting January 1980 and the other starting December 2010).

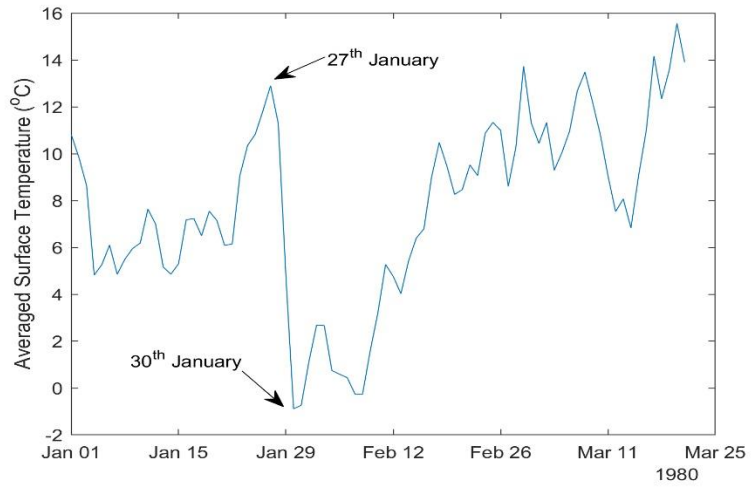

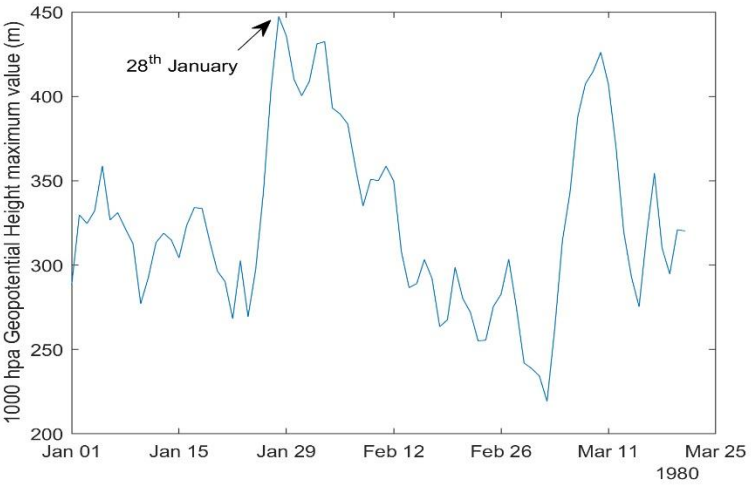

Figure 44. a) The Change in Averaged 2-m Temperature (Four-Times Daily Averaged for Each Day and Over the Region 115^{o}-120^{o}E and 25^{o}-30^{o}N) Over the Period between January 1st to March 25th 1980 b)Change in the Maximum Value of Four-Times Daily Averaged 1000 Hpa Geopotential Height with the Region 20^{o}-70^{o}N and 50^{o}-150^{o}E during the Same Period.

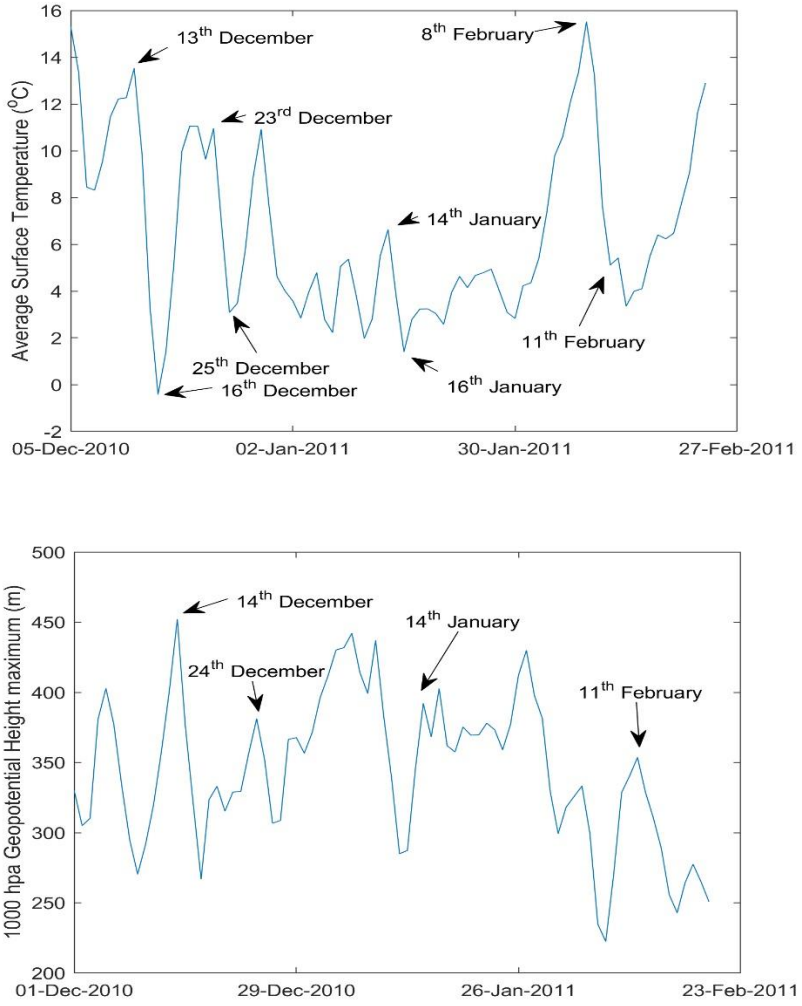

Figure 45. Like Figure 44 but for Period between 1st December 2010 and 23rd Feb 2011.

Using Reanalysis data to identify cold air outbreak events. We use the long-term reanalysis ERA5 dataset (Hersbach et al. 2020) between January 1979 and December 2017. Two different datasets are used, one being the 1000hpa Geopotential Height value and other being the 2-m Temperature value. Both over the entire Northern

Hemisphere domain (0-90^{o}N) with a spatial resolution of 0.125^{o} × 0.125^{o} are used. The four-times daily values for both these datasets which are later averaged to for each day is used. Contrary to our analysis in Chapter 2 no further spatial and temporal filtering is done other than using the data over a 1^{o} × 1^{o} domain (choosing points only over that domain size). As discussed, before we use a similar condition as Zang et al. (1997) but it is to be noted that we use 1000hpa Geopotential Height instead of using Sea Level Pressure as it helps visualizing the breaking of Siberian High better (value of Sea Level Pressure is absent over Tibetan Plateau due to its altitude).

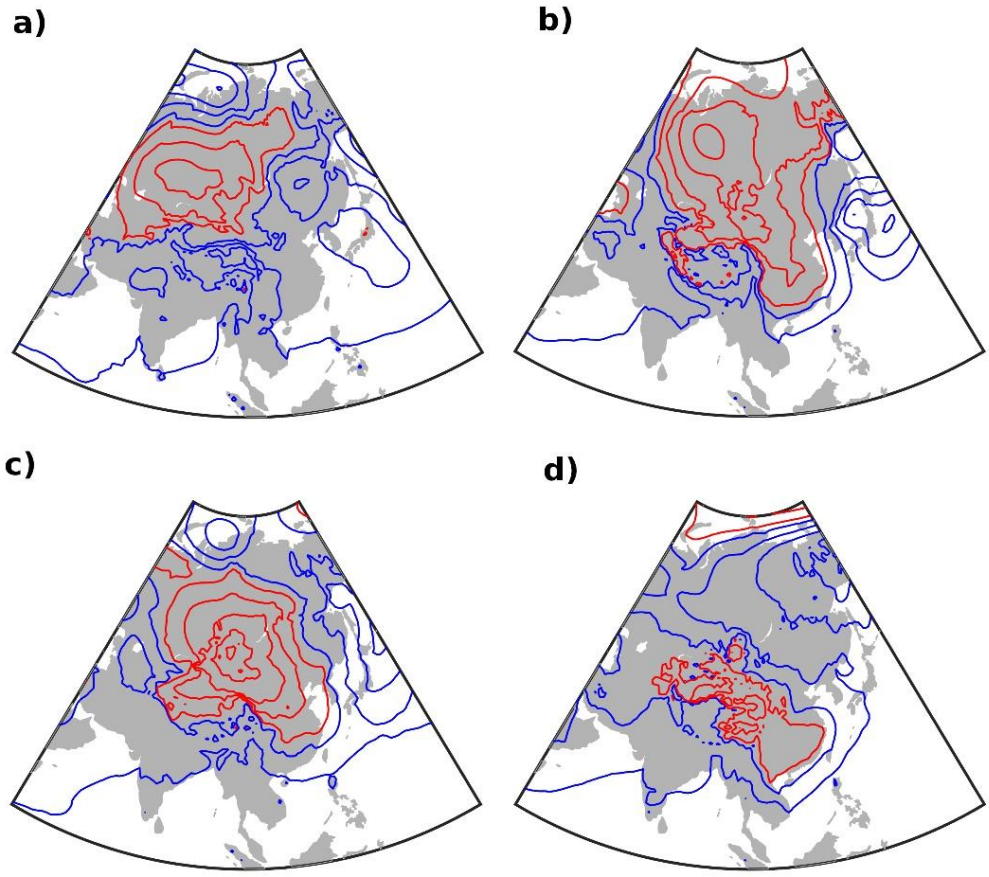

Figure 46. Geopotential Height at 1000hpa Pressure Level during Periods Identified to have Cold Air Outbreak on a) 26th January 1980, b) 30th January 1980, c) 14th December 2010, and d) 16th December 2010. Blue Contours Indicating Total Geopotential Height

Value Less Than 200m and Red Contours Indicating Values Greater than 200m with Contour Interval of 60m between Each Contour Lines over the Domain between 0^{o}-80^{o}N and 50^{o}-150^{o}E.

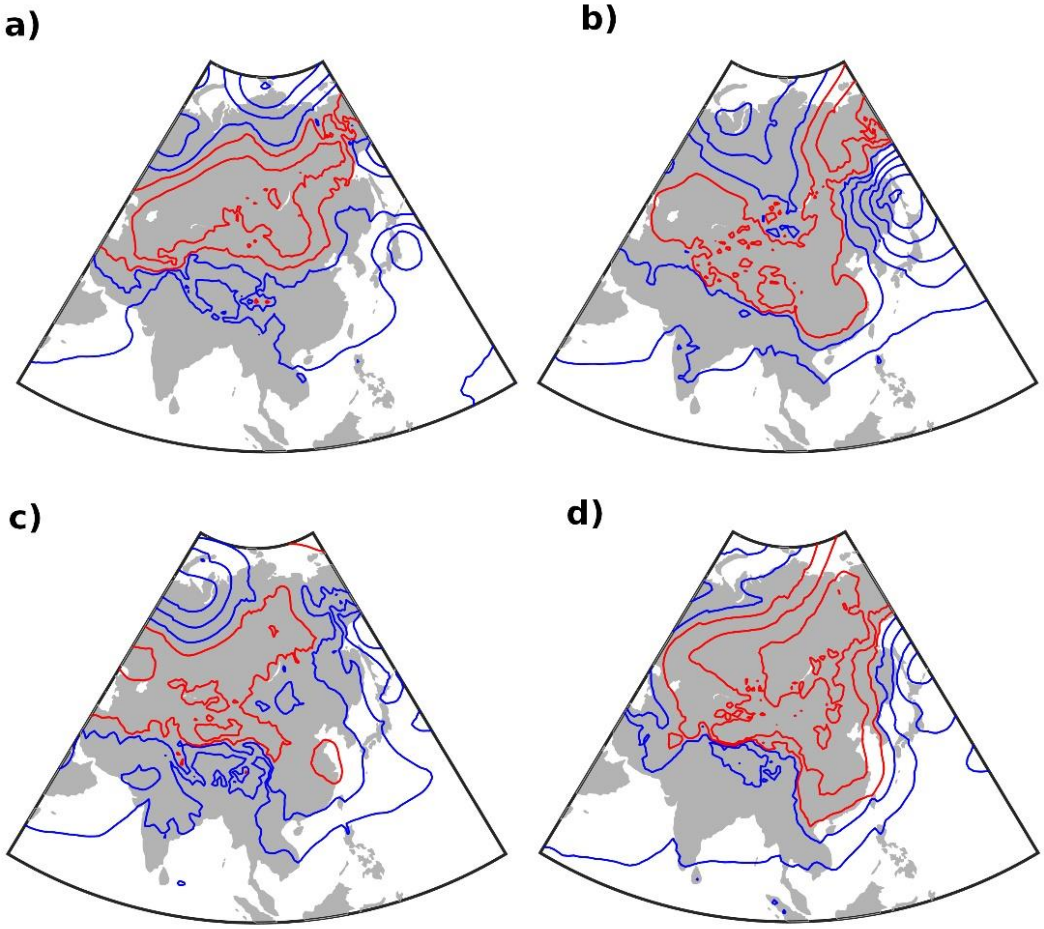

Figure 47. Like Figure 46 but for Days a) 22nd December 2010, b) 25th December 2010, c) 12th January 2011, and d) 15th January 2011.

Cold air outbreak events during winters of 1979/80 and 2010/11. Using the relation between Geopotential Height and Pressure performing a simple calculation to identify Geopotential Height at 1000 hpa for a surface pressure of 1036hpa and at approximately 10^{o}C, we can see that the value is around 300m and that surface pressure value increase by around 7hpa for every 60m increase in geopotential height. Figure 44 and Figure 45 show the evolution of 2-m Temperature (Surface Temperature) average

over a region of East Asian (similar to region 3 in Zang et al., 1997) and the Geopotential Height maximum value over the Asian continent (20^{o}-70^{o}N and 50^{o}-150^{o}E) during periods starting January 1st 1980 and December 1st 2010. Using the condition for cold air outbreak, the episodes identified during the two periods are as displayed in these figures. Of these, the evolution of 1000 hpa Geopotential Height field over East Asia and corresponding evolution of PV at 315K level for four episodes are analyzed. The breaking away of Siberian High into South East Asia is evident from these Geopotential Height maps during selected cold air outbreak events in Figure 46 and Figure 47 showing the field values before/during and after the outbreak. A simple correspondence on days with averaged Surface Temperature during the period indicate a decrease in value of more than 6^{o}C. A similar result can be seen from the Geopotential Height field during two others event between 10th – 13th February 2011 and 7th – 10th March 1980 (not shown).

Potential Vorticity during cold air outbreak. In their analysis into the mechanism of amplification of the Siberian High, Takaya, and Nakamura (2005) identified the interaction between upper level PV anomalies and cold surface temperature anomalies as a possible precursor for the intensification of Siberian High and the subsequent cold air outbreak. In a corresponding study they also identified these upper level PV anomalies of pacific origin clubbed around 67^{o}N, 107^{o}E point. When looking at the evolution of PV during the periods of cold air outbreaks discussed in the previous section, we identify similar poleward extruding PV anomalies whose timing of westward shift, seen as a movement in 1.1 PVU contour in Figure 48, corresponds with the start of cold air outbreak over East Asia and in each of these cases we can identify the low PV

anomalies to be present around that point. This can be further reaffirmed looking at four other identified cold air outbreak events during similar days of Retrograde Wave activity from Table-1 in Figure 49 with the presence of westward shift in all of the case and presence of low PV anomaly at the far east of Asian continent.

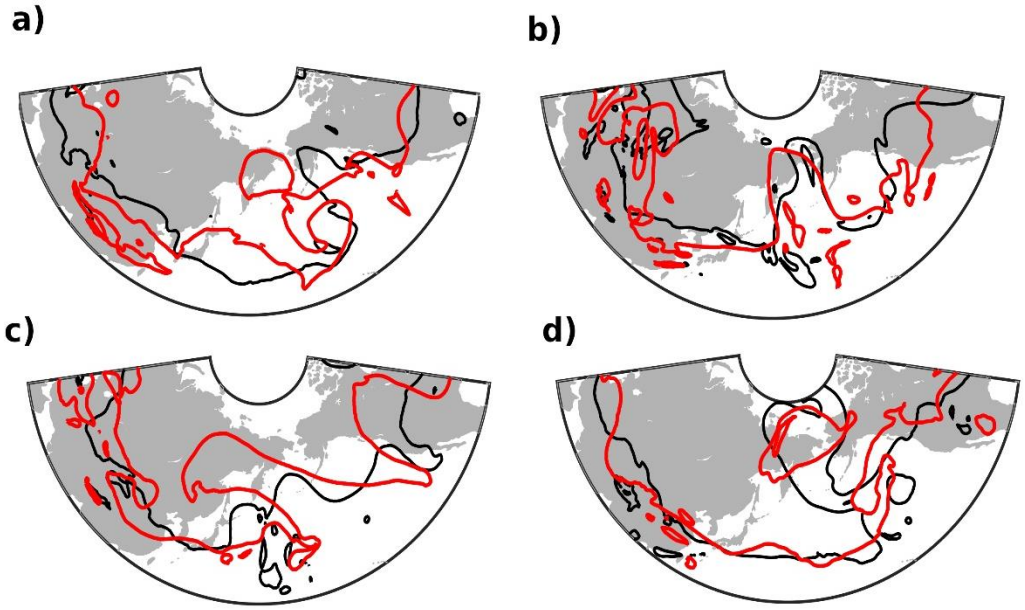

Figure 48. 1.1 PVU (10^{-6} $m^2s^{-1}K$ kg^{-1}) Potential Vorticity Contour Line over the Domain 50^o-270^oE and 20^o-80^oN) during a) Black Contour – 26th January 1980 and Red Contour - 29th January 1980, b) Black Contour – 12th December 2010 and Red Contour – 15th December 2010, c) Black Contour – 22nd December 2010 and Red Contour – 25th December 2010, and d) Black Contour – 12th January 2011 and Red Contour – 15th January 2011.

Tracking of low PV centers. A closer look at the timing of low PV disturbances movement over East Asia is possible by tracking the evolution of low PV center in the observed isentropic PV maps during cold air outbreak event. This is done using the available PV data at 315K by finding the circular radius at each point within which the average value of PV is less than 1PVU (to track low PV circulations) inside a domain 20^o-80^oN and 50^o-270^oE. To track poleward extruding PV, we then choose the topmost

point (latitude-wise) at which the radius (within which the average PV is less than 1) is at least greater 8^{o} grid size. The tracked centers and corresponding PV maps for the sequence starting 23rd December 2010 is shown in Figure 52. The result of thus tracked low PV center during the period between January 20th – 29th 1980 is shown in Figure 50. The westward movement in the tracked low PV center is seen clearly in Figure 50 and this movement in low PV center between the 26th and 29th January 1980 closer to East Asia occurs as a noticeable temperature drop occurs in the region. Figure 51 shows a similar sequence of westward moving low PV center preceding the start of another cold air outbreak event on 24th December 2010.

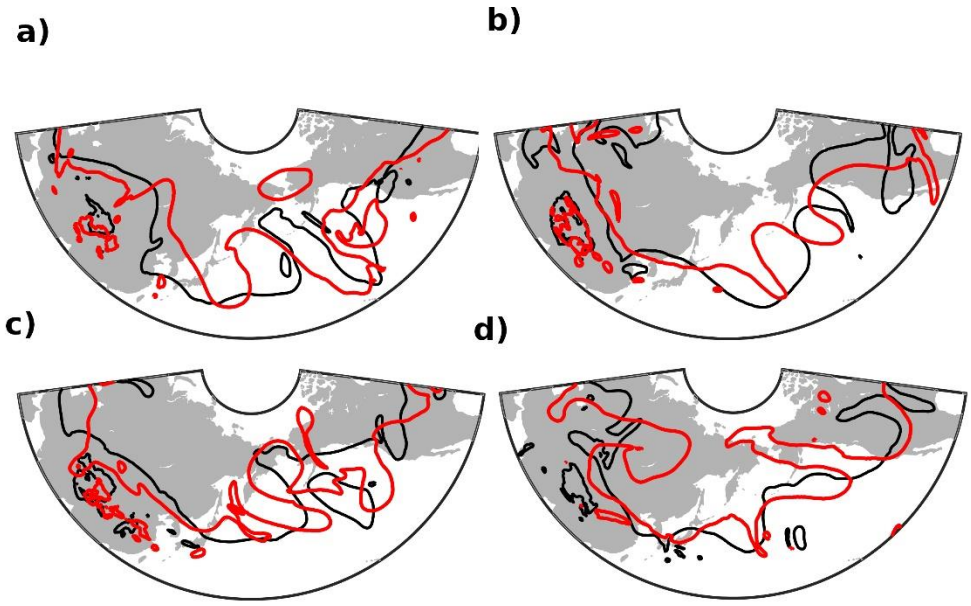

Figure 49. Like Figure 48 but During a) Black Contour – 10th March 1993 and Red Contour - 13th March 1993, b) Black Contour – 14th March 1996 and Red Contour – 17th March 1996, c) Black Contour – 28th March 1996 and Red Contour – 31st March 1996, and d) Black Contour – 9th March 2006 and Red Contour – 12th March 2006.

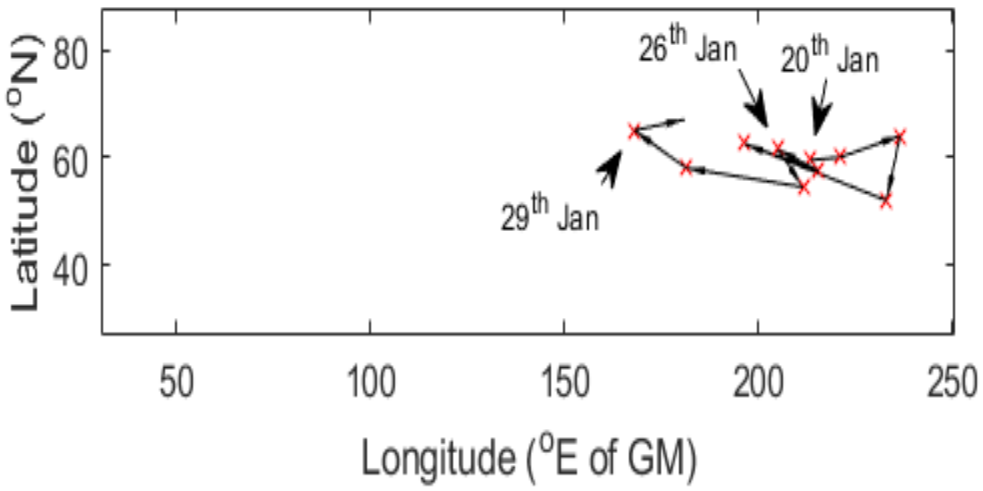

Figure 50. Position of low-PV Anomaly Center from the PV Tracking Algorithm during Each Day between 20th January 1980 and 30th January 1980 Along Corresponding Latitude and Longitude.

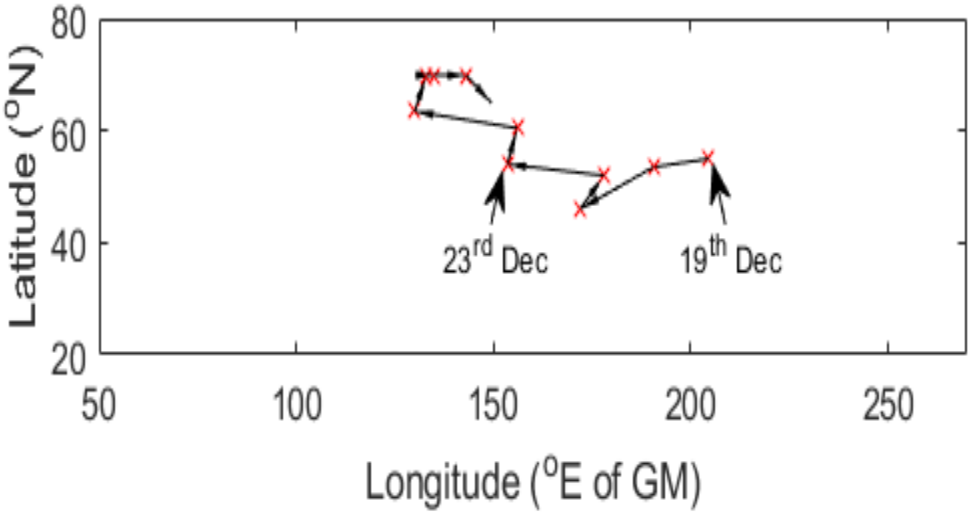

Figure 51. Like Figure 50 but for Each Day between 19th December 2010 and 29th December 2010.

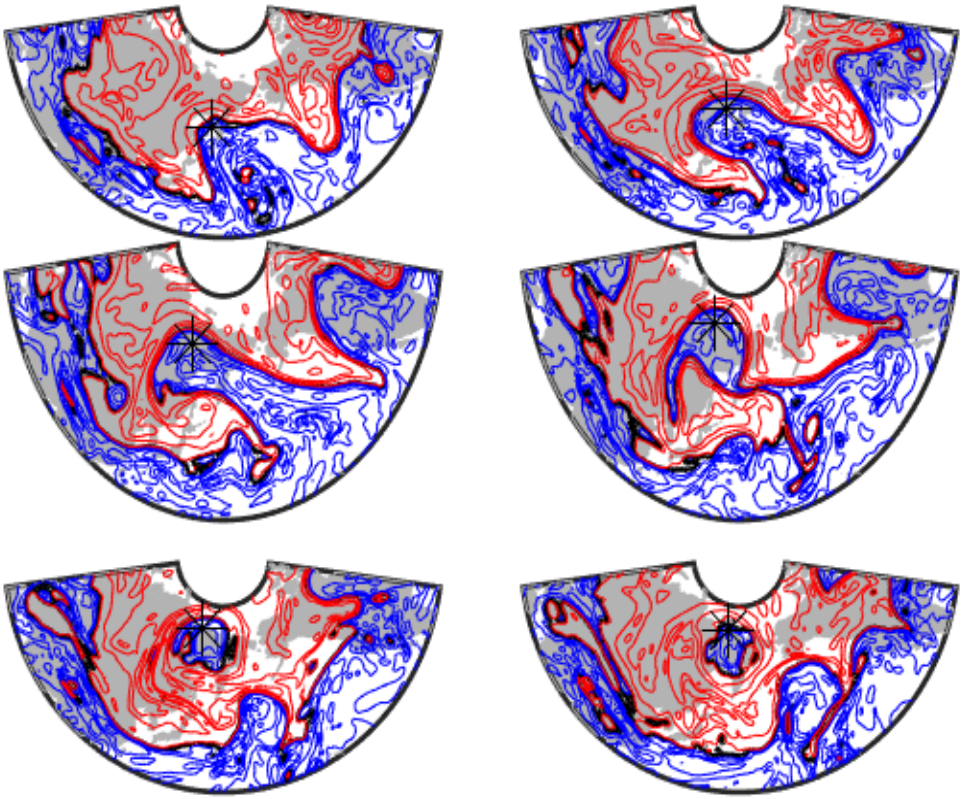

Figure 52. Like Figure 36 but for Days 23rd, 24th, 25th, 26th, 27th and 28th December 2010 (from Top Left to Bottom Right) with '*' Indicating Tracked Low-PV Centers.

Summary and Further Discussion

This work explores the mechanism of Retrograde waves a little deeper than Chapter 2 trying to understand the origin of Vortex Shedding noted often during strong retrograde events. The results indicating a strong connection between the phase of Zonal Wave-1 Geopotential Height anomaly and the start of vortex shedding event especially are quite interesting and warrants some deeper understanding. In a way, the poleward extrusions of low PV air can be looked at from a Rossby wave breaking perspective of irreversible air mass mixing from low-latitude troposphere into higher-latitude stratosphere (McIntyre and Palmer, 1983). It is also useful to quantify such poleward extrusions occurring during

Retrograde waves event in comparison with those occurring outside these events to understand if frequency of such events is higher during active period.

Another aspect explored in this study is the connection between such low PV structures and onset of East Asian cold air outbreak. By analyzing two major Retrograde event winters and outbreaks that occurred during the period, we identify a common link between the outbreaks and evolution of such westward travelling low PV structures. From tracking these low PV structures, we understand that the timing of its arrival at the East Asian continent does coincide with the start of the cold air outbreak with the positioning of low PV structures over East Asia acting as a precursor as suggested by Takaya and Nakamura (2005). With results from previous chapter indicating increased predictability of these westward travelling anti-cyclonic structures by Reforecast models, it will also be useful to check if during those periods the predictability of cold air outbreaks is improved.

CHAPTER 5

CONCLUSION AND FUTURE DIRECTION

In this thesis, the aspects of dynamics and predictability related to large-scale atmospheric waves were explored. The focus was on relative underexplored Retrograde long waves that were observed on time scales between one week and one month and with a speculated higher predictability compared to other such synoptic scale disturbances owing to their ability to maintain coherent phase propagation over several days.

With this background, this study was set out to first establish an updated catalog of Retrograde Wave events and use them to update some of the statistics along with the horizontal and vertical structure of these waves based on this new catalog (Chapter 2). From the thus established long-term catalog, it could be seen that the retrograde wave event during the winter of 1979/80 remained as one of the most prominent episodes over the 39-year period. Examination of the statistics and structure of these waves revealed similarities to the results obtained in classical observational studies. From a brief look at the PV picture during Retrograde Wave activity, a sequence of poleward ejecting low PV air, westward migration followed by vortex shedding around the region of pacific jet exit was noticed.

The predictability associated with these Retrograde disturbances over the midlatitudes measured by anomaly correlation between active and inactive period making use of the new updated catalog was studied (Chapter 3). The results indicated sustained increase in anomaly correlation values into the 16-day forecasts of 500mb Geopotential Height were noted during active period as compared to inactive period of four winter with strong Retrograde Wave activity. The 1995/96 winter in particular proved to be an

extra-ordinary case with a skillful forecast produced, on an average, 13 days prior during active period. A closer look at individual structures associated with enhanced predictability revealed retention of structures related to the westward propagating anti-cyclonic circulation originating over the pacific sector by forecasts made even 16-day prior.

Guided by the newly created catalog, investigation into possible mechanism of initiation for westward travelling low PV structures upon vortex shedding revealed the alignment of Zonal Wave-1 phase with pacific jet exit region acting as a precursor (Chapter 4). Consistent vortex shedding events were noted under the presence of this kind of alignment during major Retrograde wave events. Their subsequent role in serving as a trigger for East Asian cold air outbreak, as speculated by previous studies, was also examined. The initiation of cold air outbreaks following the positioning of low PV vortex over East Asian continent during periods of major Retrograde wave activity was seen. A closer examination on the timeline of this westward movement and initiation of cold air outbreak by tracking low PV centers proved the westward movement to be a precursor for this initiation.

This work has opened some interesting avenues for future research. For instance, the observation of vortex shedding like structures in the upper troposphere PV maps related to atmospheric wave propagation can help us view the problem from the wave breaking and vortex shedding perspective. With a subsequent analysis into their initiation revealing the consistent role of background westward propagating Wave-1 positive anomaly and the role of their shed vortices in regulating weather over East Asia, understanding the exact circumstances surrounding their occurrences become more

important. Another aspect of importance worth exploring is the dependence of Retrograde wave activity on interannual variations. From the updated catalog it can be noted that there are some winters with enhanced Retrograde activity and some with a very scanty presence. Traces of their presence in GCM simulations have been documented (May 1999). With availability of improved GCM model simulations and a better understanding of these waves because of this study, the presence of Retrograde wave structures in GCM simulations are worth looking into.

REFERENCES

Anderson, J. L., & van den Dool, H. M. (1994). Skill and Return of Skill in Dynamic Extended-Range Forecasts, *Monthly Weather Review*, *122*(3), 507-516. Retrieved Apr 4, 2021, from https://journals.ametsoc.org/view/journals/mwre/122/3/1520-0493_1994_122_0507_sarosi_2_0_co_2.xml

R. Berggren, B. Bolin & C.-G. Rossby (1949) An Aerological Study of Zonal Motion, its Perturbations and Break-down, *Tellus*, 1:2, 14-37, DOI: 10.3402/tellusa.v1i2.8501

BJERKNES, V., 1904: Das Problem der Wettervorhersage, betrachtet vom Standpunkte der Mechanik und der Physik (The problem of weather prediction, considered from the viewpoints of mechanics and physics). – Meteorol. Z. 21, 1–7. (translated and edited by VOLKEN E. and S. BRONNIMANN ¨ . – Meteorol. Z. 18 (2009), 663–667).

Branstator, G. W. (1987). A striking example of the atmosphere's leading traveling pattern. *Journal of The Atmospheric Sciences*, 44, 2310-2323. doi:10.1175/1520-0469(1987)044<2310:ASEOTA>2.0.CO;2

Branstator, G., & Held, I. (1995). Westward Propagating Normal Modes in the Presence of Stationary Background Waves, *Journal of Atmospheric Sciences, 52*(2), 247-262. Retrieved Apr 4, 2021, from https://journals.ametsoc.org/view/journals/atsc/52/2/1520-0469_1995_052_0247_wpnmit_2_0_co_2.xml

Dee, D.P., Uppala, S.M., Simmons, A.J., Berrisford, P., Poli, P., Kobayashi, S., Andrae, U., Balmaseda, M.A., Balsamo, G., Bauer, P., Bechtold, P., Beljaars, A.C.M., van de Berg, L., Bidlot, J., Bormann, N., Delsol, C., Dragani, R., Fuentes, M., Geer, A.J., Haimberger, L., Healy, S.B., Hersbach, H., Hólm, E.V., Isaksen, L., Kållberg, P., Köhler, M., Matricardi, M., McNally, A.P., Monge-Sanz, B.M., Morcrette, J.-J., Park, B.-K., Peubey, C., de Rosnay, P., Tavolato, C., Thépaut, J.-N. and Vitart, F. (2011), The ERA-Interim reanalysis: configuration and performance of the data assimilation system. *Q.J.R. Meteorol. Soc.*, 137: 553-597. https://doi.org/10.1002/qj.828

Doblas-Reyes, F., Pastor, M., Casado, M. et al. Wintertime westward-traveling planetary-scale perturbations over the Euro-Atlantic region. *Climate Dynamics* 17, 811–824 (2001). https://doi.org/10.1007/s003820000146

Feldstein, S. B. (2006). Dynamical Processes of Equatorial Atmospheric Angular Momentum, *Journal of the Atmospheric Sciences*, *63*(2), 565-581. Retrieved Apr 4, 2021, from https://journals.ametsoc.org/view/journals/atsc/63/2/jas3586.1.xml

Geophysical Flows (Omta). (2020, April 1). Retrieved April 28, 2021, from https://geo.libretexts.org/@go/page/1269

Grazzini, F., and F. Vitart, 2015: Atmospheric predictability and Rossby wave packets. *Quart. J. Roy. Meteor.* Soc., 141, 2793–2802, https://doi.org/10.1002/qj.2564.

Hamill, T. M., and J. S. Whitaker, 2007: Ensemble Calibration of 500-hPa Geopotential Height and 850-hPa and 2-m Temperatures Using Reforecasts. *Mon. Wea. Rev.*, **135**, 3273–3280, https://doi.org/10.1175/MWR3468.1.

Hamill, T. M., & Kiladis, G. N. (2014). Skill of the MJO and Northern Hemisphere Blocking in GEFS Medium-Range Reforecasts, *Monthly Weather Review*, 142(2), 868-885. Retrieved Mar 29, 2021, from https://journals.ametsoc.org/view/journals/mwre/142/2/mwr-d-13-00199.1.xml

Holton, J. R., & Hakim, G. J. (2013). An introduction to dynamic meteorology.

He, B., Liu, P., Zhu, Y. et al. Prediction and predictability of Northern Hemisphere persistent maxima of 500-hPa geopotential height eddies in the GEFS. *Clim Dyn* 52, 3773–3789 (2019). https://doi.org/10.1007/s00382-018-4347-4

Hersbach H, Bell B, Berrisford P, et al. The ERA5 global reanalysis. *QJR Meteorol Soc.* 2020;146:1999–2049. https://doi.org/10.1002/qj.3803

Hoskins, B. J., M. E. Mcintyre, and A. W. Robertson, On the use and significance of isentropic potential vorticity maps, •. J. R. Meteorol. Soc., 111,877-946, 1985. (Correction, •. J. R. Meteorol. Soc., 113, 402-404, 1987.)

Hoskins, B., 1997: A potential vorticity view of synoptic development. *Meteor. Appl.*, **4**, 325–334, https://doi.org/10.1017/S1350482797000716.

Hoskins, B. The potential for skill across the range of the seamless weather-climate prediction problem: a stimulus for our science. *Quart. J. Roy. Meteor. Soc.*, **139**, 573–584 (2013).

Hsu, C.-P.F., and J.M. Wallace, 1976: The global distribution of the annual and semiannual cycles in precipitation. Mon. Wea. Rev., 104, 1093–1101, doi:10.1175/1520-0493(1976)104<1093:TGDOTA>2.0.CO;2.

Huang, H., & Robinson, W. A. (1995). Barotropic Model Simulations of the North Pacific Retrograde Disturbances, *Journal of Atmospheric Sciences*, *52*(10), 1630-1641. Retrieved Apr 4, 2021, from https://journals.ametsoc.org/view/journals/atsc/52/10/1520-0469_1995_052_1630_bmsotn_2_0_co_2.xml

Kushnir, Y. (1987). Retrograding Wintertime Low-Frequency Disturbances over the North Pacific Ocean, *Journal of Atmospheric Sciences*, *44*(19), 2727-2742. Retrieved Apr 4, 2021, from https://journals.ametsoc.org/view/journals/atsc/44/19/1520-0469_1987_044_2727_rwlfdo_2_0_co_2.xml

Lau, N.-C., and M. J. Nath, 1999: Observed and GCM-simulated westward-propagating,

planetary-scale fluctuations with approximately three-week periods, *Mon. Weather Rev*., 127, 2324-2345.

Lavender, S. L., & Matthews, A. J. (2009). Response of the West African Monsoon to the Madden–Julian Oscillation, *Journal of Climate*, *22*(15), 4097-4116. Retrieved Apr 8, 2021, from https://journals.ametsoc.org/view/journals/clim/22/15/2009jcli2773

Lawrence, D. M., & Webster, P. J. (2002). The Boreal Summer Intraseasonal Oscillation: Relationship between Northward and Eastward Movement of Convection, *Journal of the Atmospheric Sciences*, *59*(9), 1593-1606. Retrieved Apr 8, 2021, from https://journals.ametsoc.org/view/journals/atsc/59/9/1520-0469_2002_059_1593_tbsior_2.0.co_2.xml

Lorenz, E. N. (1963). Deterministic Nonperiodic Flow, *Journal of Atmospheric Sciences*, *20*(2), 130-141. Retrieved Apr 8, 2021, from https://journals.ametsoc.org/view/journals/atsc/20/2/1520-0469_1963_020_0130_dnf_2_0_co_2.xml

Lorenz, E. N., 1969: The predictability of a flow which possesses many scales of motion. *Tellus*, 21, 289–307, https://doi.org/10.3402/tellusa. v21i3.10086.

Lorenz, E. N., 1982: Atmospheric predictability experiments with a large numerical model. *Tellus*, 34, 505–513, https://doi.org/10.1111/j.2153-3490.1982.tb01839.x

Lorenz, D. J., & Hartmann, D. L. (2006). The Effect of the MJO on the North American Monsoon, *Journal of Climate*, *19*(3), 333-343. Retrieved Apr 8, 2021, from https://journals.ametsoc.org/view/journals/clim/19/3/jcli3684.1.xml

Madden, R. A. (1979), Observations of large-scale traveling Rossby waves, *Rev. Geophys.*, 17(8), 1935– 1949, doi:10.1029/RG017i008p01935.

Madden, R. A., & Julian, P. R. (1971). Detection of a 40–50 Day Oscillation in the Zonal Wind in the Tropical Pacific, *Journal of Atmospheric Sciences*, 28(5), 702-708. Retrieved Mar 30, 2021, from https://journals.ametsoc.org/view/journals/atsc/28/5/1520-0469_1971_028_0702_doadoi_2_0_co_2.xml

Madden, R. A., & Julian, P. R. (1972). Description of Global-Scale Circulation Cells in the Tropics with a 40–50 Day Period, *Journal of Atmospheric Sciences*, 29(6), 1109-1123. Retrieved Mar 30, 2021, from https://journals.ametsoc.org/view/journals/atsc/29/6/1520 0469_1972_029_1109_dogscc_2_0_co_2.xml

Madden, R. A., & Speth, P. (1989). The Average Behavior of Large-Scale Westward Traveling Disturbances Evident in the Northern Hemisphere Geopotential Heights, *Journal of Atmospheric Sciences*, *46*(21), 3225-3239. Retrieved Apr 4, 2021, from https://journals.ametsoc.org/view/journals/atsc/46/21/1520-0469_1989_046_3225_tabols_2_0_co_2.xml

May, W. Space-time spectra of the atmospheric intraseasonal variability in the extratropics and their dependency on the El Niño/Southern Oscillation phenomenon: model versus observation. *Climate Dynamics* 15, 369–387 (1999). https://doi.org/10.1007/s003820050288

McIntyre, M., Palmer, T. Breaking planetary waves in the stratosphere. Nature 305, 593–600 (1983). https://doi.org/10.1038/305593a0

Michelangeli, P.-A. and Vautard, R. (1998), The dynamics of Euro-Atlantic blocking onsets. Q.J.R. Meteorol. Soc., 124: 1045-1070. https://doi.org/10.1002/qj.49712454803

Miller, R. L., G. M. Lackmann, and W. A. Robinson, 2020: A New Variable-Threshold Persistent Anomaly Index: Northern Hemisphere Anomalies in the ERA-Interim Reanalysis. *Mon. Wea. Rev.*, 148, 43–62, https://doi.org/10.1175/MWR-D-19-0144.1.

Mo, K. C. (1999). Alternating Wet and Dry Episodes over California and Intraseasonal Oscillations, *Monthly Weather Review*, *127*(12), 2759-2776. Retrieved Apr 4, 2021, from https://journals.ametsoc.org/view/journals/mwre/127/12/1520-0493_1999_127_2759_awadeo_2.0.co_2.xml

Nakamura, N., & Huang, C. S. Y. (2017). Local Wave Activity and the Onset of Blocking along a Potential Vorticity Front, *Journal of the Atmospheric Sciences*, *74*(7), 2341-2362. Retrieved Apr 4, 2021, from https://journals.ametsoc.org/view/journals/atsc/74/7/jas-d-17-0029.1.xml

Nakamura N, Huang CSY. Atmospheric blocking as a traffic jam in the jet stream. *Science*. 2018 Jul 6;361(6397):42-47. doi: 10.1126/science.aat0721. Epub 2018 May 24. PMID: 29794217.

Polvani, L. M., Esler, J. G., & Plumb, R. A. (1999). Time Variability and Simmons–Wallace–Branstator Instability in a Simple Nonlinear One-Layer Model, *Journal of the Atmospheric Sciences*, *56*(11), 1445-1460. Retrieved Apr 4, 2021, from https://journals.ametsoc.org/view/journals/atsc/56/11/1520-0469_1999_056_1445_tvaswb_2.0.co_2.xml

Raghunathan, G. N., & Huang, H. (2019). An Updated Analysis of Northern Hemisphere Submonthly Retrograde Waves, *Journal of the Atmospheric Sciences*, *76*(12), 3941-3954. Retrieved Apr 4, 2021, from https://journals.ametsoc.org/view/journals/atsc/76/12/jas-d-19-0143.1.xml

Rui, H., & Wang, B. (1990). Development Characteristics and Dynamic Structure of Tropical Intraseasonal Convection Anomalies, *Journal of Atmospheric Sciences*, 47(3), 357-379. Retrieved Mar 30, 2021, from https://journals.ametsoc.org/view/journals/atsc/47/3/1520-0469_1990_047_0357_dcadso_2_0_co_2.xml

Stan, C., and V. Krishnamurthy, 2019: Intra-seasonal and seasonal variability of the Northern Hemisphere extra-tropics. *Climate Dyn*., https://doi.org/10.1007/s00382-019-04827-9, in press.

Speth, P., May, W., & Madden, R. A. (1992). The Average Behavior of Large-Scale Westward-traveling Disturbances Evident in the Southern Hemisphere Geopotential Heights, *Journal of Atmospheric Sciences*, *49*(2), 178-185. Retrieved Apr 4, 2021, from https://journals.ametsoc.org/view/journals/atsc/49/2/1520-0469_1992_049_0178_tabols_2_0_co_2.xml

Takaya, K., & Nakamura, H. (2005). Geographical Dependence of Upper-Level Blocking Formation Associated with Intraseasonal Amplification of the Siberian High, *Journal of the Atmospheric Sciences*, *62*(12), 4441-4449. Retrieved Apr 4, 2021, from https://journals.ametsoc.org/view/journals/atsc/62/12/jas3628.1.xml

Takaya, K., & Nakamura, H. (2005). Mechanisms of Intraseasonal Amplification of the Cold Siberian High, *Journal of the Atmospheric Sciences*, *62*(12), 4423-4440. Retrieved Apr 4, 2021, from https://journals.ametsoc.org/view/journals/atsc/62/12/jas3629.1.xml

Tibaldi, S. and Molteni, F. (1990), On the operational predictability of blocking. Tellus A, 42: 343-365. https://doi.org/10.1034/j.1600-0870.1990.t01-2-00003.x

van Den Dool, H. M., and S. Saha, 1990: Frequency Dependence in Forecast Skill. *Mon. Wea. Rev.*, **118**, 128–137, https://doi.org/10.1175/1520-0493(1990)118<0128:FDIFS>2.0.CO;2.

Vulpiani, A. Lewis Fry Richardson: scientist, visionary and pacifist. *Lett Mat Int* 2, 121–128 (2014). https://doi.org/10.1007/s40329-014-0063-z

Watt-Meyer, O., & Kushner, P. J. (2015). Decomposition of Atmospheric Disturbances into Standing and Traveling Components, with Application to Northern Hemisphere Planetary Waves and Stratosphere–Troposphere Coupling, *Journal of the Atmospheric Sciences*, *72*(2), 787-802. Retrieved Apr 4, 2021, from https://journals.ametsoc.org/view/journals/atsc/72/2/jas-d-14-0214.1.xml

Zhang, F., Y. Q. Sun, L. Magnusson, R. Buizza, S. Lin, J. Chen, and K. Emanuel, 2019: What Is the Predictability Limit of Midlatitude Weather?. *J. Atmos. Sci.*, **76**, 1077–1091, https://doi.org/10.1175/JAS-D-18-0269.1.

APPENDIX A

BAND PASS FILTER

The band-pass filter combines a pair of standard non-recursive 8-day low-pass and 30-day high-pass filters. In physical space, the weight for the low-pass filter is

$$f_{LP}(n\Delta t) = \frac{2\sin(\omega_c\, n\Delta t)}{\omega_s\, n\Delta t} \qquad \textbf{(14)}$$

and that for the high-pass filter is

$$f_{HP}(n\Delta t) = \frac{2[\sin(\omega_s\, n\Delta\, t/2) - \sin(\omega_c\, n\Delta t)]}{\omega_s\, n\Delta t} \qquad \textbf{(15)}$$

where Δt is sampling interval (Δt = 1 day for daily data), $\omega_s = 2\pi/\Delta t$, and ω_c is the cutoff frequency given as $\omega_c = 2\pi/(8$ days) for the LP filter and $\omega_c = 2\pi/(30$ days) for the HP filter. For an M-point filter, the index n runs from $-(M-1)/2$ to $(M-1)/2$, and the weighted sum of the original data over that range yields the filtered data at $n = 0$. In actual applications, each of the filters is modified by a Hamming window,

$$w(n\Delta t) = 0.54 + 0.46\ \cos\left(\frac{2\pi n\Delta t}{M-1}\right), if\ |n| < \frac{M-1}{2}$$
$$= 0, otherwise \qquad \textbf{(16)}$$

Putting together, the fully defined filters are $F_{LP}(n\Delta t) = f_{LP}(n\Delta t)w(n\Delta t)$ for the low-pass filter, and $F_{HP}(n\Delta t) = f_{HP}(n\Delta t)w(n\Delta t)$ for the high-pass filter.

Our analysis uses a 25-point LP filter and a 121-point HP filter. The response functions for the filters are shown in Fig. 16. Over the critical window of 2-3 weeks, almost 100% of the amplitude is retained. The response function for the LP filter drops to 0.08 at 6 days, effectively suppressing the high-frequency short waves. On the low-frequency side, the response function of the HP filter drops to 0.22 at 35 days, and 0.1 at 39 days. As the

LP and HP filters are applied successively to the daily data, the end points in the time series that are not properly filtered are discarded. The excluded points are the first 72 days of 1979 and the last 72 days of 2017.

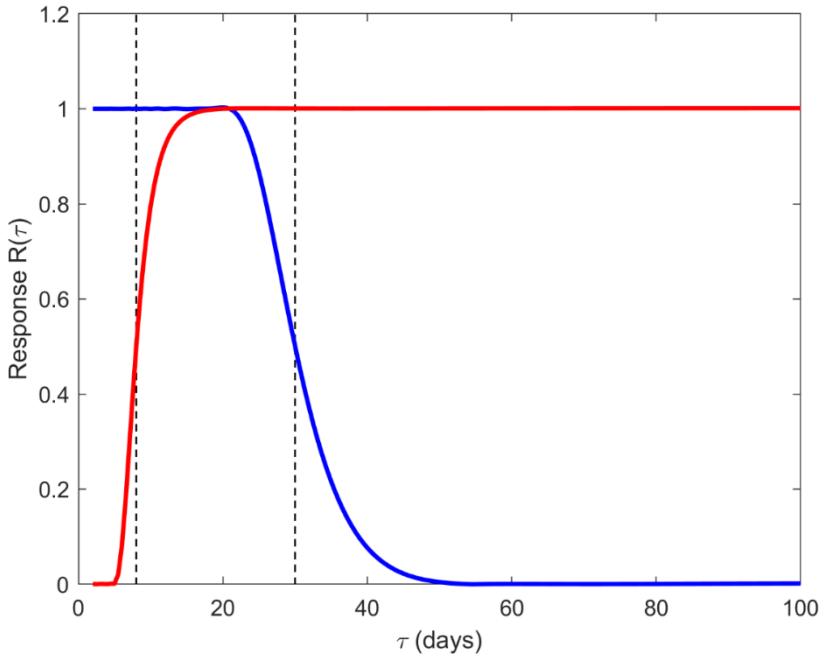

Figure 53. The Response Functions of the High-Pass (Blue) and Low-Pass (Red) Filters. The Two Dashed Vertical Lines Mark τ = 8 Days and 30 Days.

APPENDIX B

SIGNIFICANCE OF INCREASED PREDICTABILITY

The Kolmogrov-Smirnov Test and two sample student t-test are performed to test the significance of the increased Anomaly Correlation during active period as compared to the inactive period results of which are displayed below in Figure 54. The two samples in each of these plots are all Anomaly Correlation values during active period and inactive period during the corresponding Winters chosen (between November 1st – April 30th 1986/87, 1994/95, 1995/96 and 2010/11). The percentage values indicate the confidence level that the cumulative distribution function for active period of corresponding lead times is larger than that for inactive period data vector. This is performed calculating the confidence levels for values from comparing just the Zonal Wavenumbers 1 &2 500mb Geopotential Height anomaly correlation and the total Anomaly Correlation. Large values of confidence level during the years chosen proves the distribution containing Anomaly Correlation during active period is different from the one containing Anomaly Correlation during inactive period.

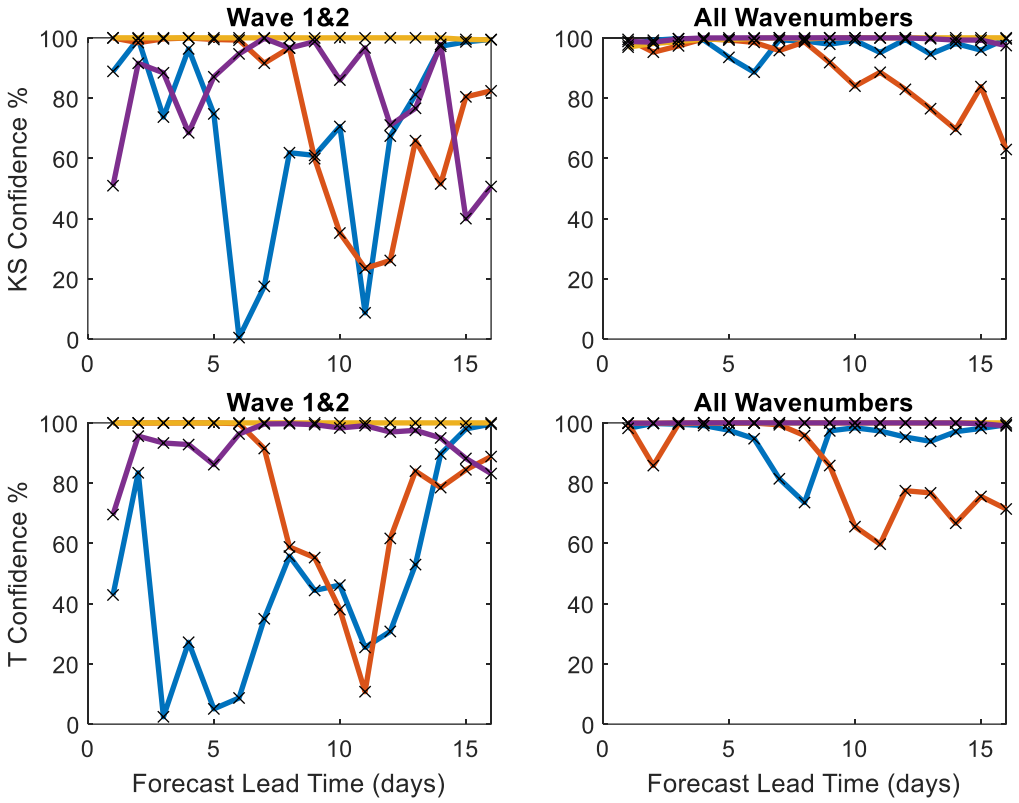

Figure 54. Percentage Confidence on the Hypothesis that Datasets Containing Event Day Anomaly Correlations has a Larger Cumulative Distribution Function Compared to the Non-Event Day Anomaly Correlations for Each of the Forecast Lead Times Based on KS and T Statistics with Purple, Red, Yellow and Blue Lines Indicating Periods November 1st to April 30th of 1986-87, 1994-95, 1995-96 and 2010-11 Respectively.